

3D in vitro co-culture models of primary breast tumour cells

Maria Manuel Vigo Osório de Valdoleiros

Dissertation for the Degree of Master of Science in Bioengineering

Supervisor: Sílvia Bidarra, Ph.D.

Co-supervisor: Cristina Barrias, Ph.D

Porto, September 2021

Maria Valdoleiros, 2021

3D in vitro co-culture models of primary breast tumour cells

Maria Manuel Vigo Osório de Valdoleiros

FEUP – Faculdade de Engenharia da Universidade do Porto

ICBAS-UP – Instituto de Ciências Biomédicas Abel Salazar, Universidade do Porto

Dissertation for Masters in Bioengineering

Supervisor:

Sílvia Bidarra, Ph.D.

Co-supervisor:

Cristina Barrias, Ph.D.

i3S – Instituto de Investigação e Inovação em Saúde, Universidade do Porto

Porto, September 2021

This page has been intentionally left blank.

Abstract

Breast cancer (BC) is a leading cause of death among women. Different categorisation systems describe the heterogeneity of this disease with implications in treatment options and patients' outcomes. Cells immunohistochemical profile is the most common categorisation system adopted and is based on the expression profile of hormone receptors (estrogen and progesterone receptors) and human epidermal growth factor receptor 2. This system defines four major BC subtypes: Luminal A and B, HER2-enriched and triple-negative (TN) BCs.

The BC microenvironment is well recognised as a critical element for tumour development and progression. This microenvironment comprises multiple cell types, extracellular matrix (ECM), soluble factors and physical properties. To address the challenges associated with BC heterogeneity, it is important to develop physiological relevant three-dimensional (3D) co-culture models. 3D culture systems offer advantages because they better reflect the *in vivo* cell – cell and cell – ECM interactions. In the literature, these models are most established from cell lines, which diminishes the biological relevance of *in vitro* models. The use of primary human cells may significantly improve 3D co-culture models and, consequently, the development of new therapeutic strategies. In this context, our work was focused on the establishment of 3D co-culture models with primary cells from patients diagnosed with Luminal A, HER2-enriched and TN BCs.

Aiming to develop 3D co-culture models, primary cell cultures were established in 2D, and characterised throughout time, for each BC subtype. We successfully produce 3D multicellular tumour spheroids (MCTS) using a scaffold-free strategy. MCTS retained *in vivo*-like properties, such as (1) extracellular matrix production rich in type I collagen and fibronectin and (2) capacity to invade and migrate. Finally, we were able to generate primary BC organoids in a well-defined 3D hydrogel matrix based on a peptide modified alginate. Although further characterisations are needed, we were able to identify the formation of multicellular clusters within these matrices.

Overall, we successfully established in our lab both 2D and 3D cultures of primary breast cancer cells giving a step forward in the development of physiologically relevant models with preclinical and clinical applicability.

This page has been intentionally left blank.

Acknowledgements

To my supervisor, Sílvia Bidarra, I would like to deeply thank the support, patience, and guidance throughout this journey. To thank every piece of knowledge and advice, every suggestion, and every moment when you believed in me more than I believed in myself. I am deeply grateful for this opportunity. I take you to the future as an example.

To my co-supervisor, Cristina Barrias, I would like to thank the opportunity to be part of this group, the support, and advice, throughout this process.

I cannot pass without acknowledging the Bioengineered 3D Microenvironments group, a pure example of teamwork. Particularly, a thank to Ana Luísa who always helped me with assertiveness and good mood.

To my friends, for all the company, the laughter, and the help with the small and big challenges we faced throughout this five-year turbulent experience.

Finally, to my family, my mother and father, Sara, Leonor, and Ricardo. The ones that most believed I would reach this moment. Thank the unconditional support and endless patience throughout the most challenging stage of my life. To my grandfather, whose eyes would be shining.

This page has been intentionally left blank.

List of contents

Abstract	v
Acknowledgements	vii
List of contents	ix
List of figures	xi
List of tables	xiii
List of abbreviations	xiv
1 General Introduction	1
1.1 Mammary gland.....	1
1.2 Breast cancer	3
2 The breast cancer microenvironment	6
2.1 Tumour cells.....	7
2.1.1 Luminal BC.....	8
2.1.2 HER2-enriched BC	9
2.1.3 Basal-like and triple-negative BCs	10
2.2 Stromal cells.....	11
2.3 Extracellular matrix (ECM).....	13
3 Models of breast cancer	14
3.1 <i>In vivo</i> models.....	14
3.2 3D <i>in vitro</i> models.....	16
3.2.1 Biomaterials as ECM-like matrices	17
3.2.2 Scaffold-free	20
3.3. Cells for breast cancer research	25
4 Motivation	27
5 Materials and methods	29
5.1 Cell maintenance.....	29
5.2 2D culture of primary tumour cells	29
5.3 Multicellular tumour spheroids of primary tumour cells.....	30

5.4 Breast cancer organoid within alginate-RGD matrices	30
5.5 Metabolic activity assay	31
5.6 MCTS morphological analysis	32
5.7 Sprouting assay	33
5.8 Immunofluorescence	34
5.8.1 2D cultures	34
5.8.2 Paraffin-embedded samples	34
5.8.3 Whole-mounted samples (fibrin)	35
5.8.4 3D culture within alginate matrices	35
5.9 Statistical analysis	35
6 Results and discussion	36
6.1 Establishment of primary tumour cells culture	36
6.2 Characterisation of cell populations in DT derived 2D cultures.	41
6.2.1 Assessment of CK8 and CK14 expression as markers of breast epithelial lineages	41
6.2.2 Expression of surface markers: E-cadherin, CD44 and CD90.....	45
6.2.3 Expression of mesenchymal markers: vimentin and α -SMA	47
6.3 Establishment of scaffold-free 3D in vitro models from DT specimens ...	49
6.3.1 Spheroid's formation and morphology	49
6.3.2 ECM production inside MCTS	54
6.3.3 Epithelial cells form the outer layer of MCTS	58
6.3.4 MCTS in fibrin as a model of cancer cells invasion	61
6.4 Formation of breast cancer organoids within RGD-alginate hydrogels ...	65
7 Concluding remarks.....	68
References	71
Supplementary information.....	79

List of figures

Figure 1. Schematic representation of the adult female mammary gland and subgross anatomy of the terminal duct lobular unit (TDLU).....	2
Figure 2. Breast cancer origin.	3
Figure 3. Schematic representation of the tumour microenvironment.	6
Figure 4. Tumour development: in situ – to – invasive transition.	7
Figure 5. Haematoxylin and eosin-stained sections of A) human breast and B) mouse mammary gland.	15
Figure 6. Alginate chemical structure and gelation process.....	19
Figure 7. Formation of physiological gradients in tumour spheroids.	21
Figure 8. Spheroid production methods.....	22
Figure 9. Graphical abstract.	28
Figure 11. Schematic representation of the production of agarose moulds.....	30
Figure 10. Experimental procedure for the preparation of the 3D cell-laden matrices.....	31
Figure 12. Schematic representation of the experimental design of the sprouting assay.	33
Figure 13. Primary breast tumour specimens cultured on collagen-coated flasks.	37
Figure 14 Metabolic activity studies of DT cells cultured in 2D monolayer.....	38
Figure 15. Metabolic activity studies of DT cells cultured in 2D monolayer.	39
Figure 16. DT cells (passage 5) cultured in 2D monolayer stained with antibodies against Ki-67.....	40
Figure 17. DT cells (passage 1) cultured in 2D monolayer stained with antibodies against cytokeratin 8 (CK8 – green) and cytokeratin 14 (CK14 – red).	42
Figure 18. Quantification of luminal epithelial (CK8) and myoepithelial (CK14) cells.	43
Figure 19. Alteration in CK14 (red) and CK8 (green) expression in HER-DT derived cultures (passage 5 cells).....	43
Figure 20. Expression pattern of CK14 (red) and CK8 (green) in LA-DT derived cultures (cells in passage 5).	44
Figure 21 Expression pattern of CK14 (red) and CK8 (green) in TN-DT derived cultures (cells in passage 5).	45
Figure 22. DT cells (passage 1) cultured in 2D monolayer stained with antibodies against surface markers: E-cadherin, CD44 and CD90.	46

Figure 23. DT cells (passage 5) cultured in 2D monolayer stained with antibodies against vimentin.	47
Figure 24. DT cells (passage 5) cultured in 2D monolayer stained with antibodies against α -SMA.	48
Figure 25. Simultaneous images of multiple spheroids.....	49
Figure 26. MCTS morphological characterisation.	50
Figure 27. MCTS morphological characterisation – (A) Solidity and (B) Roundness.	51
Figure 28. H&E staining in 3 μ m paraffin-embedded sections of MCTS derived from LA-, HER2- and TN-DT specimens in passages 2 (top) and 8 (bottom) at days 1 and 7 post-seeding.	52
Figure 29. Proliferating Ki-67+ cells in MCTS.....	53
Figure 30. Fibronectin deposition and distribution in MCTS along 7 days of culture.	55
Figure 31. Collagen I deposition and distribution in MCTS along 7 days of culture.	57
Figure 32. Fibronectin and Collagen I deposition and distribution in MCTS derived from DT specimens in passage 8 after 7 days of culture.....	58
Figure 33. Expression of epithelial markers (CK8 and 14) in MCTS along 7 days in culture.....	59
Figure 34. Expression of E-cadherin (epithelial marker) and vimentin (fibroblast marker) in MCTS along 7 days in culture.	60
Figure 35. Vimentin and E-cadherin expression in MCTS derived from DT specimens in passage 8.	61
Figure 36. Expression of vimentin and fibronectin in MCTS embedded in fibrin gel for 2 days.	63
Figure 37. Expression of vimentin and fibronectin in MCTS embedded in fibrin gel for 7 days.	64
Figure 38. RGD-Alginate hydrogel for the culture of DT cells.	66
Figure 39. Characterisation of DT cells behaviour in 3D (passages 4 and 8)...	67
Figure S1. MSCT morphological characterisation – diameter.....	79
Figure S2 Metabolic activity studies of DT cells cultured in 3D alginate matrices.	79

List of tables

Table 1. Breast cancer classification based on immunohistochemical profile.....	5
Table 2. Spheroid generation: advantages and disadvantages of different techniques.	23
Table 3. Commonly used BC cell lines.	26
Table 4. Classification of primary breast tumours at the time of diagnosis.	36

List of abbreviations

2D: Two-dimensional

3D: Three-dimensional

BC: Breast cancer

b-FGF: Basic fibroblast growth factor

BM: Basement membrane

CAAs: Cancer-associated adipocytes

CAFs: Cancer-associated fibroblasts

CAMs: Cancer-associated macrophages

CAV: Caveolin

CK: Cytokeratin

Col-I: Collagen I

CSC: Cancer stem cells

CXCL12/SDF-1: Stromal cell-derived factor-1

DCIS: Ductal carcinoma in situ

DT: Dissociated tumour

ECM: Extracellular matrix

EMT: Epithelial to mesenchymal transition

ER: Estrogen receptor

ETD: Extralobular terminal duct

FN: Fibronectin

FSP: Fibroblast specific protein

GPI: Glycosylphosphatidylinositol

HER2: Human epidermal growth factor receptor 2

IDC: Invasive ductal carcinoma

IDC-NOS: Invasive ductal carcinoma not otherwise specified

IDC-NST: Invasive ductal carcinoma of no special type

IL: Interleukin

ITD: Intralobular terminal duct

LEPs: Luminal epithelial cells

MCTS: Multicellular tumour spheroids

MMP: Matrix metalloproteases

NST: No special type

PDGFR- α/β : Platelet-derived growth factor receptor- α/β

PDGF- α/β : Platelet-derived growth factor- α/β

PI3K: Phosphatidylinositol 3-kinase

PR: Progesterone receptor

PTEN: Phosphatase and tensin homolog

TDLU: Terminal duct lobular unit

TGF- β : Transforming growth factor- β

Thy-1: thymocyte differentiation antigen-1

TME: Tumour microenvironment

TNBC: Triple-negative breast cancer

VEGF: Vascular endothelial growth factor

WHO: World Health Organization

This page has been intentionally left blank.

1 General Introduction

1.1 Mammary gland

The mammary gland is a milk-producing gland characteristic of all female mammals. In humans, two bilaterally symmetrical mammary glands are situated within the breasts. The breasts are situated within the superficial fascia of the anterior thoracic wall, above the pectoralis major, extending upwards into the axilla. In males, the mammary glandular tissue is rudimentary and, generally, non-functional [1, 2].

During embryonic life, the mammary glands derive from a modification on sweat glands which develop from a longitudinal ridge of ectoderm through a series of interactions between surface epithelial cells and underlying mesenchymal cells. The adult female mammary gland is a branched tubular organ with ducts extending radially from the nipple to form 15–20 separate lobes (**Figure 1 A**) [2]. These lobes are composed of glandular tissue (groups of secretory glandular acini) embedded in connective and adipose tissue. Each lobe is drained by its lactiferous duct leading to the nipple. The connective tissue is a fibrocollagenous stroma. Fibrous thickenings of connective tissue interdigitate between the parenchymal structures, connecting the skin with the fascia, forming fibrous suspensory ligaments, Cooper's ligaments. The Cooper's ligaments support and provide mobility to the human mammary gland. The amount and distribution of the adipose tissue determine the size and shape of the breast [1, 2].

The basic milk-producing unit of the mammary gland is the terminal duct lobular unit (TDLU). The TDLU consists of an extralobular terminal duct (ETD) and an intralobular terminal duct (ITD), which is the axial core of the lobule connecting to the acinus (**Figure 1 B**). In humans, the TDLU appears upon sexual maturity and develops during the lifetime in response to the hormone status of the female. The mammary gland acini are lined by one to two layers of cuboidal epithelial cells – the functional secretory cells during lactation [1]. Histologically, the ducts and lobules are formed by three distinct epithelial lineages: basal myoepithelial cells (MEPs) and two populations of luminal epithelial cells (LEPs) (**Figure 1 C**) [3]. The LEPs are responsible for milk production and hormone sensing. The MEPs are responsible for milk ejection during breastfeeding thanks to their contractile properties in response to oxytocin. This epithelium is

surrounded by a basement membrane (BM) and embedded in a complex stroma. In the intralobular stroma, diverse cellular elements can be found, including fibroblasts, adipocytes, nerves, microvasculature, and immune cells [1, 3].

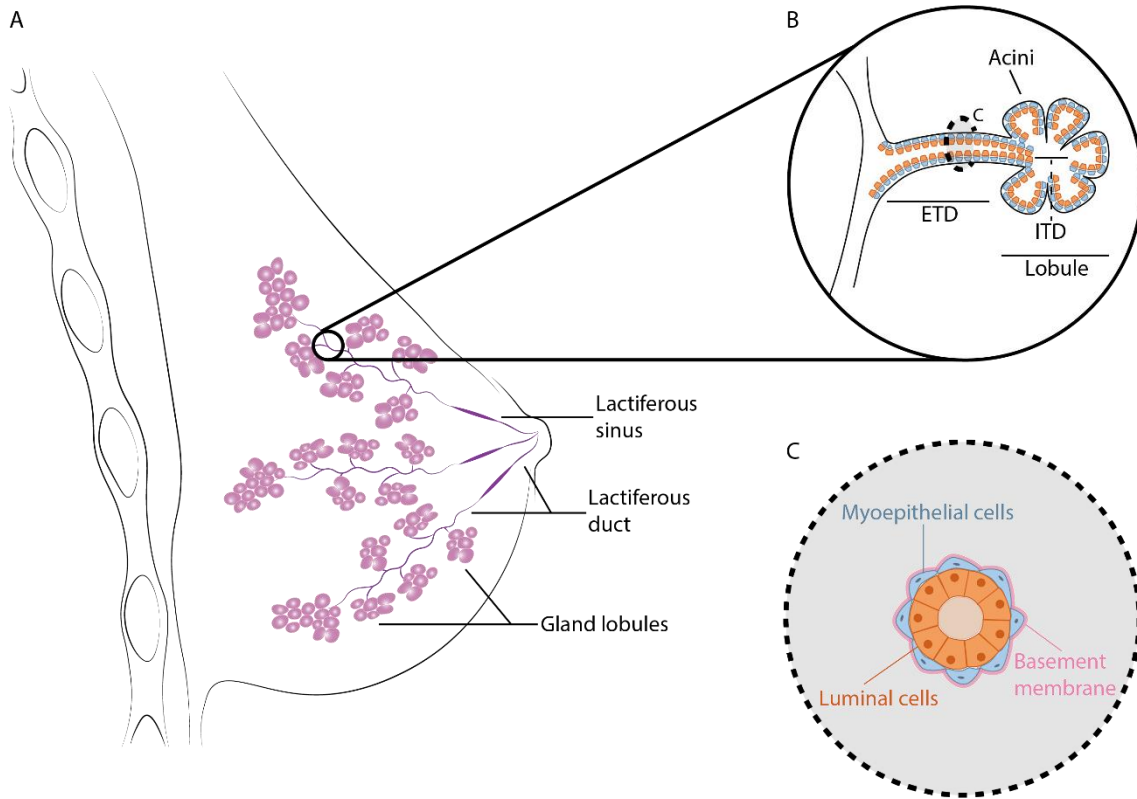


Figure 1. Schematic representation of the adult female mammary gland and subgross anatomy of the terminal duct lobular unit (TDLU). A) Human cross-sectional mammary anatomy. In humans, each lobe (gland lobules) connects with one of several major lactiferous ducts that expand to lactiferous sinuses at the base of the nipple. B) Diagram of a TDLU – the functional mammary gland unit. The TDLU consists of an intralobular terminal duct (ITD) connecting the acinus to an extralobular terminal duct (EDT). Multiple acini are found within the lobule. Adapted from Cardiff, Jindal [1], [4]. C) Cross structure diagram of the mammary gland. Ducts and lobules comprise a bilayered epithelium (myoepithelial and luminal epithelial cells) surrounded by the basement membrane. Adapted from Srivastava, Huycke [3].

1.2 Breast cancer

Breast cancer (BC) is a pathological condition that involves genetic or epigenetic alterations in ductal (**Figure 2 A**) or lobular cells (**Figure 2 B**). These alterations lead to disorganised cell replication and the formation of an aggregate/cell mass, with altered mechanical and biological properties when compared to healthy breast tissue. In women, BC accounts for 29% of new cases of cancer and 14% of cancer deaths [5] and is most commonly originated in the TDLUs [1-3, 5]. According to the American Cancer Society [6], invasive breast adenocarcinomas represent 70-80% of all BCs. Non-invasive or pre-invasive BC (ductal carcinoma *in situ* – DCIS) accounts for 1 in 5 new breast cancers cases [7].

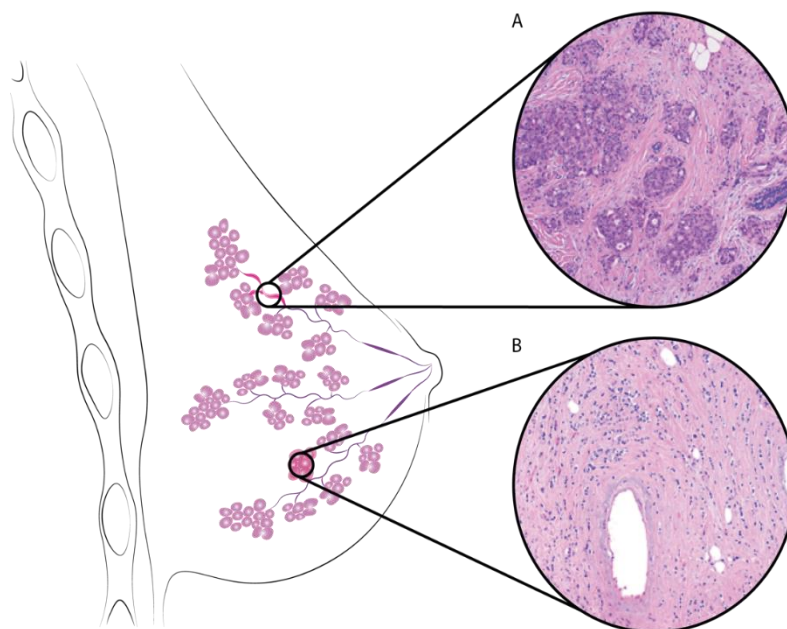


Figure 2. Breast cancer origin. A) Breast cancer of ductal origin. A histological vision of grade 2 invasive ductal carcinoma of no special type. B) Breast cancer of lobular origin. A histological vision of classical grade 2 invasive lobular carcinoma. Histological images retrieved from Erber and Hartmann [8].

Breast cancer comprises more than twenty different subtypes, that differ genetical, morphological and clinically [9]. Different categorisation systems may be adopted. Array-based gene expression profiling allowed the identification of five BC subtypes: luminal subtype A, luminal subtype B, HER2-enriched, basal-like, and normal breast-like subtypes. These distinct subtypes are associated with different molecular signatures and clinical outcomes [5, 10].

From the histological point of view, two different terminologies are important to highlight: histological grade and histological type. Histological grade refers to the degree of differentiation (associated with tubule formation and nuclear pleomorphism) and proliferative activity (*i.e.*, mitotic index) of a tumour. BC subtypes may be classified as of low or high histological grade (grade 1 to 3). This definition is correlated with tumour aggressiveness and with the genetic and transcriptomic features of BCs, being considered a strong prognostic factor [10, 11]. Low histological grade tumours (or grade 1) present with uniform cells with nuclei similar in size to normal breast epithelial cells. High histological grade tumours (grades 2 and 3) present with larger cells and nuclei of altered size and shape. Generally, low-grade tumours tend to be less aggressive than high grade [12].

Histological type refers to the growth pattern of the tumours, associated with morphological and cytological features [10]. Different tumour histological types are consistently correlated with distinctive clinical presentations and/or outcomes [8, 10]. The World Health Organization (WHO) considers the existence of more than 17 special histological types of adenocarcinomas. Tubular, mucinous, papillary, cribriform, micropapillary, or pleomorphic invasive lobular carcinomas are examples of special histological types of BC [8, 10, 11, 13]. Tubular, cribriform, and mucinous carcinomas, if at least 90% pure, are associated with a good prognosis. On the other hand, micropapillary and pleomorphic invasive lobular carcinomas are associated with poorest clinical outcome [11]. Adenocarcinomas that do not exhibit sufficient characteristics of a particular special histological type are classified as invasive ductal carcinomas (IDC) of no special type (IDC-NST)/not otherwise specified (IDC-NOS) [8, 10, 11].

Apart from the histological-based classification, BCs are more often distinguished based on cells immunohistochemical profile, a well-established biomarker for BC diagnosis and guidance for treatment [14]. For immunohistochemical profiling, the expression status of hormone receptors (estrogen receptor – ER – and progesterone receptor – PR) and human epidermal growth factor receptor 2 (HER2) are considered. Based on this categorisation, invasive breast adenocarcinomas are commonly classified into four major molecular subtypes (**Table 1**).

Table 1. Breast cancer classification based on immunohistochemical profile [6].

Classification	Epidemiologic incidence	Immunohistochemical profile			
		Hormone receptors			
		ER	PR	Her2	
Luminal	A	30 – 40 %	+	+	-
	B	20 – 30 %	+	-	-
HER2 enriched	12 – 20 %	-	-	+	
Triple-negative	15 – 20%	-	-	-	

ER – estrogen receptor; PR – progesterone receptor; HER2 – human epidermal growth factor receptor 2.

Cancer prognosis depends on multiple factors, such as the stage and type of tumour, patient genetics, age, tumour microenvironment (TME), available treatment option, and patient's response to therapy [15]. Accumulation of mutation is a critical point in breast cancer. Usually, a higher degree of mutations is associated with worst prognosis and diminished treatment options [14]. Generally, the presence of hormone receptors and HER2 is associated with a better prognosis [14, 16]. These receptors are cancer-specific therapeutic targets that have demonstrated a survival benefit beyond that provided by cytotoxic therapy (chemotherapy) alone. Anti-estrogen (endocrine) therapies are applied to patients whose tumours express ER and/or PR. Anti-HER2 therapies are applicable in the treatment of tumours that demonstrate amplification of HER2. In triple-negative breast cancer (TNBC), in which the cells express neither ER and PR nor HER2, patients cannot benefit from the above-mentioned therapies, been chemotherapy the current mainstay treatment [5, 11]. Therefore, to understand the BC dynamics and develop new approaches, it is fundamental to study the molecular biology behind each BC subtype and to create three-dimensional (3D) models that better recapitulate the breast cancer microenvironment complexity and structure.

2 The breast cancer microenvironment

The breast cancer microenvironment is well recognised as a critical element for tumour development and progression. The BC microenvironment (**Figure 3**), at both local and metastatic levels, comprises multiple cell types, ECM, soluble factors and physical properties [17]. In this section, we will describe tumour cells according to each molecular subtype, stromal cells (fibroblast, adipocytes, macrophages, and endothelial cells) and a brief overview of ECM mechanical properties.

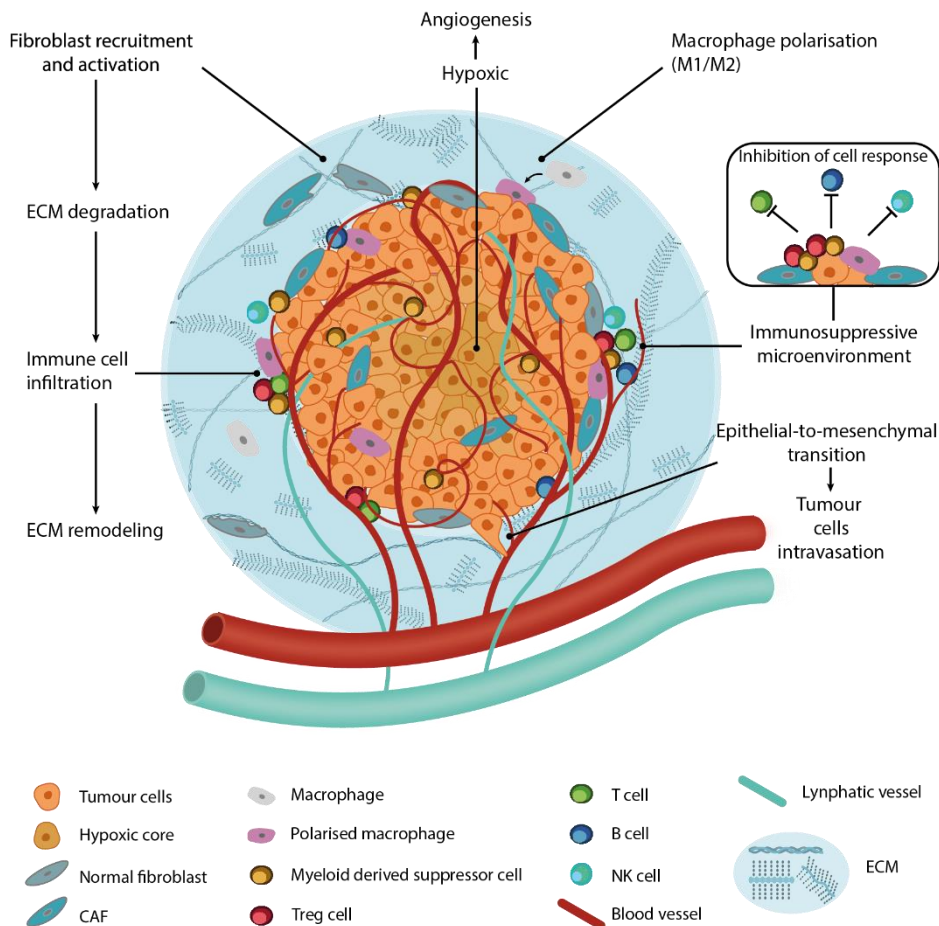


Figure 3. Schematic representation of the tumour microenvironment. The complexity of TME involves three main components: tumour cells, stromal cells, and immune cells. Processes such as fibroblast recruitment, macrophage polarisation, immunosuppression and angiogenesis shape the microenvironment and promote ECM degradation and remodelling enabling tumour cell intravasation and potential metastatisation. Abbreviations: CAF, Cancer-associated macrophage; Treg cell, regulatory T cell; NK cell, Natural Killer cell; ECM, extracellular matrix.

2.1 Tumour cells

Tumour development is characterised by diminished cell adhesion that promotes the dissociation of the epithelium [14, 18] and the destabilisation of the BM [18]. In this way, tumour cells invade the lumen forming DCIS (solid tumour masses in the lumens of epithelial tissues). On the other hand, tumour development is characterised by an uncontrolled cell division that allows rapid cell proliferation and accumulation of cellular mutations [14, 18]. Alterations in the TME associated with disruption of the BM enable cells to invade the stromal compartment and form IDC (tacking place an *in situ* – to – invasive transition – **Figure 4**) [18].

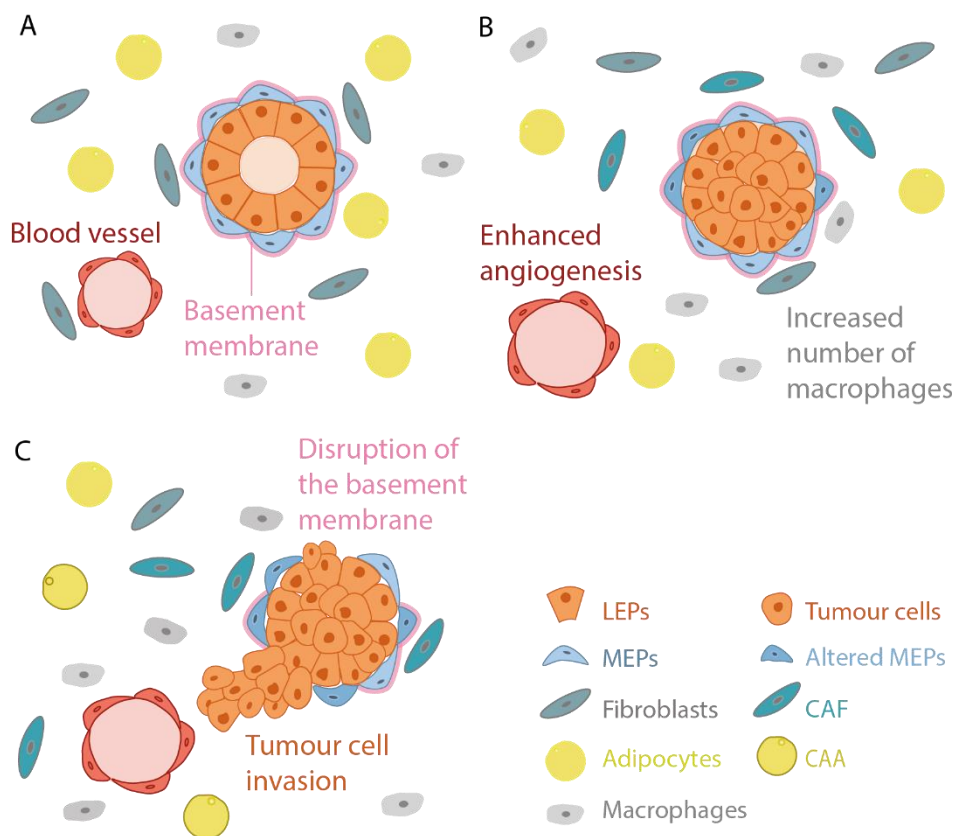


Figure 4. Tumour development: in situ – to – invasive transition. A) Normal breast microenvironment. Luminal epithelial cells (LEPs) form a lumen surrounded by myoepithelial cells (MEPs) and a basement membrane. Diverse stroma cells can be found in the microenvironment, namely, fibroblasts, adipocytes, and macrophages. B) In situ ductal carcinoma. Characterised by increased proliferation of LEPs that occupy the central lumen surrounded by the MEPs. The tumour microenvironment is characterised by enhanced angiogenesis, increased number of macrophages and appearance of cancer-associated fibroblasts (CAFs) and adipocytes (CAAs). C) Invasive ductal carcinoma. Characterised by disruption of the basement membrane and loss of the MEPs outer ring, associated with invasion of the stromal compartment by tumour cells.

In solid tumours, such as BC, cells form a core of necrotic and apoptotic cells (in a hypoxia environment) surrounded by a middle layer of senescent cells and an outer layer of rapid proliferative cells. This organization is due to differential oxygen and nutrient supply to cells at different sites in the tumour. Uncontrolled cell division and hypoxic gradients increase cells heterogeneity (phenotypic and/or genotypically) [14, 19]. Moreover, hypoxia induces alteration in protein expression promoting angiogenesis and reinforcing cell heterogeneity [14].

As referred, epithelial cells from the TDLU have been proposed as the site of origin of most BCs. The abnormal expression of the three most common biomarkers (ER, PR and HER2) introduces different proprieties to each molecular BC subtype [5]. Luminal, HER2-enriched and triple-negative BCs will be further characterised below.

2.1.1 Luminal BC

Approximately 70% of breast cancers express estrogen receptors. Estrogen plays a critical role in the development of both normal breast epithelium and breast cancer. Estrogen interacts with epithelial cells via a cell-specific receptor – the ER – which has two subtypes – alpha (ER α) and beta (ER β). These proteins act as nuclear transcription factors regulating the development and function of different organs. The ER α has a more prominent role on the mammary gland and uterus and is closely associated with BC [5, 20]. In luminal BC, epithelial cells express the ER α (i.e., they are ER-positive (ER+)). ER+ tumours usually grow more slowly and appear better differentiated than ER-negative (ER-) tumours [5].

The presence of PR will determine the subtype of luminal BC and is a prognostic marker. The PR is encoded by an estrogen-regulated gene and occurs as two different isoforms – PRa and PRb. Polymorphisms in isoform b are most associated with the development of BC [5]. Luminal A BC is characterised by the expression of the PR, while in luminal B BC this receptor is not present [5, 11].

Luminal A BCs are characterised as small tumours with low aneuploid events and nodal involvement [5]. Considering the histological characterisation, these tumours are of low histological grade – presenting low degrees of nuclear pleomorphism and mitotic activity [5, 10, 21, 22]. The luminal A molecular subtype includes some special histological types, such as tubular, invasive cribriform, mucinous and lobular carcinomas [23]. In addition to being ER+/PR+, immunohistochemical studies describe these tumours as those that (1) express low molecular weight luminal epithelial cytokeratins (CK) 8 and 18, (2) have low expression rates of Ki-67 (a proliferative cell marker), [10,

21, 23] and (3) express ER-activated genes [10]. Overall, luminal A BC tends to be associated with good outcomes [5, 10, 21] and anti-estrogen therapy is the most applied therapeutic strategy [5, 21].

Luminal B BCs are immunohistochemically defined as ER+/PR- and express high levels of Ki-67. Usually, these tumours are of high histological grade and associated with high proliferation rates [8, 10, 24]. Regarding the histological type, the luminal B subtype is most commonly IDC-NST [25]. In some cases, these tumours present with papillary, mucinous, [25] micropapillary [11, 25], lobular pleiomorphic and atypical lobular [11] histology's. Luminal subtype B is associated with a worse prognosis than subtype A [8, 10, 24]. This worse prognosis is related to the poor outcome with endocrine therapy, and with relative resistance to chemotherapy compared with other highly proliferative BCs [24, 26]. Therefore, this subtype is considered the most aggressive form of ER+ BCs [26]. Considering the certain degree of resistance to endocrine therapy, luminal B BC is considered to share molecular features with ER- subtypes (such as HER2-enriched and basal-like BCs) [23, 26].

2.1.2 HER2-enriched BC

ERBB2 (or HER2) is a growth-signalling molecule, a member of the family of four membrane tyrosine kinases (ERBB1 – EGFR, ERBB3 – HER3, and ERBB4 – HER4), expressed on the surface of normal breast cells. HER2 is overexpressed, or amplified, in approximately 20% of BCs (classified as HER2-positive [HER2+]) and contributes to the growing autonomy and genomic instability of these tumours [5, 23]. HER2+ status can be assessed by immunohistochemical membrane staining of HER2 or by an amplification of ERBB2 detected by an in situ hybridisation method [11].

HER2 overexpression is a consequence of the amplification of the HER2/neu gene on chromosome 17q. The activation of HER proteins depends on hetero- and homodimerization [5, 23]. When overexpressed, HER2 activation often relies on homodimerization [23]. Heterodimerization with HER3 has a strong oncogenic effect predominantly exerted through activation of intracellular signalling through the phosphatidylinositol 3-kinase (PI3K)-Akt-mTOR pathway [5]. Once activated, these phosphorylated tyrosine residues interact with intracellular signalling molecules, leading to activation of downstream signalling pathways such as the ones involved in cell proliferation, survival, differentiation, angiogenesis, invasion and metastasis [5, 23].

HER2-enriched tumours are, usually, classified as ER-/HER2+. Histologically, these tumours are characterised as high histological grade, been highly proliferative [23],

presenting usually as IDC-NST or pleiomorphic lobular and micropapillary carcinomas [11]. HER2-enriched tumours have a more aggressive clinical course and can be associated with intracranial metastases [5, 23], being the BC subtype most likely to metastasize in the brain [11].

As referred, HER2-enriched tumours benefit from anti-HER2 therapies, such as trastuzumab and pertuzumab, humanized monoclonal antibodies [5, 11]. These drugs interact with the extracellular domain of HER2, blocking downstream signalling pathways [5]. The development of trastuzumab revolutionised the treatment of HER2-enriched BCs reducing the risk of recurrence and mortality in patients compared with the same chemotherapy regimen without anti-HER2 therapy [5, 11].

2.1.3 Basal-like and triple-negative BCs

Basal-like BC and TNBC are terms frequently used as synonyms, however, not all TNBC are basal-like, and *vice versa* [13, 27, 28]. TNBC is defined as a tumour that does not express ER and PR and has no overexpression of HER2 (ER-/PR-/HER2-) [13, 27-29]. Basal-like BC is characterised by low/absence levels of expression of ER and expression of genes typically found in basal epithelial cells of the normal breast [13, 27, 30], such as CK5 and CK17 [13, 30]. Usually, cells from basal-like tumours have an absence of HER2 overexpression [13, 27, 30], however, approximately 23% of these tumours are HER2+ [27]. Even not synonyms, these two BCs subtypes frequently overlap [13, 27, 28] – 75% of TNBCs are basal-like [27]. Both TNBC and basal-like BC show considerable overlap with BRCA1-mutated tumours. BRCA1 is a tumour suppressor gene involved in DNA repair [5, 28].

Triple-negative and basal-like BCs are considered high histological grade tumours (most frequently of grade 3) [13]. Regarding the histological type, TNBCs are usually IDC-NST [13]. However, in some cases, these tumours present characteristics of some special histological types [5, 13], such as medullary [5, 27, 28], adenoid cystic [5, 28], metaplastic [27, 28] and apocrine [28] carcinomas.

TNBCs are usually larger than other subtypes of BC [5, 31] and associated with an adverse prognosis since no specific biologic therapy is available. Chemotherapy is currently the mainstay of systemic medical treatment; however, the efficiency is limited: in general, patients with TNBC have a worse outcome after chemotherapy than patients with other subtypes of BC [11, 13, 27, 28]. Poor outcomes are also associated with the fact that (1) it is frequently diagnosed in young women (<50 years) [28], (2) early relapse is common even in early-stage TNBC (first two to three years after initial diagnosis) [27,

28], (3) these tumours are most likely to visceral metastasis (in the lungs and brain), and less likely to metastasize in bone [11, 13, 28], (4) metastases tend to be more aggressive than in other BC subtypes [28], and (5) there is a shorter post-recurrence survival [13, 27].

2.2 Stromal cells

Crosstalk between epithelial and stromal cells is essential for the normal development and differentiation of the mammary gland [18]. Tumour progression and metastasis do not depend exclusively on tumour cells and their molecular phenotype. Stromal cells, especially fibroblast, play a critical role in BC dynamics [14, 32-36].

In normal tissue, fibroblasts assume an important role in the synthesis, remodelling and turnover of the ECM [34]. Activated fibroblasts, known as cancer-associated fibroblasts (CAFs), are one of the major components of breast TME and are considered a key player in cancer progression [14, 32]. Different studies indicate that CAFs may originate from a variety of sources, such as bone-marrow-derived mesenchymal stem cells, local tissue fibroblasts, and cancer cells that have undergone an epithelial to mesenchymal transition (EMT) process [14, 36]. Transforming growth factor- β (TGF- β) and stromal cell-derived factor-1 (CXCL12/SDF-1) are considered key factors in fibroblast activation, along with platelet-derived growth factor- α/β (PDGF- α/β), basic fibroblast growth factor (b-FGF) and interleukin IL-6 [34, 36]. CAFs are considered a heterogeneous population that may be characterized by (1) high expression of α -SMA, fibroblast specific protein (FSP)-1, fibroblast associated protein (FAP), platelet-derived growth factor – α/β receptors (PDGFR- α/β), and vimentin, (2) downregulation of tumour suppressor genes (caveolin (CAV)-1, phosphatase and tensin homolog (PTEN), p53 and p21), and (3) TP53 mutation [36]. Moreover, these cells present enhanced proliferation, increased migration, and the ability to promote tumour growth in co-culture experiments [33]. Alteration in their secretome include increased expression of matrix metalloproteases (MMP) – 2 [34], 9 [34, 35] and 13 [35], collagen [34], vascular endothelial growth factor (VEGF) [34, 35], hepatocyte growth factor (HGF) and TGF- β [34]. This altered secretome induces CAF-associated tumour initiation and progression, EMT, invasion, angiogenesis, and therapy resistance [14, 34, 36].

Adipocytes represent a major component in the normal breast. Over the last years, these cells have been associated with the BC dynamic [14, 34, 36]. Adipocytes are classified into two populations: white adipocytes and brown adipocytes. The firsts

are lipid storage cells and produce hormones, such as leptin and estrogen, and growth factors, such as VEGF. The seconds are known as thermogenic cells which dissipate chemical energy as heat and are characterised by densely packed mitochondria. In the TME, adipocytes can assume a pro-tumorigenic phenotype (cancer-associated adipocytes (CAAs)). The secretome of CAAs includes overexpression of inflammatory cytokines (IL-6 and TNF α) and MMPs [34, 36]. This abnormal secretion profile combined with the release of free fatty acids, results in the recruitment of immune cells to the TME, promoting a chronic inflammation environment, EMT and an invasive tumour phenotype [14].

Other cellular components of the BC microenvironment are important, namely, cancer-associated macrophages (CAMs) [14, 36]. CAMs are a mixed cell population of M1/M2 macrophages [14]. M1 is a proinflammatory macrophage phenotype characterised by the production of TNF- α , IL-1 and IL-6, being more common in the early phases of repair. M2 is the “alternatively activated” phenotype that macrophages can assume and is characterised by the production of TGF- β , VEGF and insulin-like growth factor-1. M1/M2 transition is assumed to require a phenotype switch from inflammatory to proliferative [37]. The presence of this mixed cell population promotes the expression of immunosuppressive cytokines, assisting tumour cells to escape immune surveillance [14]. In BC, CAMs correlate with poor prognostic features, higher tumour grade, high vascular grade and increased necrosis [36].

As previously referred, the establishment of hypoxic conditions in the core of solid tumours promotes angiogenesis. Hypoxic conditions induce the expression of hypoxia-inducible factor (HIF). The activation of the HIF signalling pathway upregulates the secretion of VEGF. VEGF interacts with VEGF receptors (VEGFR) on endothelial cells activating downstream signalling pathways that promote vascular permeability, angiogenesis, and neovascularization [14, 34]. Apart from hypoxia, CAFs can recruit endothelial cells by secreting high levels of CXCL12 [35, 36, 38]. Moreover, ECM degradation, particularly induced by MMP-9 secretion, enables the release of entrapped VEGF, reinforcing endothelial cells recruitment [35, 39]. Additionally, in HER2-enriched BC, HER2 overexpression induces an increase in VEGF mRNA [39]. Overall, several mechanisms recruit endothelial cells to the TME promoting the formation of a deficient vascular network. Endothelial cells in the TME have reduced coverage of pericytes and their binding is aberrant. Therefore, a disorganised, immature and highly permeable vascular network is formed, facilitating the metastatic spread of cancer cells [38].

2.3 Extracellular matrix (ECM)

The ECM has a critical role in the development and maintenance of epithelial tissues. In the human breast, the ECM is composed of (1) proteins, which provide structural support and resistance to tensile forces, and (2) glycosaminoglycans, such as hyaluronan chains, that provide resistance to compressive forces [15, 40]. In the protein components, it is possible to highlight collagen – the main protein component – and laminins and fibronectin [15, 18, 40]. These proteins can modulate the specific distribution of cell adhesion receptors [15], cytokines and growth factors [18].

When compared with a normal tissue microenvironment, the TME is characterised by alterations in the architecture and composition of the ECM and BM [19, 41]. Tumour cells enzymatically degrade and rebuild their surrounding ECM by secreting proteases, such as MMPs. ECM remodelling during tumour progression creates a spatially controlled cellular compartment (tumour capsule). In the tumour capsule, interactions between cancer cells and stromal cells are promoted, inducing tumour growth and altering cellular response to therapy [15, 18].

In breast cancer, cells directly affect the ECM mechanical properties leading to tissue stiffening [14, 18, 42]. Additionally, abnormal cell proliferation and tumour growth in a constrained physical volume lead to an increased pressure (increased solid stress) [14, 42]. Moreover, increased stiffness can be related to lysyl oxidase (LOX) secretion, which crosslinks collagen fibres [18]. Studies indicate that in BC the ECM elastic modulus ranges from 1000 to 4000 Pa, contrasting with values between 150 - 200 Pa in normal mammary gland tissue [14].

Overall, the tumour ECM becomes more stiff, dense and crosslinked, the porosity is diminished, and the protein composition is altered (with increased collagen I deposition, for example) [19, 41]. These alterations on biochemical and biophysical properties of the ECM promote tumour angiogenesis and modulate the immune system response [18].

3 Models of breast cancer

3.1 *In vivo* models

In vivo models, such as rodents (mouse and rat), have allowed a great understanding of the molecular mechanisms involved in the development and progression of BC and drug metabolism. However, there are major differences between rodents and human mammary glands [14, 40, 43, 44].

In gross analysis, the differences begin with the number of mammary glands. The mouse has five pairs of mammary glands (three thoracics and two inguinal), and the rat has six pairs (three of each thoracic and inguinal) [1, 43]. In rodents, a gradient of specification is found, being the first thoracic pair the less differentiated and the last inguinal pair the most differentiated [43]. In terms of organization, rodents present a single complex branching system with a major lactiferous duct that forms 5 to 10 secondary ducts that further branch. Humans present a system of 10 or more lactiferous ducts in the nipple that branch to form a segmentally branched ductal system with separate lobes.

Histologically, rodents and humans share similar epithelial cells [1, 43] expressing the same CK proteins [43]. However, structurally, the mouse mammary gland is formed by alveolar buds subdivided in rudimentary alveolar structures – the lobuloalveolar (LA) unit. In contrast, rats do not present a LA unit, sharing with humans the mature functional glandular unit – TDLU. Nevertheless, the epitheliums of humans and rodents are surrounded by different stroma (**Figure 5**) [1, 43]. In rodents, when comparing with humans, the stroma has large amounts of fat and lacks connective (fibrocollagenous) tissue, being this present mostly surrounding quiescent ducts [1].

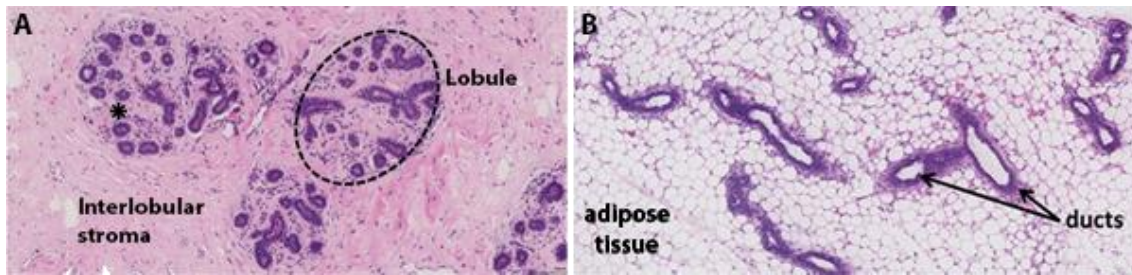


Figure 5. Haematoxylin and eosin-stained sections of A) human breast and B) mouse mammary gland. The human breast section shows epithelial lobules with a collagenous intralobular (asterisk) and interlobular stroma, contrasting with the epithelial ducts of the mouse mammary gland surrounded by a collagen sheath within an adipocyte-rich tissue. Retrieved from McNally and Stein [43].

Within *in vivo* models, patient-derived xenografts (PDX) models are one of the most used human-derived BC models and have contributed to the translation of BC research into the clinic [9]. PDX models are established with surgically obtained tumour samples of cancer patients that are implanted in immunodeficient mice [15]. Studies have shown that PDX models may accurately replicate tumour growth, diversity of tumour cells and tumour progression, including metastatic potential [45]. Therefore, these models are promising for personalised therapy [15, 45], however, some drawbacks are associated. Since these models are established in immunodeficient mice, tumour development may not be fully recapitulated and certain BC cells have low engraftment potential which might compromise the results [14, 15]. Overall, *in vivo* models are costly, laborious, and time-consuming for researchers to produce and maintain [14]. PDX models, in particular, have two other disadvantages: the low-throughput and difficulty to scale up [15].

Considering the differences both in structure and cellular microenvironment, and the drawbacks of *in vivo* models, modelling the human breast morphogenesis and cancer progression *in vitro* may allow us to further explore the molecular and cellular mechanisms that drive these phenotypic events [44].

3.2 3D *in vitro* models

To improve the understanding of cancer biology, the TME should be recapitulated as best as possible [14, 19] and the selected cells must represent the heterogeneity and complexity of BC [19].

Two-dimensional (2D) cell culture models have been an important primary tool in cancer research [46]. However, 2D microenvironments do not adequately recapitulate the complexity of the TME [46]. In 2D systems, cells grow in non-physiological conditions that induce them to adhere to the flat and rigid culture surfaces, lose polarization, and increase their exchange area to culture media. This increased exchange area introduces cells to excessive nutrition and oxygenation and deficient molecular gradients. In consequence, extracellular matrix production suffers modifications in terms of the amount, configuration, and composition of proteins. Moreover, after multiple *in vitro* passages, cells cultured in 2D are more resistant to apoptosis since they tend to immortalize [14, 47, 48].

Regarding gene expression profiles, studies indicate that there is a significant gap between gene expression *in vitro* and *in vivo*. Comparing 2D and 3D culture systems, it seems easier to mimic physiological gene expression when cells are cultured in 3D systems [49]. Moreover, 2D cancer models are not able to mimic the wide range of cellular states found in solid tumours (proliferative, senescent, and necrotic and apoptotic cells) [48]. Also, cells in 2D are normally immortalize and more prone to drug targeting than rapidly dividing cells [47, 48]. In this way, pre-clinical studies of therapeutic applications are limited in 2D cancer models and thus fail to reflect the actual response of tumours to the developed drugs [14].

In vivo, cells have important crosstalk with the ECM which is particularly important in tumour progression. The ECM can modulate not only soluble cytokines, but also signalling pathways, which are vital for cancer cell proliferation, migration, and apoptosis. In 2D platforms, the cells – ECM crosstalk is constrained, and the model may not represent the true tumour progression [48]. 3D culture systems offer advantages because they better reflect the environment cells face *in vivo* (contemplating cell – cell and cell – ECM interactions and recreating the ECM biochemical signalling and mechanotransduction) [47-49]. By opting for 3D models, it is possible to study the contribution of microenvironmental factors in cancer progression [50] and to discover new clinically relevant therapeutic approaches [49].

3.2.1 Biomaterials as ECM-like matrices

Regarding the modulation of cell – cell and cell – ECM interactions of the TME, biomaterials assume an important role [14, 41, 47-49]. In 3D models, both naturally derived and synthetic polymers can be applied, as well as basement membrane extracts (Matrigel) and decellularized ECM.

In general, naturally derived materials, such as collagen and Matrigel, intrinsically recapitulate the tissue microenvironment by promoting cell – ECM interactions [14, 15]. Matrigel is a reconstituted BM used as a *gold standard* 3D scaffold to support the formation of epithelial structures. This biomaterial is extracted from mouse sarcoma tumours and is formed by laminin, type IV collagen, entactin, heparan sulphate proteoglycans and growth factors [15, 51]. In Matrigel models, cells can aggregate and remodel the ECM, creating conditions for self-organization in polarized structures – particularly relevant as breast models [51]. However, Matrigel has complex compositions with uncertain proportions of ingredients between different batches [15, 51], which difficult the dissection of molecular mechanisms.

Collagen is a major component of the ECM in mammals and is widely used to construct biologically relevant 3D models [14, 15]. Collagen hydrogels can be produced in a controlled way to ensure specific stiffness and pore sizes to study the effects of these properties on tumour progression, migration and invasion [14]. Carter, Gopsill [46] highlighted the capacity of collagen hydrogels to promote native cell organization in a 3D model established with primary MEPs and LEPs isolated from mammaplasty specimens.

One major concern with natural biomaterials is the fact that it is not possible to predict the impact of one single biophysical factor since alterations in one parameter affects other matrix properties. As referred, stiffness and porosity are important parameters for tumour progression. Stiffness can be modulated by alterations in the material concentration or in the crosslinking density. Increased stiffness is correlated with alterations in adhesive properties of the matrix, pore size, and 3D architecture. Therefore, it is not possible to study stiffness as an independent parameter. Regarding porosity, collagen matrices, are frequently used to study their influence on cancer cell migration. Comparing with synthetic biomaterials, the fact that collagen is an MMP sensitive biomaterial represents a drawback in these studies since cells can dynamically modulate the matrix porosity [14, 51, 52]. Besides the lack of mechanical properties control, natural biomaterials present batch-to-batch variations that reduces consistency and reproducibility [14, 51].

Synthetic biomaterials represent an improvement of natural biomaterials regarding the two above-mentioned drawbacks. With synthetic biomaterials (polyethylene glycol (PEG), polylactic acid (PLA), polycaprolactone (PCL), and polyurethane (PU)) it is possible to produce matrices of controlled stiffness, degradation rate, and structure. However, these matrices lack cell-interactive domains – crucial to models the TME – and cannot be degraded by cells [14, 44, 52]. Therefore, these matrices need to be chemically modified to ensure cell – ECM interactions [14, 35, 52] by grafting cell adhesion ligands and biodegradable crosslinkers [32, 52]. Moreover, the 3D architecture of synthetic matrices often does not mimic the filamentous nature of natural ECMs which controls the spatial organization of cells [15]. Comparing both natural and synthetic polymers, the first have improved biocompatibility and lower toxicity, while the synthetic polymers have higher versatility, reproducibility, and enhanced workability.

3.2.1.1 Alginate

One example is alginate that has been explored in our group for the development of 3D models of breast cancer. Alginate is a naturally occurring anionic polymer derived from brown seaweed (*Phacophyceae*). Structurally, alginate is a linear polysaccharide composed of sequences of (1,4)-linked β -D-mannuronate (M) and α -L-guluronate (G) residues (**Figure 6 A**) [53-55]. After crosslinking, alginate forms hydrogels that have been previously described as scaffolds to culture mammalian breast cells *in vitro* [56-60].

Usually, alginate hydrogels are formed by ionic crosslinking G-blocks by certain divalent cations, such as Ca^{2+} , Ba^{2+} and Sr^{2+} (**Figure 6 B**) [54, 55]. These hydrogels have high biocompatibility, low toxicity [54, 55], and form scaffolds with an ECM-like structure [55]. Moreover, alginate hydrogels have high pore interconnectivity that allows easy diffusion of nutrients and growth factors while cells are embedded in the polymer network [54].

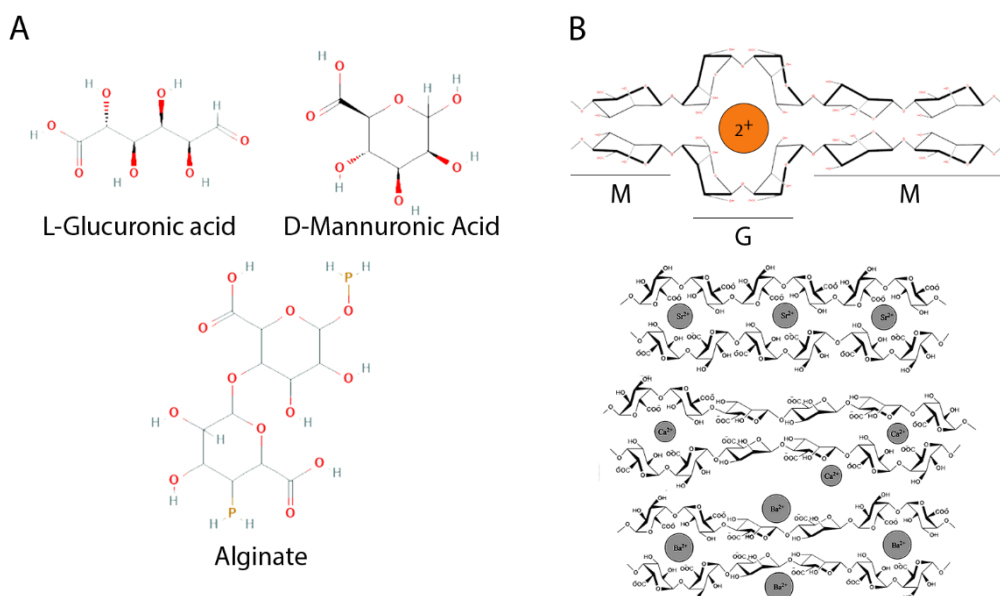


Figure 6. Alginate chemical structure and gelation process. (A) 2D chemical structure of alginate and its components (L-guluronic acid – G residues – and D-mannuronic acid – M residues). Images retrieved from PubChem website (components IDs: CID 21145305, CID 439630, and CID 131704328). (B) The “egg-box” model for the gelation process of alginate with ionic crosslinking between alginate residues by divalent cations. Different divalent cations crosslink in specific conformations: Sr²⁺ binds to G-G blocks solely, Ca²⁺ binds to G-G and M-G blocks, and Ba²⁺ binds to G-G and M-M blocks. Images retrieved from Paredes Juarez, Spasojevic [61].

Alginate is an easily tuneable biomaterial. The hydrogel mechanical properties can be modulated by adjusting parameters such as (1) M/G ratio, (2) sequence and length of different G-blocks, (3) alginate concentration and molecular weight and (4) crosslinking density [54, 55]. Moreover, alginate lacks cell responsive properties and needs to be chemically modified to introduce adhesion sites for mammalian cells [15, 54, 55]. The RGD (arginyl-glycyl-aspartic acid) sequence is one of the most used bioactive peptides. Overall, these hydrogels represent a good equilibrium between protein-based and synthetic materials.

In the context of BC research, both human and murine cell lines have been studied in alginate matrices. Cavo, Fato [60] described the 3D cellular behaviour of MCF-7 cell line (human cell line, ER-positive/PR-positive) embedded in alginate hydrogels of different stiffnesses (150 – 200 kPa, 300 – 350 kPa and 900 – 1800 kPa). When cultured in softer hydrogels (150 – 200 kPa), cells presented a round shape morphology and increased viability. Moreover, cells presented increased proliferation forming cell clusters of higher dimensions in comparison with cells embedded in stiffer hydrogels. Comparing to cellular behaviour in 2D, cells in the 3D alginate matrices presented a multicellular, cluster-like, conformation that better resembled the *in vivo* solid tumour organisation. In

the work of Bidarra, Oliveira [57] and co-workers, EpH4 cell line (of murine origin) shown a similar behaviour in 3D, with cells forming larger multicellular spheroids and presenting higher cell viability when cultured in softer alginate hydrogels (200 Pa). Moreover, the authors studied the induction of an EMT-phenotype *in vitro*. As reported, TGF β 1 can induce a mesenchymal phenotype (decreased expression of E-cadherin and increased fibronectin and vimentin expression) in epithelial EpH4 cells, after 7 days in culture. Removal of TGF β 1 from the culture medium led to the acquisition of a partial epithelial-like phenotype, in which E-cadherin expression at cell membrane was recovered, while expression of fibronectin and vimentin was still present. Together, the presented results highlight the importance of ECM biochemical and mechanical properties in cell behaviour and BC progression.

3.2.2 Scaffold-free

Apart from 3D models based on decellularized matrices and polymeric scaffolds (namely, hydrogels), spheroids are emerging as gold standards in *in vitro* cancer research [62, 63].

Spheroids are cell aggregates that may grow in suspension or embedded in 3D matrices [4, 62, 63]. Multiple factors contribute to the success of these models, namely the workability (simple workflow combined with high-throughput capabilities), and the possibility to incorporate different elements of the TME (biological gradients, ECM cues and cellular heterogeneity) [63].

Multicellular tumour spheroids (MCTS) are one of the most well characterised *in vitro* models for cancer research [4]. These models offer advantages since they recapitulate the 3D architecture (particularly, cell – cell interactions) [14, 62] and transport properties [62] of the TME. MCTS are used as platforms to study tumour biology (growth and proliferation, invasion, angiogenesis and immune interaction) and for drug screening [62]. In a size-dependent behaviour, MCTS may recapitulate oxygen and nutrient gradients, proliferation gradients and the formation of necrotic core observed in tumours *in vivo* (**Figure 7**) [4, 14, 62, 63]. Overall, protein and gene expression profiles [4, 14, 62], as well as morphology and heterogeneity [4, 14], of cells cultured in MCTS are more physiologically relevant than the profile of those cultured in 2D.

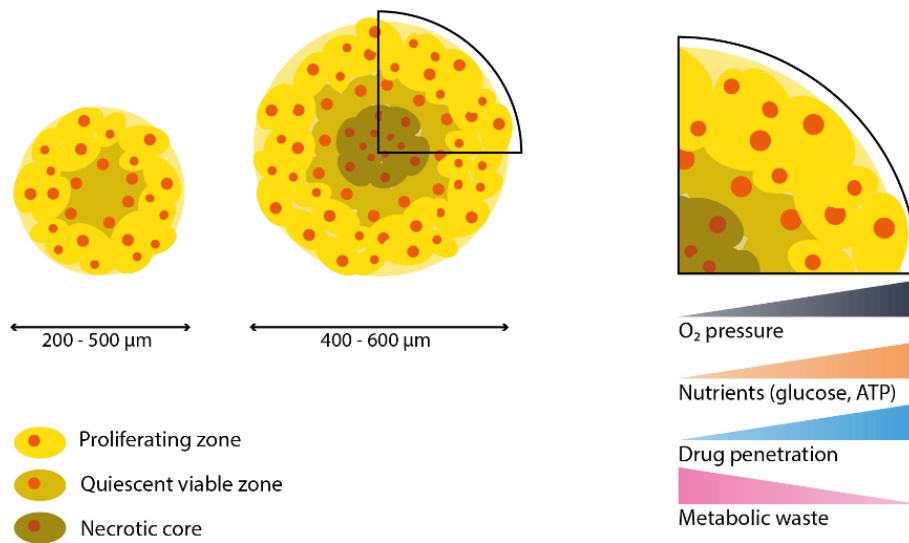


Figure 7. Formation of physiological gradients in tumour spheroids. Spheroids have a layered cellular organisation with an outer proliferating and an inner quiescent zone. Moreover, a potential necrotic core may be formed in the centre of MCTS with a diameter over 400 µm. These zones are the result of the 3D physiological geometry that stimulate the establishment of gradients of oxygen, nutrients, and metabolites over time, better resembling the microenvironment of solid tumours in which distance from blood vessels gives rise to these gradients. Moreover, drug penetration gradients may be established reinforcing the utility of MCTS in pre-clinical studies. Based on Lv, Hu [53].

MCTS can be produced using different techniques (**Figure 8**) with underlying advantages and disadvantages (**Table 2**). In terms of cell sources, MCTS may be generated from cell lines, patient cells, or xenograft material [4, 63].

Spheroid size and cellular heterogeneity are critical parameters in biochemical assays and high-throughput screenings. Therefore, techniques that allow the generations of spheroids of uniform size and complexity must be preferred to increase the robustness of an assay [4, 63]. As previously referred, spheroid diameter is critical for the formation of oxygen and nutrient gradients [4, 14, 62, 63], implying that this parameter must be taken into consideration to understand if spheroids formed by a specific technique are valid to study a pathophysiological condition, such as hypoxia [4].

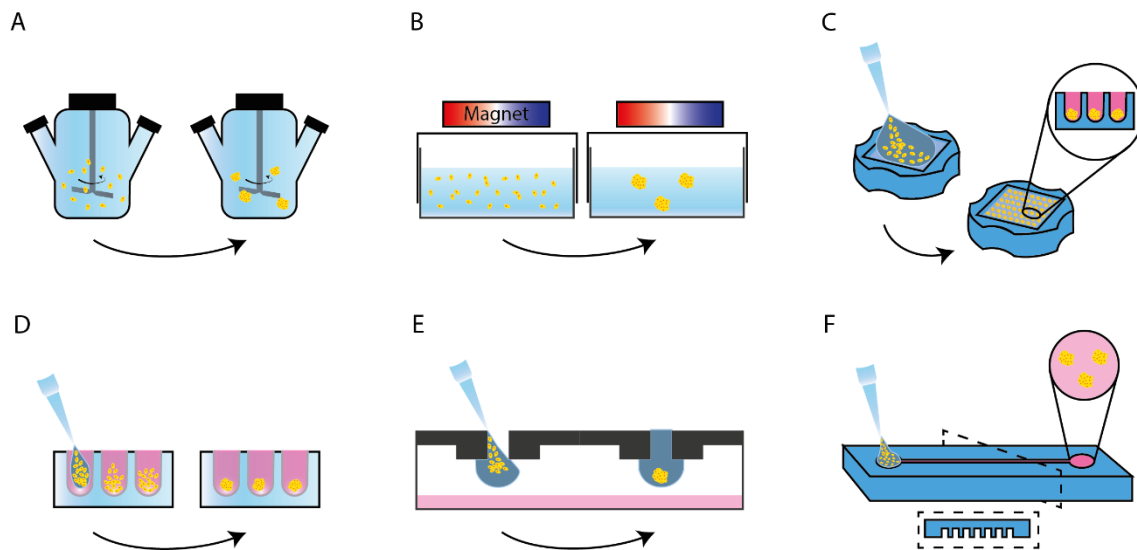


Figure 8. Spheroid production methods. A) Spinner-flasks. Spheroids are produced in a bioreactor system that ensures continuous stirring allowing cells in suspension to aggregate. B) Magnetic levitation. Cells are incubated with magnetic nanoparticles (e.g., SPIONS) and seeded in low attachment plates. Under magnetisation, induced by a magnet on top of the culture plate, cells levitate off the bottom and self-aggregate into spheroids. C) Micropatterned moulds. Cells are seeded on moulds with microwells of a uniform size where self-aggregation into spheroids occurs. D) Ultra-low attachment plates. Cells are seeded on wells coated with non-adherent inert substrates (e.g., polystyrene) allowing cell aggregation. E) Hanging drop method. The cell suspension is dropped onto a culture plate where the micro-liquid adhesion with the substrate surface is greater than its own weight. Cells self-aggregation into spheroids at the liquid-air interface of the medium drop. F) Microfluidic devices. Spheroid formation occurs in micrometre-sized channels of the microfluidic device. Based on Nath and Devi [4], Lv, Hu [53].

Table 2. Spheroid generation: advantages and disadvantages of different techniques [4, 53].

	Technique	Advantage	Disadvantage
Cell suspension culture	Spinner-flasks	<ul style="list-style-type: none"> - Simple procedure. - Large-scale production. - Uniform distribution of nutrients and oxygen throughout the medium. 	<ul style="list-style-type: none"> - Fluid shear force caused by agitation may affect cellular physiology and cause cell damage.
	Magnetic levitation	<ul style="list-style-type: none"> - Simple procedure. - Can be multiplexed with bioimaging techniques. 	<ul style="list-style-type: none"> - Limited production of spheroids. - Magnetic nanoparticles need to be pre-loaded into cells – an expensive procedure that might induce cytotoxicity.
	Non-adherent surfaces (e.g.: Micropatterned moulds)	<ul style="list-style-type: none"> - Simple and efficient procedure. - Large-scale production. - Uniform dimensions. - Allow post culture recovery. 	<ul style="list-style-type: none"> - Long-term culture is difficult. - Formation of multiple spheroids in a well reduces the assay reproducibility.
	Ultra-low attachment plates	<ul style="list-style-type: none"> - Simple procedure. - Large-scale production. - Allow post culture recovery 	<ul style="list-style-type: none"> - Formation of heterogeneous spheroids.
	Hanging drop	<ul style="list-style-type: none"> - Uniform spheroids with controlled size. - Allow coculture with defined cell types. 	<ul style="list-style-type: none"> - Long-term culture is difficult. - Low number of cells per spheroid. - Low efficiency.
	Microfluidic devices	<ul style="list-style-type: none"> - Faster spheroid formation. - Spheroids of controlled size and growth parameters. - Continuous perfusion. - Allows the formation, maintenance, and testing of spheroids within a single device. 	<ul style="list-style-type: none"> - Difficulty in collecting cells for analysis. - Increased risk of necrosis due to confinement.

Different research groups have applied spheroids to BC research. Pal, Ashworth [64] described the formation of monoculture and co-culture spheroids, with ultra-low attachment plates, from MCF7 and MDA-MB-231 alone or with bone marrow-derived mesenchymal stem cells. The authors report that in co-culture spheroids, BC cells have enhanced proliferation and invasion capacities, particularly with MCF7 cells (ER-positive/PR-positive). Results confirmed with spheroids of PDX derived cells (BR15 and BR8). Moreover, co-culture promoted a partial EMT phenotype in BC cell lines (downregulation of E-cadherin and upregulation of SNAIL, EMT markers). The work developed by Mokhtari, Qorri [65] describes the acquisition of a stemness phenotype in spheroids produced with non-adherent surfaces from MCF7, ZR-75-1, and MDA-MB-231 cell lines. Cancer stem cells (CSCs) are a heterogeneous population with clinical significance since they modulate patients' responses to treatment. These spheroids possess enhanced proliferation, self-renewal, and differentiation potentials under stem cell factor-enriched medium. Moreover, when co-cultured with human fetal lung fibroblasts (representing the stromal compartment), spheroids presented enhanced efficiency in establishing orthotopic xenografts exhibiting a CSC phenotype (high riboflavin uptake and expression of CD44, CD47, CD24, CD131, and HIF2- α) in the athymic nude rat model of human BC. More, the multicellular stem-like spheroids presented increased chemoresistance comparing with their 2D counterparts. These works allowed the study of luminal (MCF7 and ZR-75-1) and TN (MDA-MB-231) breast cancers *in vitro* and prove the importance of the stromal compartment and cellular heterogeneity (CSC) in BC progression.

Halfter, Hoffmann [66] reported the establishment of tumour-derived MCTS from HER2-enriched breast cancer samples. Halfter and co-workers compared the effect of cytostatic drugs *in vitro* on the tumour-derived MCTS with their effect on spheroids produced with HER2-negative breast cancer cell lines (MCF7, T-47D, HCC1143 and HCC1937) and shown that patient-derived MCTS better reflect clinical findings with HER2-negative patients than cell line spheroids. Hofmann, Cohen-Harazi [67] described MCTS derived from different primary BC samples with distinct molecular signatures. Independently from BC origin, MCTS were successfully formed, particularly when fibroblasts were present in high ratios (1:3 tumour cells for fibroblasts). Epithelial cells within the MCTS retained their original molecular signature and responded differentially to chemotherapeutic drugs. Together, the reported results highlight (1) that MCTS better reflect the heterogeneity of the TME which impacts drug resistance, and (2) the relevance of patient-derived models in preclinical studies.

3.3. Cells for breast cancer research

3D models may be established from immortalised or primary cells, from human or murine origin. Regarding mammary gland development and BC, 3D models of immortalised human mammary epithelial cells have allowed the dissection of human-specific cell biology [3]. Cell line models have been extremely useful as *in vitro* models to study the basis behind the biology of breast cancer [9, 16, 19, 68]. According to Burdall, Hanby [68], a *bona fide* cell line is characterized by “altered cytomorphology, increased growth, reduced serum dependency, increased clonogenicity, a tendency toward anchorage-independent growth, changes in ploidy, tumourigenicity in nude mice and an infinite lifespan”. However, these common models do not reflect the multiple cell types found *in vivo* and suffer from molecular changes associated with long-term culture and immortalization [3, 19, 68].

Established cell lines (**Table 3**) are a rich source of easily replaceable, homogeneous, and easily propagated material, providing an excellent tool for molecular and cellular characterisation of BC. However, these models do not fully capture the BC spectrum, since they are usually derived from advanced-stage tumours (isolated from metastatic lesions, especially aspirates and pleural effusions, and rarely from primary tumours) [9, 16, 68]. Moreover, as described, the TME is a niche of a heterogeneous population and, therefore, the use of metastatic homogeneous cells brings into question the relationship between these and the primary tumour cells [16, 19], especially when cell lines are used as valid models to evaluate the pathobiology of BC and the likely response to novel therapies [19, 68].

Because most cell lines are from more aggressive and often metastatic tumours, it may be more clinically relevant to use cells derived from primary tumours [68]. Tissue banks provide researchers access to normal and tumour-derived patient cells [3, 46]. Primary cells and, particularly, human-derived organoids, retain *in vivo*-like cellular heterogeneity [3, 46] and BC subtypes [9], and are prone to form physiologically relevant structures, increasing knowledge about early stages of BC [3, 9, 16]. Moreover, usually, detailed pathology is available to allow the cellular characterisation and comparison with the original tumour [68, 69].

Scientists often experience several challenges when trying to establish cultures of BC epithelial cells. Primary cell cultures may be established from tissue explants (mixed cell populations) or as enriched populations of a defined cell type [68, 70]. Tissue explants are associated with limited success since stroma cells (namely, fibroblasts) have an outgrowth comparing with the epithelial cells, dominating the culture [68]. On

the other hand, the isolation of enriched populations is a time-consuming process that is difficult to reproduce [70].

Primary cells have a slow doubling time and can only be maintained in culture for a finite length of time. Therefore, experimental techniques that require high cell density may be difficult to realise in the first passages [68, 70, 71]. Lastly, cell – cell and cell – ECM interactions are crucial to ensure to maintain the tumours-phenotype *in vitro* and, therefore, primary cells may behave differently during culture as compared with *in vivo* conditions. Once again, 3D culture systems offer advantages for primary tumour culture since *in vivo*-like cellular interactions may be recreated under controlled conditions [68].

Considering that early stages of BC are under-represented by the current *in vitro* and *in vivo* models [16], the development of patient-derived primary cell models is important. Future improvements in primary cell organoids and high-throughput drug screening technologies may allow the development of personalised therapies that better corroborate patient responses [9].

Table 3. Commonly used BC cell lines.

Represented BC subtype	Cell line	Origin	Ref.
Luminal A	T-47D	Pleural effusion	[72, 73]
	MFC-7	Pleural effusion	[68, 72, 73]
Luminal B	BT-474	Breast	[73]
	ZR-75 (27 and 30)	Ascites	[73, 74]
HER2-enriched	HCC-1954	Breast	[72]
	MDA-MB-453	Pleural effusion	[68, 74]
TNBC	BT-549	Lymph node metastasis	[72]
	MDA-MB-231	Pleural effusion	[68, 72]
	BT-20	Breast	[68, 73]
	MDA-MB-468	Pleural effusion	[68, 73, 74]

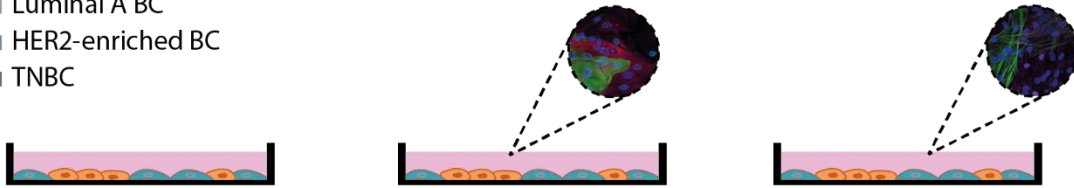
4 Motivation

There is a growing recognition of the importance of the tumour microenvironment (TME), especially cells within the stroma, in determining biological characteristics of cancer cells such as proliferation, invasion and drug resistance. 3D spheroid models represent a simple strategy, comparing to *in vivo* models, to mimic human BC. 3D spheroids potentially provide a useful system for modelling heterotypic interactions and are increasingly being used for drug screening and drug penetration studies. In spheroids, cells grow in aggregates that result in cell – cell interactions and, under some conditions, the nutrition and oxygen gradients observed in real tissue. Although we can find in the literature several papers using multicellular-based spheroids for breast cancer research, the majority are limited to cell lines, which are unable to replicate the heterogeneity found in patient tumours. Physiological relevant 3D co-culture models established from primary human cells may significantly improve the biological relevance of *in vitro* models and, consequently, the development of new therapeutic strategies. In this context and to address the challenge of culturing for the first time primary BC cells in our lab, the key goals of this thesis were to (**Figure 9**):

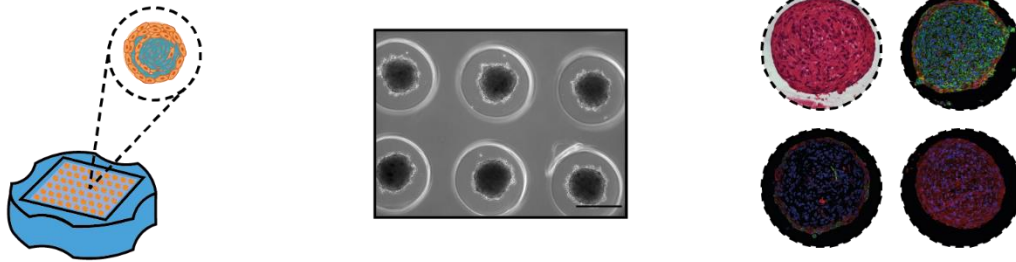
- 1) establish a primary 2D breast cancer cell culture of three different BC: luminal A, Her2-enriched and TNBC.
- 2) culture the different primary breast cancer cells in 3D using micropatterned moulds to form multicellular spheroids.
- 3) develop breast cancer organoids (tumoroids) in a well-defined hydrogel matrix.

1. 2D culture and characterisation

- Luminal A BC
- HER2-enriched BC
- TNBC



2. MCTS characterisation



3. Breast tumoroid in a well-defined hydrogel matrix

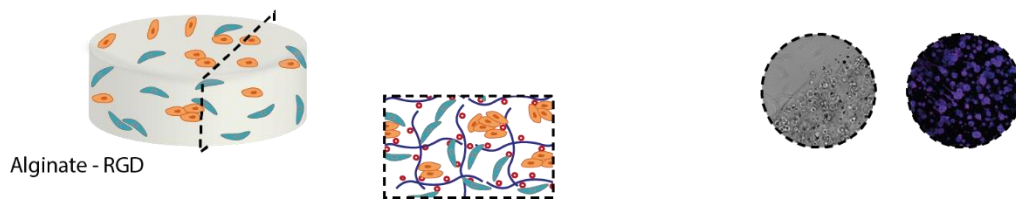


Figure 9. Graphical abstract. Schematic representation of the proposed strategy to establish 3D *in vitro* co-culture models of primary breast tumour cells. Abbreviations: 2D, two-dimensional; BC, breast cancer; TN, triple-negative; 3D, three-dimensional; MCTS, Multicellular tumour spheroids; RGD, arginyl-glycyl-aspartic acid peptide.

5 Materials and methods

5.1 Cell maintenance

Tumour specimens of primary breast tumours from three different donors were obtained from the Breast Cancer Now Tissue Bank. Each donor was diagnosed with a different subtype of breast cancer: luminal A, HER2-enriched and TNBC. Cells were cultured in collagen type I coated flasks in epithelial medium prepared by supplementing Dulbecco's Modified Eagle's Medium/Nutrient Mixture F-12 Ham (DMEM-F12, Sigma-Aldrich) with 10% of fetal bovine serum (FBS), 1% of fungizone, 1% of penicillin/streptomycin, 0.5 µg/mL of hydrocortisone (Sigma-Aldrich), 0.5 µg/mL of apo-transferrin (Sigma-Aldrich), 10 ng/mL of human epidermal growth factor (EGF) (Sigma-Aldrich) and 5 µg/mL of human insulin (Sigma-Aldrich). Collagen coating was prepared by diluting collagens type I in 0.02M acetic acid in PBS to reach a final concentration of 10 µg/cm². Cells were maintained in a 5% v/v CO₂ incubator at 37 °C and media was changed every two days. All experiments were performed with cells at passage 10 or lower.

5.2 2D culture of primary tumour cells

Cells were trypsinised, centrifugated (5 min, 1100 rpm) and the supernatant was removed.

For 2D characterisation of the populations present in the BC, cells were resuspended in culture medium and seeded at 2x10⁴ cells/cm² on collagen type I coated TCPS coverslips (13 mm diameter) placed in 24-well plates. Cells were cultured for 6 days.

To assess the metabolic activity of tumour cells in 2D culture, cells were seeded at 1 x 10⁴ cells/cm² in 48-well plates and maintained in a 5% v/v CO₂ incubator at 37 °C for 21 days. Culture media was replaced every two days.

5.3 Multicellular tumour spheroids of primary tumour cells

Multicellular tumour spheroids (MCTS) were produced in agarose moulds. Agarose moulds were prepared according to manufacturer specifications (Microtissues Inc., USA). Briefly, molten 2% w/v agarose in 0.9% w/v NaCl was filtered through a 0.22 μm filter, and 550 μL were poured into a positive silicon template (*MicroTissues® 3D Petri Dish® Micro-molds*, **Figure 11 A and B**). Each template contained 81 U-bottom microwells of 800 μm in diameter and 800 μm in depth. After casting, agarose moulds were carefully detached from the template (**Figure 11 C**), transferred to a 12- well plate and equilibrated in culture medium overnight.

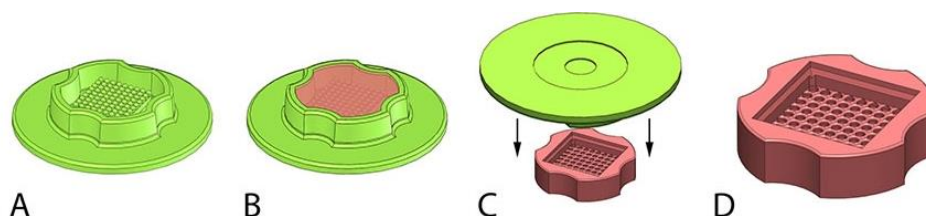


Figure 10. Schematic representation of the production of agarose moulds. (A) Commercially available precision mould. (B) Mould filled with molten agarose. (C) Detachment of agarose mould. (D) Final microwell array of gelled agarose. Flow chart retrieved from Microtissues, Inc. website.

Cells were trypsinised and 10000 cells/spheroid (81×10^4 cells/mould) were resuspended in culture medium (200 μL). Cell's suspension was pipetted to each mould. Cells were allowed to settle for 30 minutes at room temperature to allow spheroids formation. Then, 2 mL of medium was added to the wells and cells were incubated at 37 $^{\circ}\text{C}$ under a 5% v/v CO_2 humidified atmosphere. The medium was changed every other day, and spheroids were collected for analysis on days 1, 3, and 7. Brightfield images were taken on days 1 and 7 using the Inverted Fluorescence Microscope Axiovert 200M (Zeiss).

5.4 Breast cancer organoid within alginate-RGD matrices

In situ forming alginate hydrogel matrices were prepared by internal gelation, using calcium as an ionic crosslinker, as previously described [57]. For that, RGD-alginate precursor solutions were sterile-filtered (0.22 μm) with a sterile suspension of CaCO_3 in 0.9% wt.% NaCl at a $\text{Ca}^{2+}/\text{COO}^-$ molar ratio of 0.288, and the gelling process was triggered through the addition of a filtered (0.22 μm) fresh GDL in 0.9% wt.% NaCl

at a CaCO_3/GDL molar ratio of 0.125. A final RGD-modified alginate concentration of 1 wt.% with 200 μM of RGD is obtained by adding the previous solution to the cell suspension (5×10^6 cells/mL). Cells were trypsinised and, centrifugated (1100 rpm, 5 min) and, after removing the supernatant, cells were resuspended in 0.9% wt.% NaCl.

Finally, the cell suspension was homogeneously mixed with the RGD-alginate solution and crosslinking agents. The 3D matrices were obtained by quickly applying 14 μL drops of the mixture between Teflon plates separated by 500 μm -thickness spacers (**Figure 10**). Then the Teflon plates with the 3D matrices were kept in a petri dish, at 37°C in a 5% v/v CO_2 incubator and removed 20 minutes counting after adding GDL. The 3D matrices were transferred to a 24-well plate and incubated with culture medium at 37°C. After 30 minutes the medium was replaced and subsequently changed every two days.

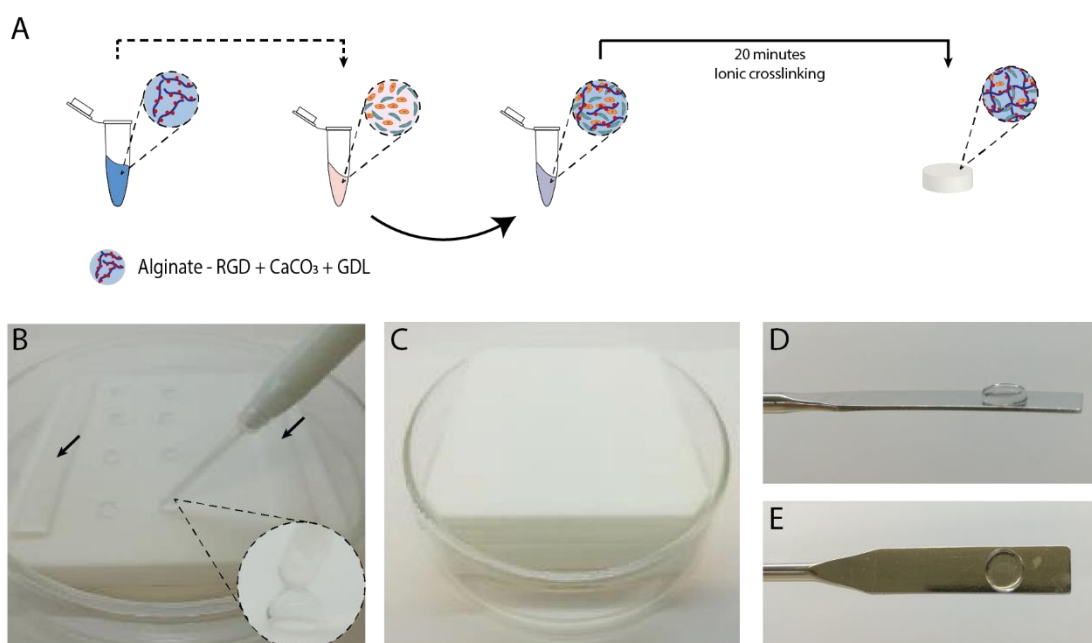


Figure 11. Experimental procedure for the preparation of the 3D cell-laden matrices. (A) Schematic description of the experimental procedure. (B) Small drops of cell-laden alginate are applied on the top of a Teflon plate between two spacers (black arrows) and (C) covered with another Teflon plate on top of those spacers. (D, E) After gelation, 3D matrices are obtained.

5.5 Metabolic activity assay

Metabolic activity quantification of cells cultured in 2D and cells embedded within alginate matrices was assessed through the resazurin-based assay. In brief, cells were incubated with 500 μL of 20% v/v of resazurin solution in complete culture medium for 2h at 37°C protected from light. Fluorescence from the supernatant (200 μL), arising from

resazurin reduction to the fluorescent compound resorufin, was measured at 530 nm excitation and 590 nm emission using the fluorescence microplate reader Synergy Mx™ (BioTek, Winooski, VT). The metabolic activity assays were performed at culture days 1, 7, 14 and 21.

5.6 MCTS morphological analysis

Images of all spheroids were taken at days 1 and 7 to determine spheroids diameter, roundness and circularity using an Axiovert 200M (Zeiss) microscope in brightfield with a 5x objective.

A macro was written in Fiji-ImageJ to automate the characterisation process based on Ivanov, Parker [75]. Briefly, this macro uses the Zeiss Vision Image (ZVI) format files (containing image captured and the metadata of camera and microscope settings) to avoid the necessity of using a calibration slide to determine the scale of images.

Each image is treated to clean any artefacts and converted to an 8-bit format to which a threshold is applied. Before analysing the spheroids with the *analyze particles* function of Fiji-ImageJ, particles are individualised using the *watershed* binary option. To filter the results, small particles with an area under 1000 μm^2 and the ones on the edges of the image (incomplete spheroids) are excluded. The macro saves a file with the area and shape descriptors (roundness and solidity indexes, equations (1) and (2), respectively) of each analysed spheroid and the result of the treatment applied to the images.

$$(1) \text{ Roundness} = 4 \times \frac{\text{Area}}{\pi \times \text{Major Axis}^2}$$

$$(2) \text{ Solidity} = \frac{\text{Area}}{\text{Convex Area}}$$

Data from the macro was treated in Microsoft Excel. Spheroid's diameter was calculated from the area with equation (3). Data analyse was performed in GraphPad Prism 8.

$$(3) \text{ Diameter} = 2 \times \frac{\sqrt{\text{Area}}}{\pi}$$

Solidity is an indicator of MCTS density and is a measure of spheroids regularity. Roundness is maximum for perfect circles (i.e., with constant radius). In both cases, the values range from 1 to 0.

5.7 Sprouting assay

To determine cells invasion capacity, spheroids with 24 hours were incorporated within fibrin gel. Spheroids were aspirated from the moulds using a 100uL pipette. A first layer of fibrin was formed on the bottom of μ -slides 4-well (Ibidi), 3 to 4 spheroids were placed on top of the polymerised layer, and a second layer of fibrin was laden over the spheroids (**Figure 12**). After incubation for 25 minutes at 37°C, 5% CO₂, complete medium was added to each well and replaced every other day.

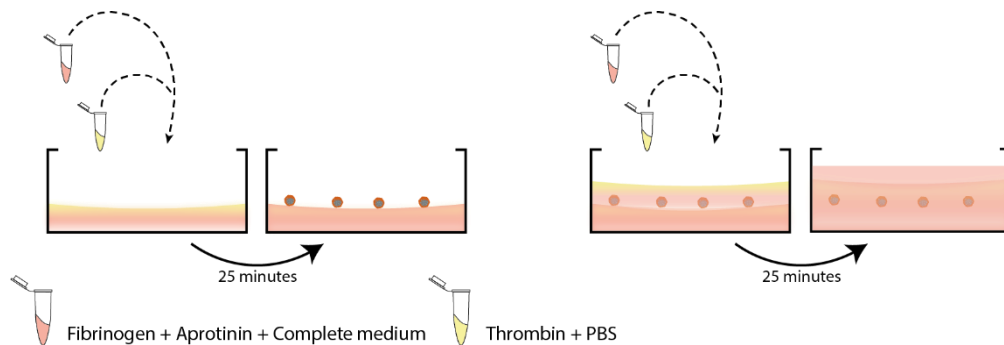


Figure 12. Schematic representation of the experimental design of the sprouting assay.

Fibrin gel was formed with a volume of 55.7 μ L of complete medium added to 166.7 μ L of fibrinogen (4mg/mL in 0.9% NaCl, Sigma) and 22.3 μ L of aprotinin (500 μ g/mL in PBS, Sigma). This solution was mixed with 15.2 μ L of thrombin (25 U/mL in PBS, Sigma) and 166.7 μ L of 1x PBS and incubated at 37°C for 25 minutes to allow for gel formation.

5.8 Immunofluorescence

5.8.1 2D cultures

Cells in 2D (collagen-coated TCPS coverslips) and were washed twice in PBS, fixed in 4 wt.% PFA in PBS for 20 minutes at room temperature and washed twice again. The samples were kept in PBS at 4 °C. Cells cultured in 2D were fixed at day 3.

Cells cultured on coverslips were stained for CK8 (catalogue number C5301, Sigma, 1:200) and CK14 (catalogue number Ab51054, Abcam, 1:100) by permeabilising with 0.2% Triton™ X-100 in PBS and blocking with 1% BSA in PBS/0.05% Tween 20. For stainings for E-cadherin (catalogue number 3195, Cell Signalling, 1:100), cells were permeabilised with Na₄Cl (50 mM) and blocked with 1% BSA in PBS/0.3% Triton™ X-100. Stainings for vimentin (catalogue number Sc-6260, Santa Cruz, 1:50), EGFR (catalogue number D38B1, Cell Signalling, 1:50), CD90 (catalogue number AF2067, R&D Systems, 7.5:100), CD44 (catalogue number 156-3C11, Cell Signalling, 1:200), α-SMA (catalogue number Ab5694, Abcam 1:50; and A5288, Sigma, 1:400) and Ki-67 (catalogue number Ab15580, Abcam, 1:100) were performed without the pre-permeabilization step and blocked with 5% FBS/0.3% Triton™ X-100 in PBS. Samples were incubated with the primary antibodies and with Flash phalloidin 647 (Invitrogen, 1:1000) diluted in antibody dilution buffer (1% BSA in PBS) overnight. Subsequently, samples were incubated in a species-appropriate fluorescent secondary antibody and with 1µg/mL DAPI for 1 hour before the addition of *Vectashield*.

5.8.2 Paraffin-embedded samples

MCTS were fixed at days 1, 3 and 7, directly in agarose moulds, with 2% w/v PFA (30 min, RT). Each mould was sealed with 200 µL of molten HistoGel™ (ThermoFisher) and processed in an automatic rotational tissue processor (Microtom STP-120-1). Samples were then paraffin-embedded in an EC-350 embedding centre and sectioned into 3 µm sections for Hematoxylin/Eosin (H&E) staining and 12 µm sections for immunohistochemistry. Sections were then deparaffinized in xylene and rehydrated in sequentially decreasing ethanol (96%, 70% and 50%). Antigen retrieval was performed by boiling the section in citrate buffer (10 mM, pH = 6) for 30 minutes. The MCTS were permeabilized with 0.25% Triton-x100 in PBS and blocked with 1.5% BSA/5% FBS in PBS. Samples were incubated with the primary antibodies diluted in blocking solution overnight and subsequently in a species-appropriate fluorescent secondary antibody and 1µg/mL DAPI for 1 hour before being mounted with *Vectashield*. Primary antibodies used were CK8 (catalogue number

C5301, Sigma, 1:200), CK14 (catalogue number Ab51054, Abcam, 1:100), E-cadherin (catalogue number 3195, Cell Signalling, 1:100), vimentin (catalogue number Sc-6260, Santa Cruz, 1:50), fibronectin (catalogue number F3648, Sigma, 1:200), collagen I (catalogue number 600-401-103-0.1, Rockland, 1:100) and Ki-67 (catalogue number Ab15580, Abcam, 1:100).

5.8.3 Whole-mounted samples (fibrin)

Fibrin-embedded spheroids were fixed directly in the μ -slide at days 2 and 7 using 2% w/v PFA (30 min, RT). Samples were permeabilized in 0.25% v/v Triton X-100 (Fisher Scientific) in PBS for 20 min, washed twice with 0.05% v/v Tween-20 (Fisher Scientific) in PBS for 10 minutes, blocked with 5% w/v BSA for 1h at RT and incubated overnight (ON) with Phalloidin 647 (Invitrogen, 1:1000) and the following primary antibodies diluted in 1.5% w/v BSA: vimentin (catalogue number Sc-6260, Santa Cruz, 1:50), fibronectin (catalogue number F3648, Sigma, 1:100).

5.8.4 3D culture within alginate matrices

3D matrices were washed twice with HBSS (1x), fixed with 4% v/v PFA in HBSS (20 min at RT) and washed again with HBSS (1x). Then, 3D matrices were permeabilized with 0.2% v/v Triton X-100 for 10 min and blocked for 1h with wt.% BSA solution in HBSS. After that, 3D matrices were incubated ON at 4°C with Phalloidin 647 (Invitrogen).

5.9 Statistical analysis

Statistical analyses were performed using GraphPad Prism 8.0 software version 8.0.1. To compare the organoids diameter (3D culture within alginate matrices), Kruskal-Wallis test was used. Results for all analysis with 'p' value less than 0.05 were considered as statistically significant differences.

6 Results and discussion

6.1 Establishment of primary tumour cells culture

As previously mentioned, BCs are normally categorised based on cells immunohistochemical profile - the expression status of hormone receptors (estrogen receptor – ER – and progesterone receptor – PR) and human epidermal growth factor receptor 2 (HER2) are considered. Based on this categorisation, invasive breast adenocarcinomas are commonly classified into four major molecular subtypes. In this work the following breast cancer were considered: ER+/HER-, ER-/HER+, and ER-/HER- (**Table 4**). These three dissociated tumour (DT) specimens were obtained from women undergoing mastectomy for primary breast cancer and specimens were identified at the time of diagnosis.

Table 4. Classification of primary breast tumours at the time of diagnosis.

Patient ID	Immunohistochemical profile	Breast cancer subtype	Adopted nomenclature
1902	ER+/HER-	Invasive ductal carcinoma Luminal A	LA-DT
1704	ER-/HER+	Invasive ductal carcinoma HER2-enriched	HER-DT
1997	ER-/HER-	Invasive ductal carcinoma Triple-Negative	TN-DT

As illustrated in **Figure 13** dissociated tumour specimens formed heterogeneous 2D cultures and these cultures were successfully maintained for at least 10 passages. Independently of cancer origin, it was possible to identify cells with epithelial-like and fibroblast-like morphology. Epithelial-like cells are polygonal in shape with more regular

dimensions and grow attached to a substrate in discrete patches as visualized in **Figure 13 C**. On the other hand, fibroblast-like cells have elongated shapes as observed in **Figure 13 B**.

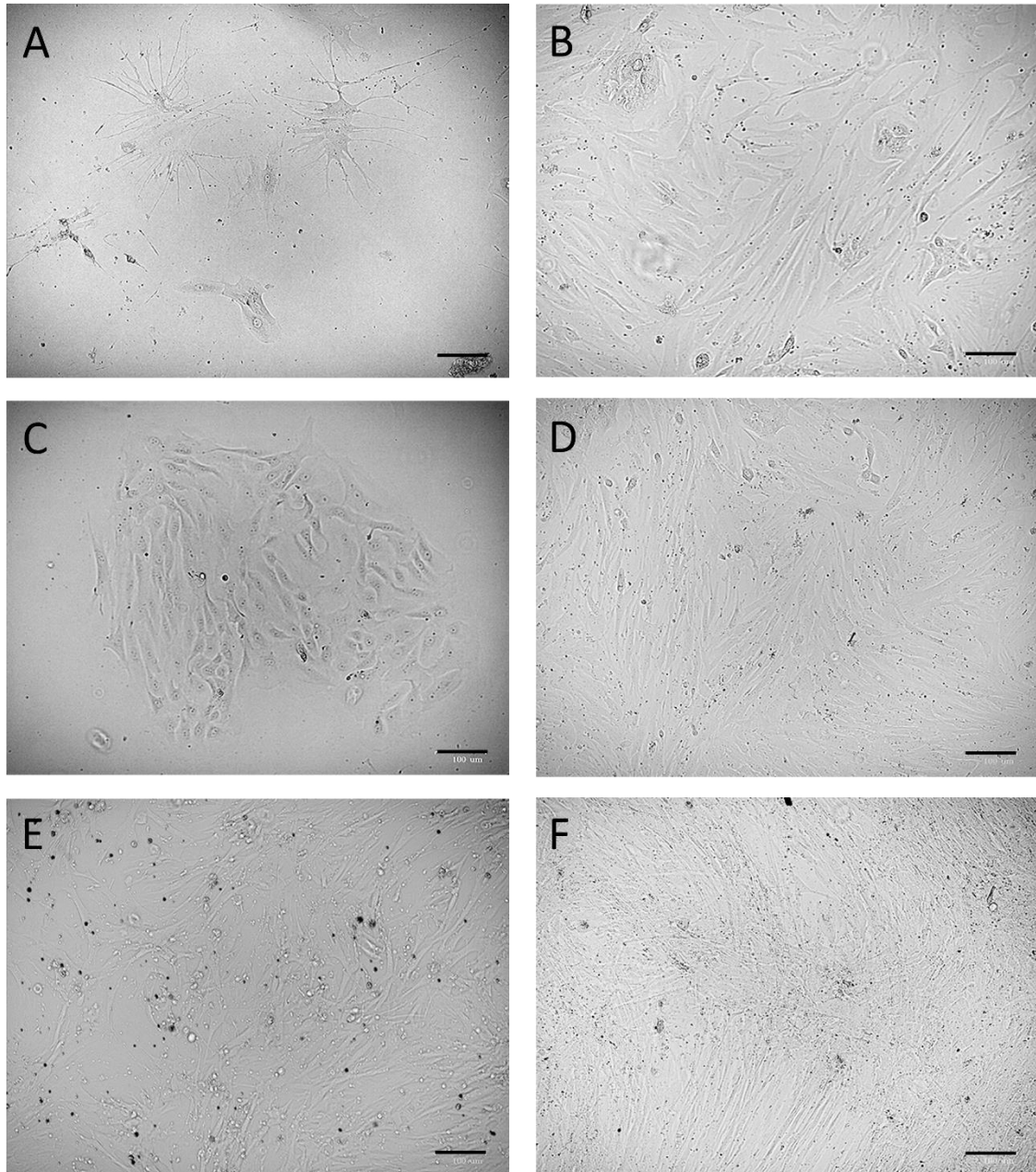


Figure 13. Primary breast tumour specimens cultured on collagen-coated flasks. Cultures derived from (A-B) LA-, (C-D) HER-, (E-F) TN-DT specimens (passages 0-1). Images acquired with ZOE Fluorescent Cell Imager (BioRad). Scale bar: 100µm.

In cultures originated from the LA- and HER-DT specimens was possible to observe a heterogeneous cell population with both epithelial and fibroblast-like cells (**Figure 13 A-D**). Although, HER-DT appears to form bigger epithelial-like colonies

(**Figure 13 C**). Cultures originated from TN-DT specimens (**Figure 13 E-F**) present an early enrichment in fibroblast-like cells. Nonetheless, over time all cultures become dominated by fibroblasts-like cells (**Figure 13 B, D and F**).

Fibroblast enrichment is a common difficulty during the establishment of cultures derived from tissue explants, such as primary tumours [68]. To originate epithelial cell-enriched cultures, differential centrifugation methods and FACS sorting must be applied. The establishment of defined cell-type cultures may be relevant to characterise the involvement of both the tumour and the stromal compartment in tumour progression. In the present work, a simplest strategy was applied: DT specimens were cultured directly without prior cell enrichment. Therefore, fibroblast enrichment was expected and, over time, cells from epithelial lineages may be lost in the 2D culture.

To evaluate 2D cell behaviour through metabolic activity, studies were performed on days 1, 7, 14 and 21 after seeding for different cell passages. Independently from tumour origin, cells metabolic activity tends to increase over time (**Figure 14**) indicating cell viability and proliferating capacity.

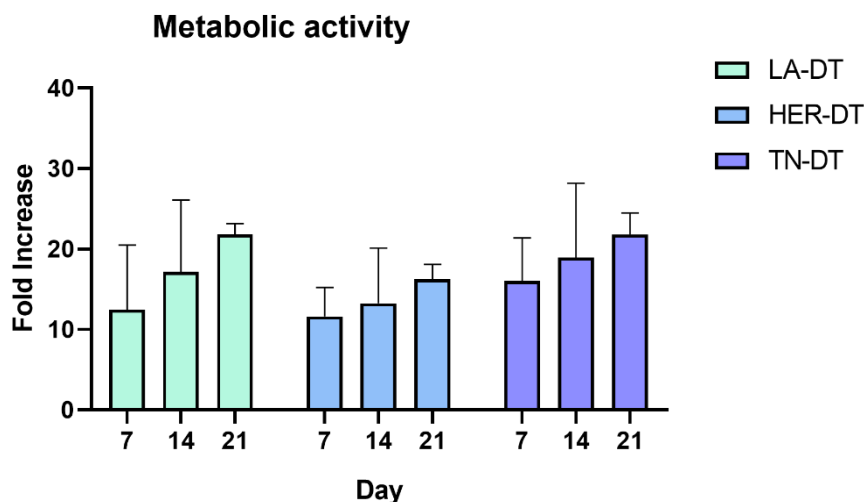


Figure 14 Metabolic activity studies of DT cells cultured in 2D monolayer. Resazurin-based assay performed with cells in passages 1, 4, 8 and 9. Results presented as the average of the four cell passages and normalised in relation to day 1.

According to our results, cells immunohistochemical profile does not influence the 2D metabolic activity profile (**Figure 15**). Cells from different cancer origins, in the same passage and experimental setup, present the same tendency of behaviour. Over time, TN-DT cells present the higher fold increase values (passages 8 and 9). Since fibroblasts have been described as highly metabolically active cells, even when in a quiescent state [76], this result reinforces that fibroblasts might have completely dominated these

cultures. By contrast, HER-DT cells present, consistently, lower fold increase values, which may be related to the presence of bigger epithelial-like colonies in HER-DT specimens (**Figure 13 C**).

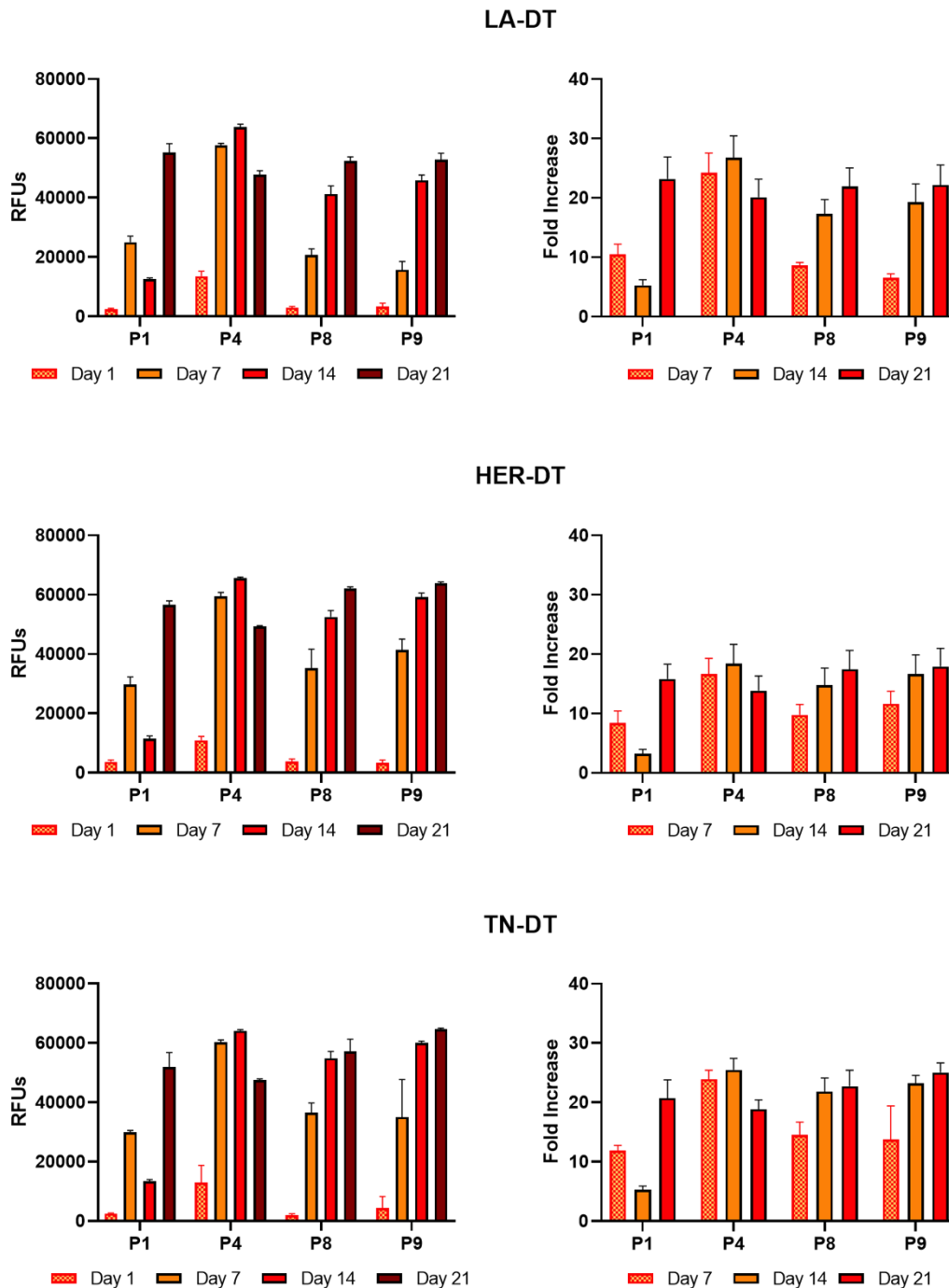


Figure 15. Metabolic activity studies of DT cells cultured in 2D monolayer. Resazurin-based assay performed with cells in passages 1, 4, 8 and 9. Results for each passage are presented (left) with relative fluorescent units (RFUs) normalised to the autofluorescence of the resazurin solution and (right) with the fold increase values in relation to day 1. N = 4.

To assess cell proliferation, we performed immunostaining for Ki-67 protein, which has been widely used as a proliferation marker for human tumour cells. Expression of Ki-67 has been correlated with molecular BC subtypes [77-79]. Studies indicate that Luminal A BC rarely presents high expression levels of Ki-67; HER-2 enriched and, particularly, TN BCs are consistently characterised by higher Ki-67 expression. Nevertheless, in the literature, there is no standard level of expression that defines the high expression of Ki-67. However, on average, samples in which less than 15% of cells are Ki-67+ are considered to have "low expression levels" [77-79]. We observed in our samples only a small percentage of Ki-67+ cells (**Figure 16**). Therefore, we could state that none of the DT specimens was clearly characterised by high expression of Ki-67. Nevertheless, in terms of relative expression, LA-DT derived cultures present higher Ki-67 expression.

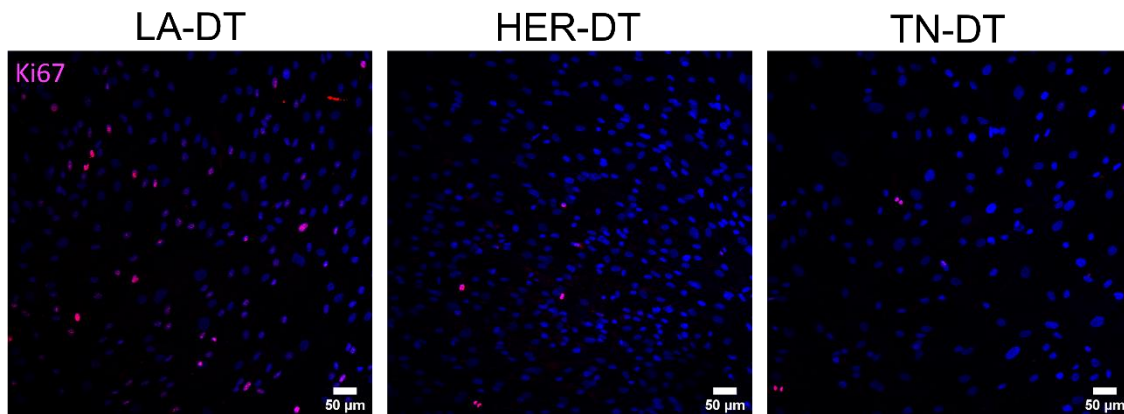


Figure 16. DT cells (passage 5) cultured in 2D monolayer stained with antibodies against Ki-67. Cells were immunostained with Ki-67 (red) to identify proliferative cells (pink) – colocalization of Ki-67 with DAPI (staining blue for DNA). Images acquired using a 20x magnification objective. Scale bar: 50 μ m.

6.2 Characterisation of cell populations in DT derived 2D cultures.

6.2.1 Assessment of CK8 and CK14 expression as markers of breast epithelial lineages

As previously cited, BC origin is frequently associated with epithelial cells from the TDLUs. Normal breast epithelial lineages are characterized by the expression of CK8 and CK14 by LEPs and MEPs, respectively. To study the presence of breast epithelial cells, DT specimens cultured in a 2D monolayer were stained for the referred markers. We were successfully able to establish the immunostaining protocol in the lab and we were able to identify both cell populations. As expected, and according to previous brightfield images (**Figure 13**), epithelial cells represent a small population within the DT specimen (**Figure 17**). In LA- and HER-DT derived cultures, breast epithelial lineages represent, approximately, 2.32% and 1.86% of the DT specimens, respectively, contrasting with 0.25% in TN-DT derived cultures (**Figure 18**).

DT specimens present different proportions of CK8+/CK14+ cells. In TN-DT, CK8+ cells are not detected and CK14+ cells present a diffuse cytoplasmic expression contrasting with LA- and HER-DT (**Figure 17**). LA- and HER-DT specimens present both CK8+ and CK14+ cells, although in different proportions (**Figure 18**). LA-DT appear to have more epithelial cells expressing CK8 than the HER-DT specimens.

Different clinicopathologic studies have been focused on the expression pattern of luminal and basal cytokeratin's (CK8/18 and CK5/6/14, respectively) in breast cancer. Focal and complete loss of CK8 expression has been previously described [80-82], particularly in TNBC. According to Rädler, Wehde [83], during BC progression, some typical luminal-type cells (CK8+) start to co-express CK14. These dual-positive cells occupy the luminal space and progressively lose CK8 expression associated with acquisition EMT characteristics. The cells may further evolve for mesenchymal-like cells that exhibited a significantly reduced or complete loss of CK14 expression. Noteworthy, it has been reported that only 2-18% of IDC-NST present CK14 expression [84]. Therefore, a progressive loss of CK8+ cells may explain the results obtained with TN-DT derived cultures.

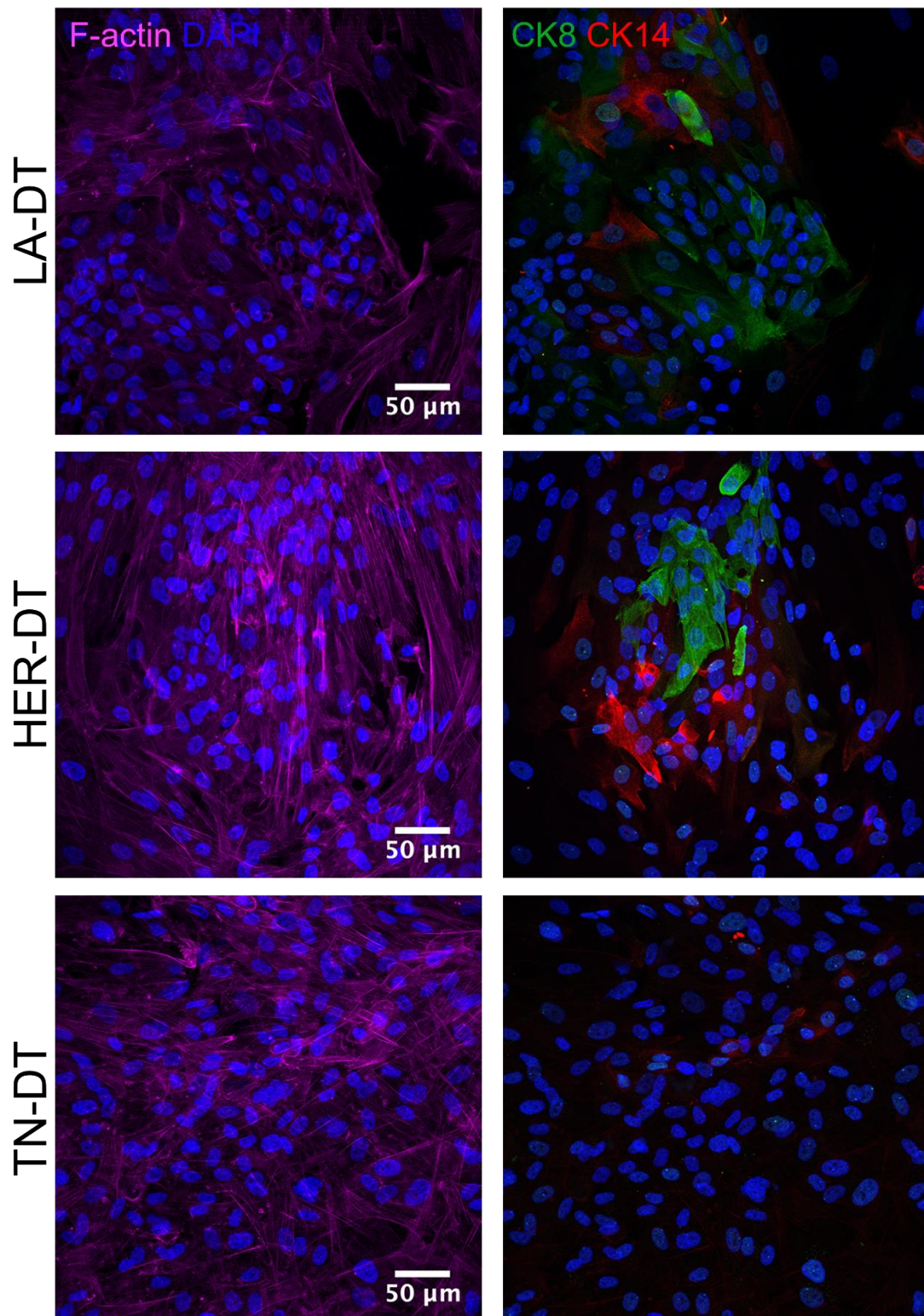


Figure 17. DT cells (passage 1) cultured in 2D monolayer stained with antibodies against cytokeratin 8 (CK8 – green) and cytokeratin 14 (CK14 – red). CK8/CK14 staining's reveal the presence of both breast epithelial lineages (luminal epithelial cells – CK8, myoepithelial cells – CK14) in LA- and HER-DT specimens. In TN-DT specimens only cells positive for CK8 were identified. DAPI stains for DNA. Images acquired using a 40x magnification objective. Scale bar: 50 μ m.

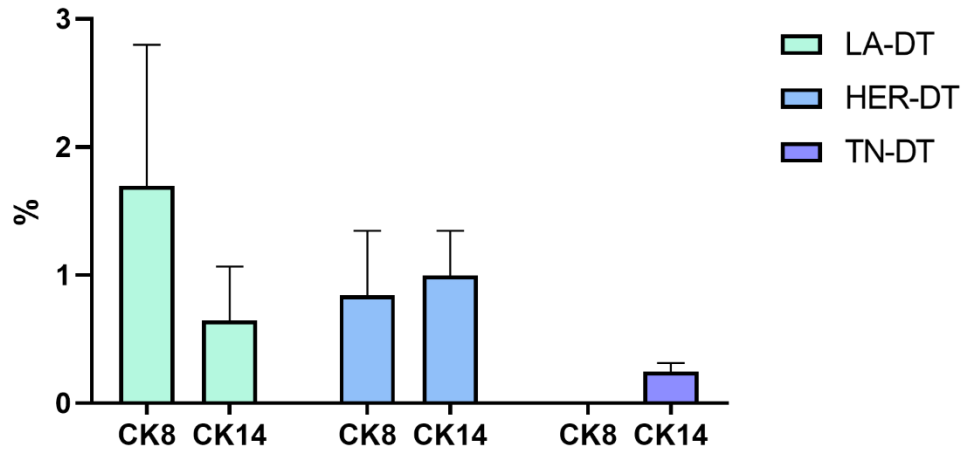


Figure 18. Quantification of luminal epithelial (CK8) and myoepithelial (CK14) cells. Percentage of cells staining for CK8/CK14 in relation to the total number of nuclei (DAPI staining). LA- (N=10), HER- and TN-DT (N=6) specimens in passage 1 cultured in 2D monolayer.

In normal human breast, LEPs and MEPs exist in a 1:1 proportion [46]. Results on the quantification of CK8/CK14 expression evidence a more physiological proportion in the HER-DT specimen (**Figure 18**). Over time, cells start to present a diffuse cytoplasmic expression of CK14 and a decrease in CK8 expression (**Figure 19**), contrasting with results obtained with cells in passage 1 (**Figure 17**). Furthermore, it is possible to identify dual-positive cells (CK8+/CK14+). These results further support a progressive acquisition of CK14 expression by LEPs followed by loss of CK8 expression.

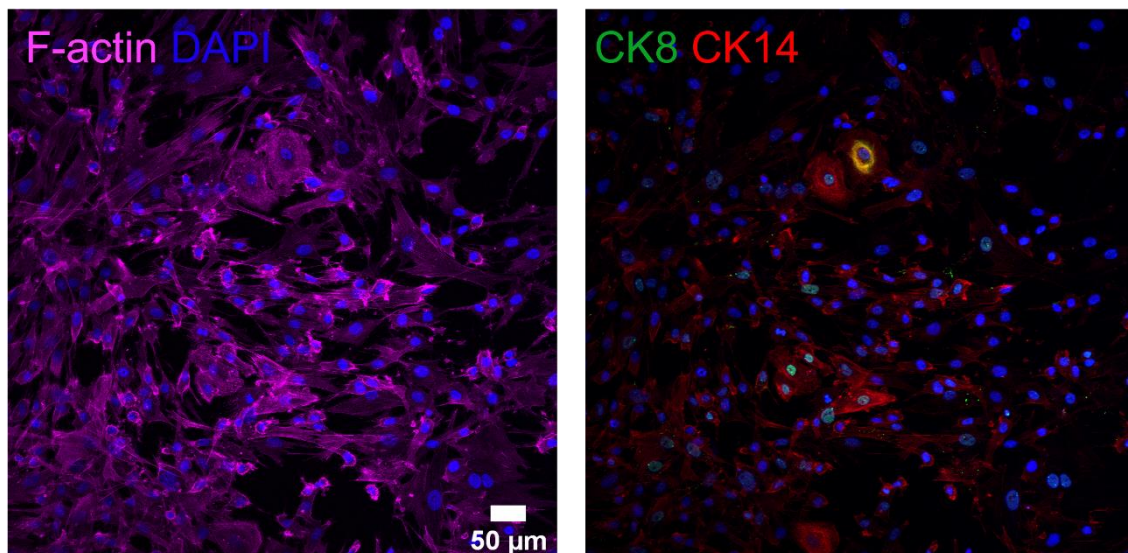


Figure 19. Alteration in CK14 (red) and CK8 (green) expression in HER-DT derived cultures (passage 5 cells). Notice the decreased expression of CK8 and the presence of dual-positive (CK8+/CK14+) cells. Images acquired a 20x magnification objective. Scale bar: 50 μm .

Luminal-A tumours are characterised by the expression of CK8/18 [10, 21, 23]. Therefore, it was expected to have high levels of CK8+ cells in LA-DT derived cultures. In passage 1, CK8+ cells were, approximately, two times more than CK14+ cells and dual-positive cells were not detected. Over time, LA-DT derived cultures appear to better conserve CK8 expression, however, an alteration in the expression pattern is detected: (1) the signal intensity decreases and (2) nuclei colocalization appears (**Figure 20**).

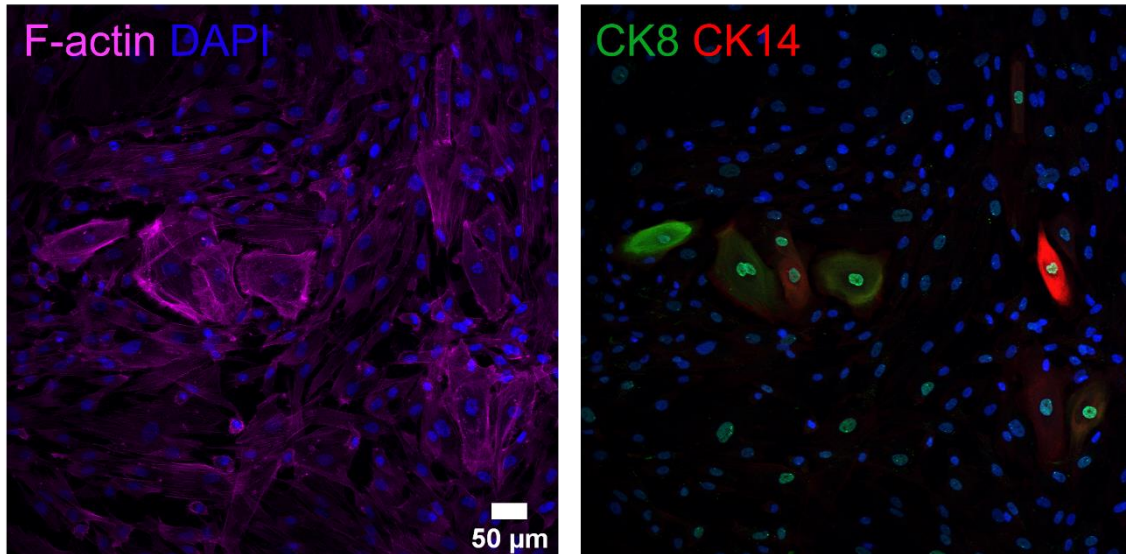


Figure 20. Expression pattern of CK14 (red) and CK8 (green) in LA-DT derived cultures (cells in passage 5). Images acquired using a 20x magnification objective. Scale bar: 50 µm.

Nevertheless, progressive loss of CK8 and CK14 expression is transversal to all DT specimens (**Figure 19, 20 and 21**). Therefore, it may be related to the cell passage process since we observed that epithelial-like cells present greater resistance to trypsinisation. Trypsin, used to detach the cells, is a proteolytic enzyme that breaks peptidic bonds. The presence of more adhesion proteins in epithelial cells, comparing with mesenchymal-like cells (such as fibroblasts), may explain this increased resistance. Theriault, Portelance [85] describe a partial trypsinisation method to propagate epithelial ovarian primary cancer cells that can, in the future, be considered to overcome this challenge.

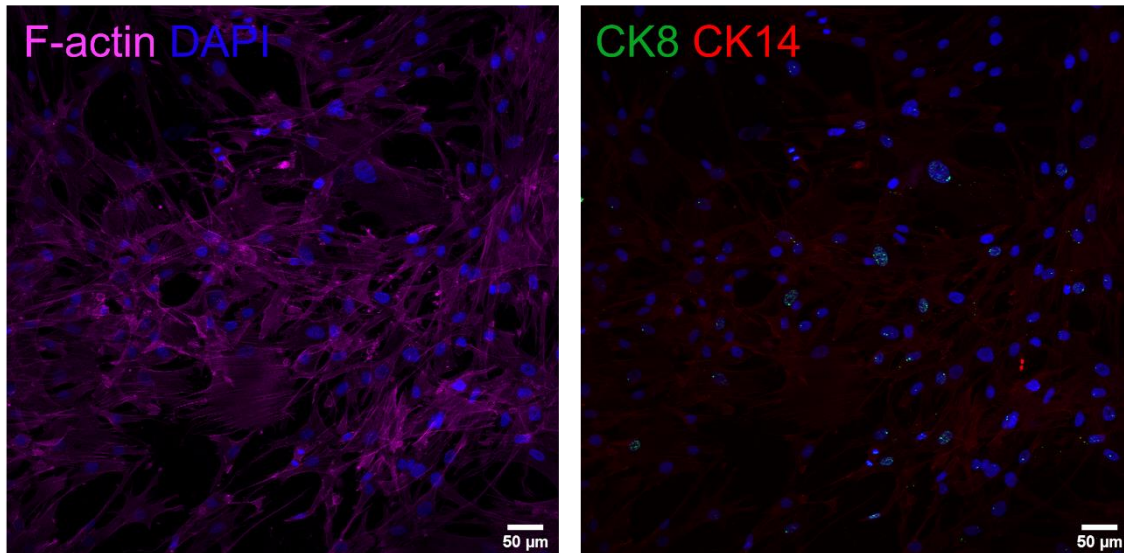


Figure 21 Expression pattern of CK14 (red) and CK8 (green) in TN-DT derived cultures (cells in passage 5). Images acquired using a 20x magnification objective. Scale bar: 50 µm.

6.2.2 Expression of surface markers: E-cadherin, CD44 and CD90

E-cadherin, also known as CDH1, is a cadherin from the family of Ca^{2+} -dependent cell – cell adhesion proteins [86, 87]. This cell adhesion molecule plays a role in initiating adhesion and cell sorting during development, and is virtually expressed in all epithelial tissues [87]. In cancer biology, its disruption is a common occurrence in metastatic cancers as a consequence of EMT programs [86, 87]. The activation of EMT induces the acquisition of mesenchymal features. We were able to identify E-cadherin positive cells in all DT specimens (**Figure 22**), but in lower amounts in HER- and TN-DT, corroborating the previous results. In fact, E-cadherin expression follows a similar proportion to CK8 and CK14.

CD44 is a single-chain non-kinase transmembrane proteoglycan widely expressed in normal adult and foetal tissues (in epithelial cells, keratinocytes and macrophages, for example) [88, 89]. Nevertheless, CD44 has been associated with cancer progression (migration/invasion, angiogenesis, and metastasis) and with CSCs characterisation [88, 89]. CD44 positive cells were found in all DT specimens (**Figure 22**) and in close contact with epithelial cells, which could be related to a CSC-like phenotype. To confirm this further analysis should be performed such as CD24, ALDH1, EpCAM [16, 90-92]. Noteworthy, CSCs have been associated with drug resistance and relapse of solid tumours [93].

CD90, also known as Thy-1 (thymocyte differentiation antigen-1), is a GPI (glycosylphosphatidylinositol)-anchored glycoprotein involved in cell – cell and cell – matrix interactions. CD90 expression has been identified in fibroblasts, leukocytes, neurons, and activated endothelial cells [94]. On the other hand, this glycoprotein has been increasingly associated with cancer development and CSCs characterisation. Regarding CD90, its expression is detected throughout the different cultures (**Figure 22**) suggesting the presence of activated fibroblast [95]. Independently from DT specimen origin, an apparent colocalization of CD44 and CD90 is presented. CD44-positive/CD90-positive cells have been previously reported [96, 97] and might be related to a CSC-like phenotype.

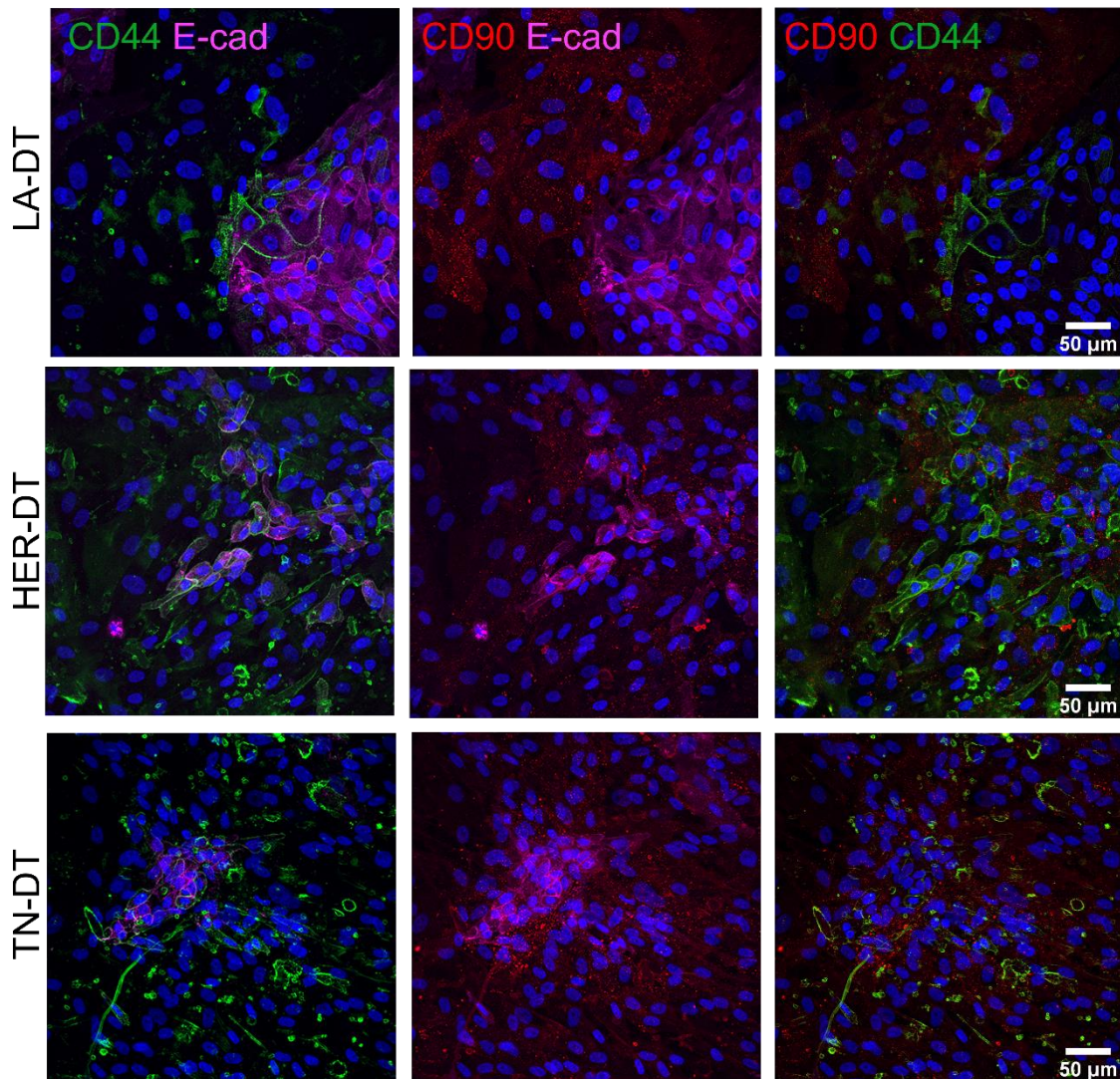


Figure 22. DT cells (passage 1) cultured in 2D monolayer stained with antibodies against surface markers: E-cadherin, CD44 and CD90. Images acquired using a 40x magnification objective. Scale bar: 50 μm.

6.2.3 Expression of mesenchymal markers: vimentin and α -SMA

Vimentin, a type III intermediate filament cytoskeletal protein [98, 99] of approximately 57 kDa [99], is widely expressed in cells of mesenchymal origin. However, not associated with normal epithelial cells, it has been shown to be expressed in epithelial tumour cells due to the activation of EMT programmes [98-101]. In our work, vimentin staining's were performed to identify mesenchymal-like cells, such as fibroblast. We observed that vimentin-positive cells were similar in all DT specimens (**Figure 23**).

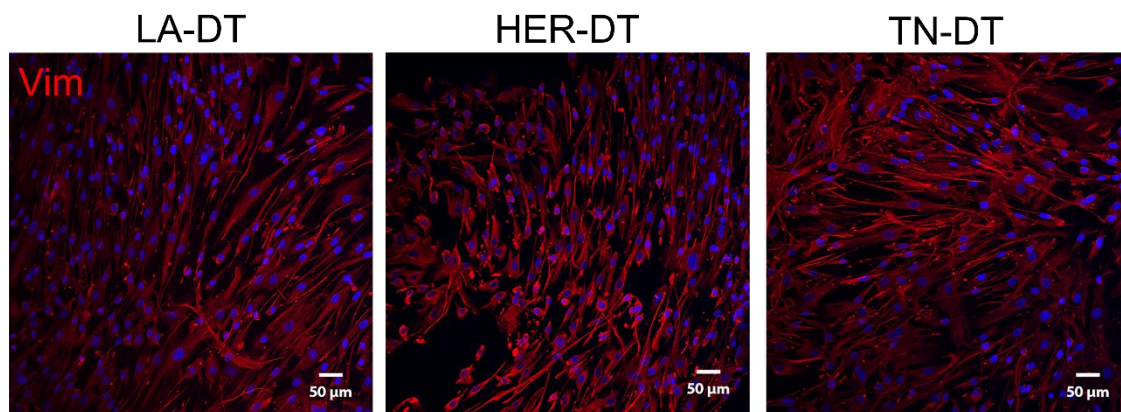


Figure 23. DT cells (passage 5) cultured in 2D monolayer stained with antibodies against vimentin. Images acquired using a 40x magnification objective. Scale bar: 50 μ m.

Since vimentin is an EMT-related marker, the involvement of this protein in BC progression has been extensively studied. According to previous studies, vimentin expression is positively correlated with tumour grade and negatively correlated with the expression of CK 8/18 and ER expression. Notable, vimentin expression is strongly associated with grade 3 IDC, and ER- tumours, with implications in chemotherapy resistance [100, 101]. Therefore, it was expected an increased expression of vimentin in TN-DT specimens. Although not directly demonstrated by vimentin expression, since cells from the same passage do not present expression of CKs, particularly CK8 (**Figure 21**), we may conclude that these samples present an *in vivo*-like expression of vimentin. Moreover, the difficulty in identifying differences in vimentin expression among the different DT may be related to the dominance of fibroblasts on the culture.

As previously mentioned, CAFs are an important component of the TME. Since CAFs are a heterogeneous population, a specific marker has not yet been identified, however, α -SMA is widely accepted [102-104]. High expression of vimentin has been

positively correlated to α -SMA expression [101]. Considering our previously presented results, it is expected a strong α -SMA staining in TN-DT cells.

The presence of α -SMA fibres is recognised as a characteristic of activated fibroblasts, namely, myofibroblasts [105, 106]. Myofibroblasts are cells that have acquired an intermediate phenotype between fibroblasts and smooth muscle cells [106]. These cells have been identified in normal and pathological tissues, such as breast cancer [105, 106].

Our results show α -SMA expression independently from cancer origin (**Figure 24**). However, different expression patterns were observed. LA-DT specimens present formation of α -SMA fibres (**Figure 24 A**). In turn, HER- and TN-DT cells present diffuse cytoplasmatic expression of α -SMA, although, more positive cells are identified in these samples. In the TN-DT culture it was possible to identify an occasional formation of weak α -SMA fibres (**Figure 24 B**).

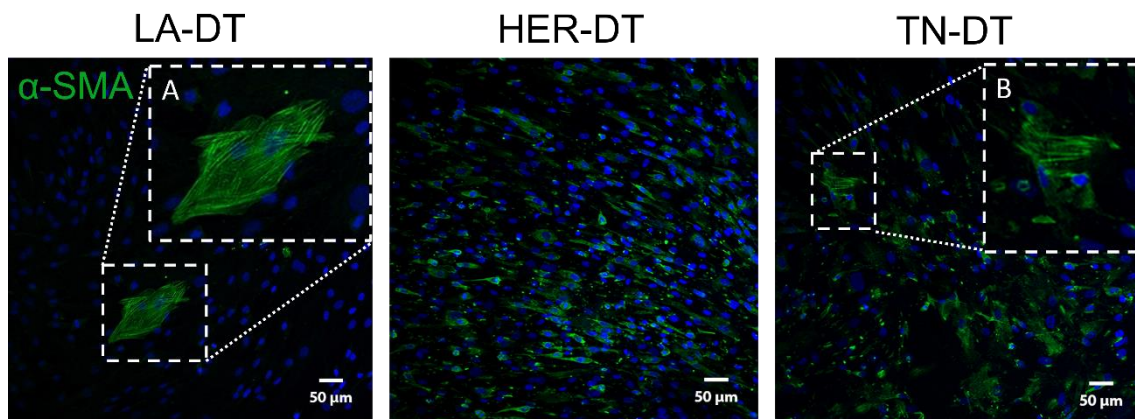


Figure 24. DT cells (passage 5) cultured in 2D monolayer stained with antibodies against α -SMA. Images acquired using a 40x magnification objective. Scale bar: 50 μ m.

Myofibroblast in the TME, known as CAFs, are characterised by high proliferative activity [105]. The hypothesis that these activated fibroblasts present a CAFs phenotype may explain the high expression of Ki-67 and the metabolic activity values in LA-DT specimens (section 6.1). However, TN-DT cells were not distinguished by the expression of α -SMA. Moreover, it was not possible to establish a positive correlation between vimentin and α -SMA expression.

6.3 Establishment of scaffold-free 3D in vitro models from DT specimens

In the present work, MCTS were produced in micropatterned agarose moulds. This nonadherent surface enables the formation of 81 monodispersed spheroids per mould and allows live cell image of multiple spheroids at once (**Figure 25 A**). Therefore, an easy spheroid's characterisation over time can be performed. Moreover, without prior removing the spheroids from the mould, it is possible to do paraffin embedding with several spheroids being present in each section (**Figure 25 B-D**). This approach is suitable for more high throughput biochemical, histological and immunohistochemical analysis, an important characteristic in BC research.

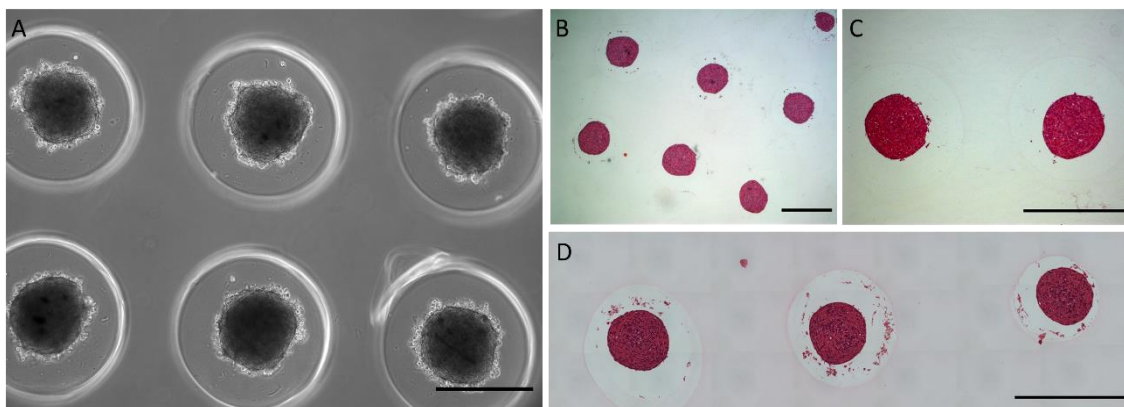


Figure 25. Simultaneous images of multiple spheroids. (A) Brightfield images of MCTS acquired using a 5x magnification. (B-D) Images of H&E staining in 3µm paraffin-embedded sections acquired using (B) 10x and (C, D) 40x magnification. Scale bar = 500µm.

6.3.1 Spheroid's formation and morphology

MCTS were visualised 24 hours and 7 days after cell seeding with Axiovert 200M (Zeiss) microscope. The recorded images were analysed to evaluate spheroids morphological characteristics: size distribution (diameter), solidity and roundness.

Images showed spontaneous aggregation of cells as a single mass per well. Approximately one day after seeding, the DT specimens had formed dense aggregates presenting round-type morphology (**Figure 26 A**). A decrease in MCTS diameter over time indicates spheroid's compactness – which is evident independently from the cell passage of the DT specimens. However, in higher cell passages, spheroids are smaller

at day 1 (**Figure 26 B**). Round-type morphology [107] and total compactness [108] are associated with strong cell – cell interactions and ECM production. Fibroblast enrichment (ECM producing cells, *par excellence*), previously confirmed in 2D characterisation (section 6.2.2), might explain earlier compactness in MCTS from higher passages. On average, spheroids size decreased from a mean size of around 220 μm to $\sim 180 \mu\text{m}$ in 7 days (**Figure S1**, supplementary information). No significant differences were associated with cell sources. Overall, completely formed MCTS of homogenous size were reproducibly obtained independently from DT specimen origin, supporting the possible application of the system for high-throughput biochemical assays.

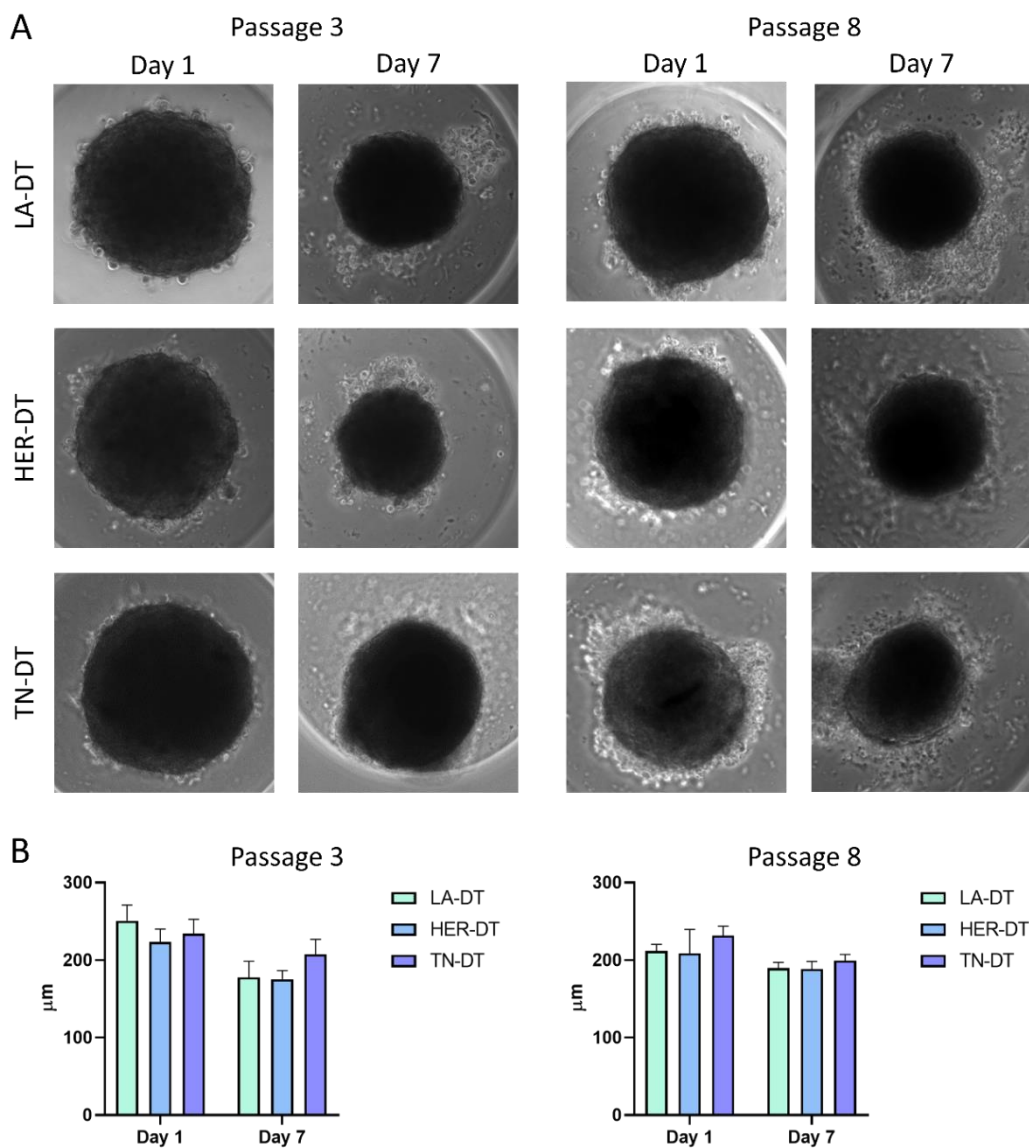


Figure 26. MCTS morphological characterisation. (A) Brightfield images of MCTS from LA-, HER- and TN-DT in passages 3 and 8 in different timepoints (days 1 and 7). Images acquired using 5x magnification. (B) Diameter of MCTS derived from DT specimens in passage 3 and passage 8.

To further characterise MCTS morphology, solidity and roundness indexes were considered, as previously described [108-110]. Solidity is an indicator of MCTS density [109] and is a measure of spheroids regularity [108]. Roundness is a parameter that defines how close the shape of the 2D projection of the spheroid approaches a circle [108]. This parameter is mainly dependent on the sharpness of angular protrusions (convexities) and indentations (concavities) [111]. Both indices range from 1 (perfect sphere) to 0 (elongated shape). Compact and well-shaped regular spheroids are characterized by solidity values above 0.90 [108, 110]. The results show that MCTS derived from the three DT reach a proper spheroid shape 1 day after seeding, which is maintained throughout the 7 days of culture (solidity index over 0.93 – **Figure 27 A**).

Independently from DT specimen origin, MCTS present high roundness values (~0.9 – **Figure 27 B**) indicating a smooth surface associated with high ECM production and total compactness. After 7 days in culture, a slight decrease is observed, as previously described [108]. According to Zanoni, Piccinini [112], this decrease may influence the number of cells exposed to high levels of nutrients and oxygen, therefore, influencing the percentage of actively proliferating cells and their response in biochemical assays (e.g., drug screening).

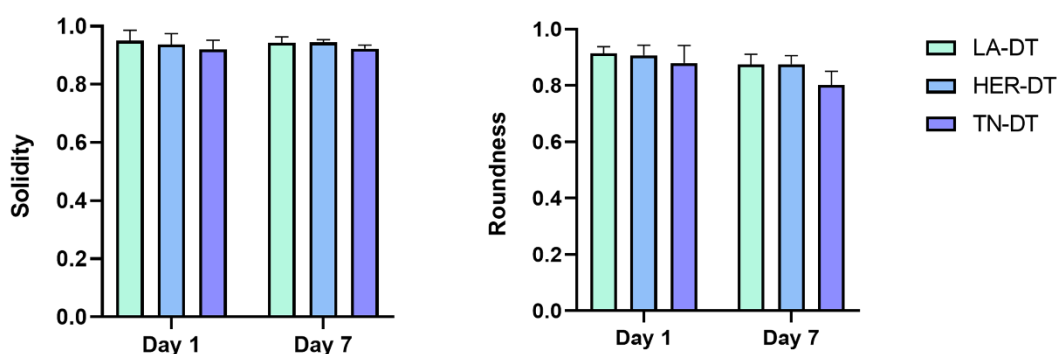


Figure 27. MCTS morphological characterisation – (A) Solidity and (B) Roundness. Results for MCTS derived from DT in different cell passages.

To analyse the internal structure of the spheroids (cell arrangement) and further confirm that compact and uniformed MCTS have been produced, H&E staining was performed (**Figure 28**). Independently from DT specimen origin, MCTS of a well-defined outer perimeter were observed on day 1. Cells within the spheroids present densely packed and with no sign of formation of an apoptotic core cavity. The formation of multiple cavities was occasionally observed, particularly on HER-DT derived MCTS.

However, this can be a technical artefact caused by tissue detachment during processing. Cells nuclei exhibited pronounced elongation and circumferential alignment around the core of the spheroid, which is enhanced on day 7 (**Figure 28 F and J**). Moreover, it was frequently observed the organisation of cells into a peripheral monolayer (**Figure 28 A - E**). Occasionally, large round cells (**Figure 28 B and L**) are detected in the core of the spheroids. Overall, H&E staining confirmed that total compact MCTS were obtained within 24 hours post-seeding and maintained for 7 days in culture.

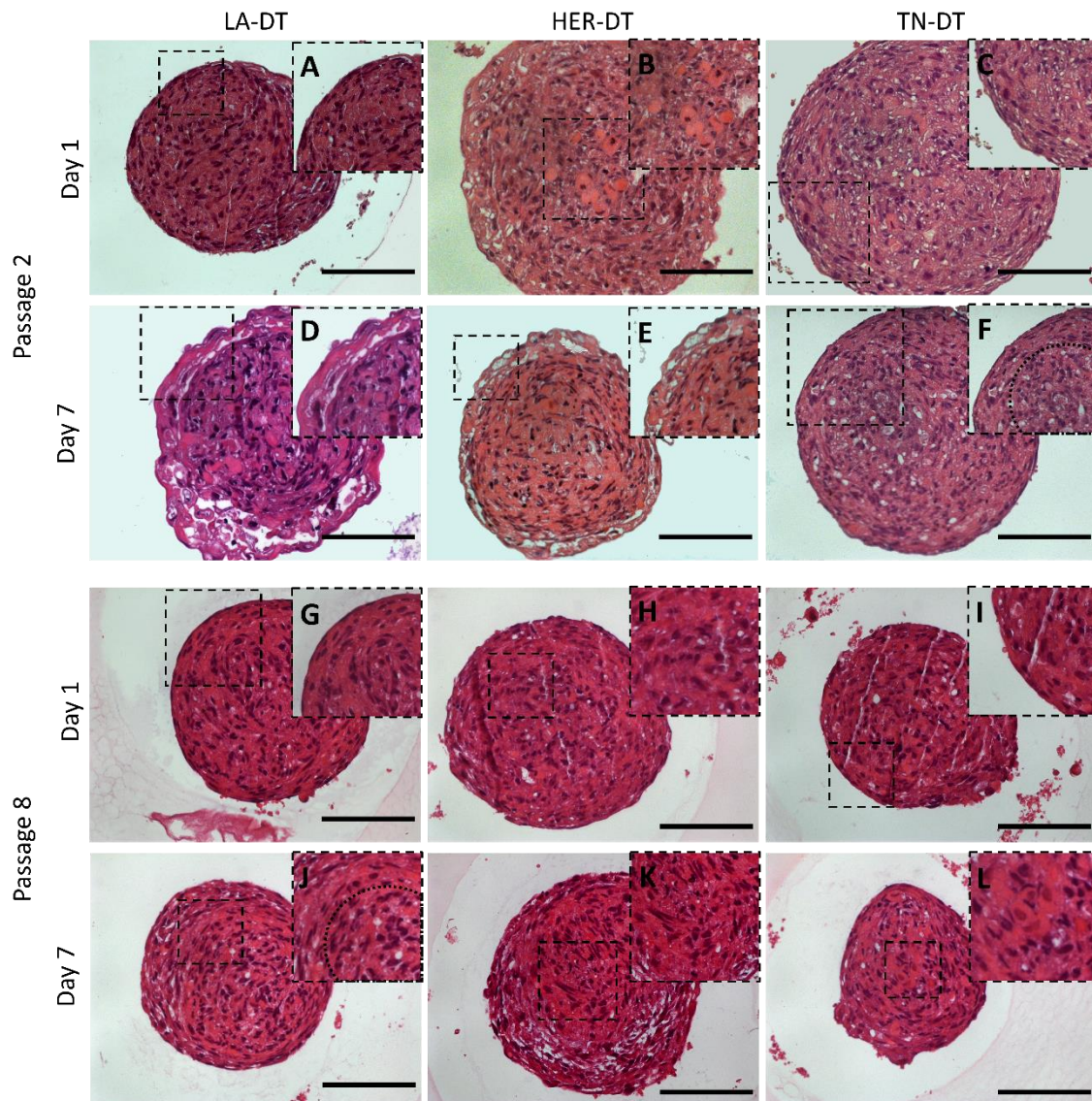


Figure 28. H&E staining in 3 μ m paraffin-embedded sections of MCTS derived from LA-, HER2- and TN-DT specimens in passages 2 (top) and 8 (bottom) at days 1 and 7 post-seeding. (A-L) Highlights of different regions of the MCTS. Brightfield images acquired using a 40x magnification. Scale bar: 100 μ m

Spheroid formation is commonly associated with the establishment of physiological gradients and cellular zones. Considering the diameter range of the

produced MCTS (under 400 μm), two cellular zones might be established (a proliferating and a quiescent zones). Ki-67 is a proliferation marker used to assess the formation of a proliferating outer zone in the MCTS.

Day 1 MCTS presents Ki-67 expression throughout all spheroid (**Figure 29**). Comparing with the expression levels in 2D, cells in MCTS appear to be more proliferative. Over time, the expression significantly decreases and is circumscribed to the periphery.

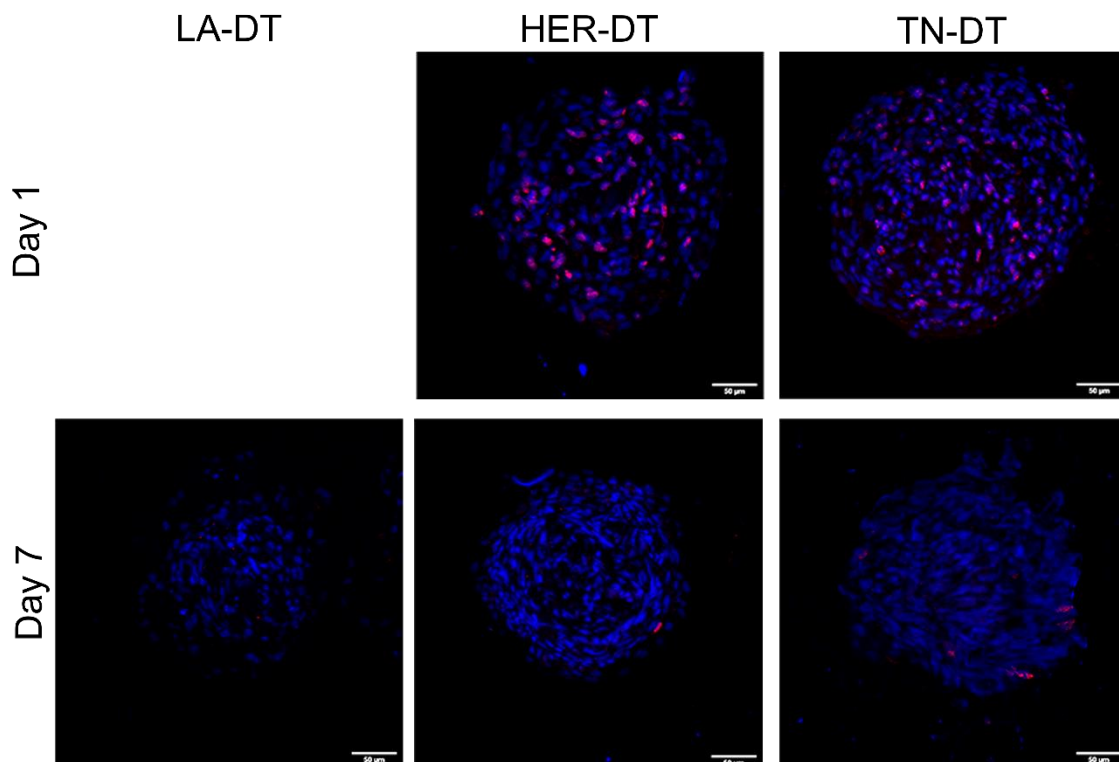


Figure 29. Proliferating Ki-67+ cells in MCTS. Representative images of MCTS at days 1 (upper row) and 7 (bottom row) from LA-, HER- and TN-DT samples (respectively, from left to right). Images of MCTS from LA-DT at day 1 missing due to tissue detachment during processing. Scale bar = 50 μm .

Considering DT specimens origin, HER-MCTS present higher Ki-67 expression at day 1. However, TN-MCTS appear to better maintain the expression, presenting more positive cells at day 7. Luminal A breast cancer is characterised by low expression of Ki-67. Unfortunately, due to tissue detachment during processing, it was not possible to acquire images of Ki-67 expression on LA-DT derived MCTS on day 1. Regarding day 7, Ki-67+ cells were not detected in these MCTS. These results differ from the ones obtained with DT specimens cultured in 2D (section 6.2.2) where LA-DT specimens presented the higher Ki-67 expression levels.

The presented results contrast with results obtained by Imamura, Mukohara [72], that reported that Luminal BC cells (MCF-7 cell line), comparing with HER2-enriched BC cells (BT-549 and BT-474 cell lines) present, in both 2D and 3D spheroids, lower levels of Ki-67 expression. Moreover, the authors report less Ki-67+ cells in 3D cultures, compared to their 2D counterparts, which is not the case in our results with HER- and TN-MCTS. Overall, our 3D culture system may better reflect *in vivo* features than the 2D system; reinforcing the importance of 3D models in BC research.

In terms of expression level, a decrease in the number of Ki-67+ cells was expected following the decrease in the roundness index value on day 7, although not as significant. Moreover, it was not possible to demonstrate the establishment of a proliferative gradient in the MCTS, as previously reported [113].

6.3.2 ECM production inside MCTS

The ECM provides an important context for cell regulation. ECM biochemical properties can directly affect both epithelial and stromal cells. Several alterations in the ECM have been described in BC, and it has even been proposed as a therapeutic target.

High levels of cell – cell /cell – ECM interactions within 3D spheroids have been reported to regulate cell functionality; better capturing *in vivo* cellular features when compared to 2D cultured systems [114]. Therefore, the capacity to develop a tissue-specific ECM is considered an important feature in 3D tissue constructs and, consequently, in cancer research [115]. During BC progression, increased deposition of a fibrotic stromal matrix is observed. Within the deposited molecules, collagen type I, III and V, elastin, and fibronectin are reported [115, 116]. The previously described MCTS morphological characterisation has proposed that high ECM deposition has occurred. Therefore, to evaluate whether the MCTS replicate the native TME *ex vivo* by producing ECM, the expression of major ECM proteins, such as collagen I (Col-I) and fibronectin (FN), was analysed.

Immunohistochemical evaluation of cells in MCTS showed sustained expression of FN between days 1 and 7 *in vitro*, independently from DT origin (**Figure 30 A**). However, in LA-MCTS less FN deposition was observed. Moreover, FN remained mainly non-polymerised throughout the culture (**Figure 30 B**). In turn, FN deposition in HER- and TN-MCTS is consistently polymerised with the formation of fibres since day 1 (**Figure 30 B**).

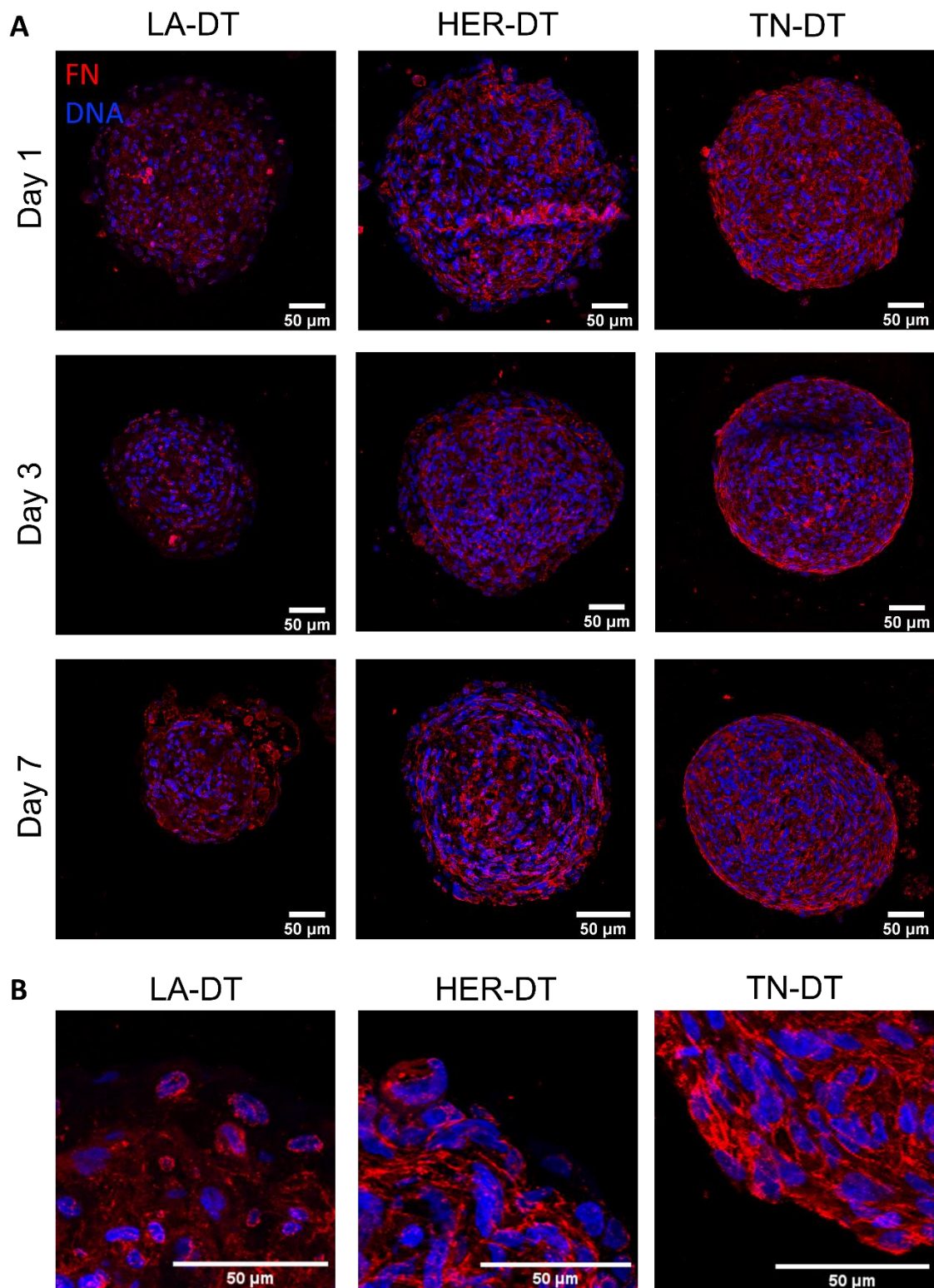


Figure 30. Fibronectin deposition and distribution in MCTS along 7 days of culture. (A) Immunostaining of FN (red) and DAPI (blue) in 3 μm paraffin-embedded sections of MCTS spheroids derived from LA-, HER- and TN-DT specimens (passage 2) along 7 days of culture. (B) Highlights of different regions of the MCTS at day 1 to show the deposition pattern of FN. Images acquired with a 40x magnification. Scale bar 50 μm.

Previous studies have correlated FN expression with BC subtypes. According to Park and Helfman [117], a significantly higher expression of FN is identified in TNBC compared to HER2-enriched and, particularly, with hormone receptor-positive BCs (such as Luminal A). These findings have been further confirmed in epidemiological studies [118, 119], indicating that FN expression may be considered a useful marker of poor prognosis in BC. Taken together, these findings support that FN expression in MCTS replicates the native TME.

Over time, polarised FN forms an outer layer of circumferentially aligned fibres surrounding a more disorganized core (**Figure 30**), particularly in HER-MCTS. In TN-MCTS, between days 3 and 7, the other layer gives rise to FN elongated fibres assembled at the periphery. This deposition pattern in the spheroid periphery has been previously reported in spheroids of other aggressive cancers (e.g., colorectal cancer [120]). Moreover, the presence of FN has been positively correlated with (1) higher levels of Ki-67+ cells [121] and (2) enhanced migration capacity [117, 122]. Therefore, the deposition of FN may indicate that a tumour-like gradient is established within the MCTS with cells of increased proliferation and/or motility capacities been segregated to the periphery.

The formation of collagen fibres has been described in DCIS and associated with a higher propensity to develop IDC [123-125]. Immunohistochemical studies on Col-I expression revealed that all spheroids present Col-I deposition since day 1 (**Figure 31**). However, HER- and TN-MCTS present higher expression levels throughout the culture time. HER2-enriched and TNBCs have been previously associated with abundant deposits of fibrillar collagens that significantly stiff the matrices comparing with less aggressive luminal BCs [123]. Taken together, the deposition of Col-I resembles *in vivo* BC features, which support that a tissue-specific ECM is produced in the MCTS.

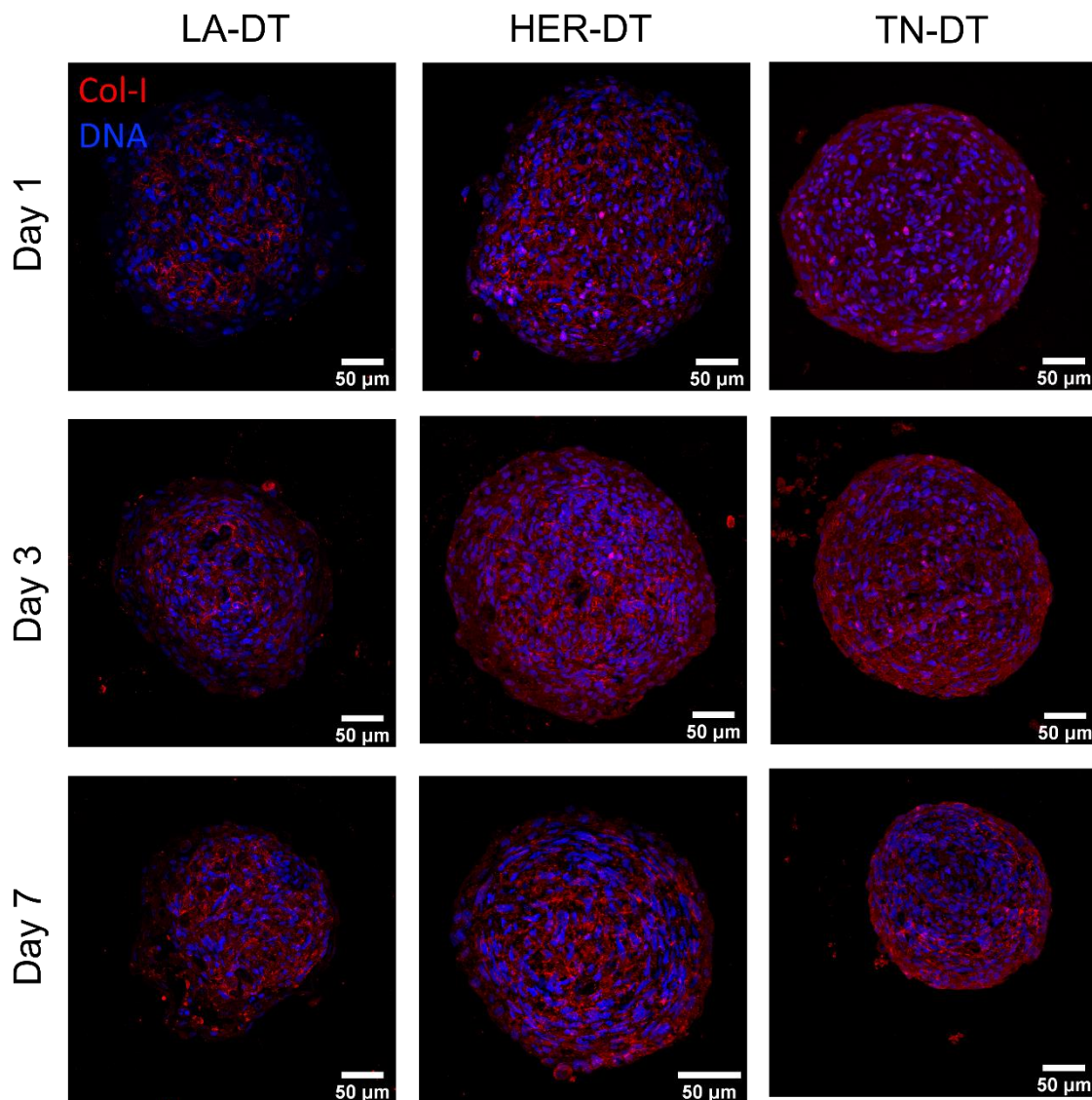


Figure 31. Collagen I deposition and distribution in MCTS along 7 days of culture. Immunostaining of Col-I (red) and DAPI (blue) in 3 µm paraffin-embedded sections of MCTS spheroids derived from LA-, HER- and TN-DT specimens (passage 2) along 7 days of culture. Images acquired with a 40x magnification. Scale bar 50 µm.

Particularly in MCTS derived from HER-DT specimens, polymerised Col-I deposition occurs essentially at the inner layer of the spheroids. MCTS's morphological characterisation did not indicate the formation of a hypoxic core. However, enhanced Col-I polymerisation has been reported in hypoxic conditions [126, 127]. Therefore, the spatial deposition of polymerised Col-I might be related to an oxygen gradient established within the spheroid.

Overall, the expression patterns of FN and Col-I in the different MCTS are maintained in the ones derived from DT specimens of higher passages (**Figure 32**), supporting the reproducibility of the model.

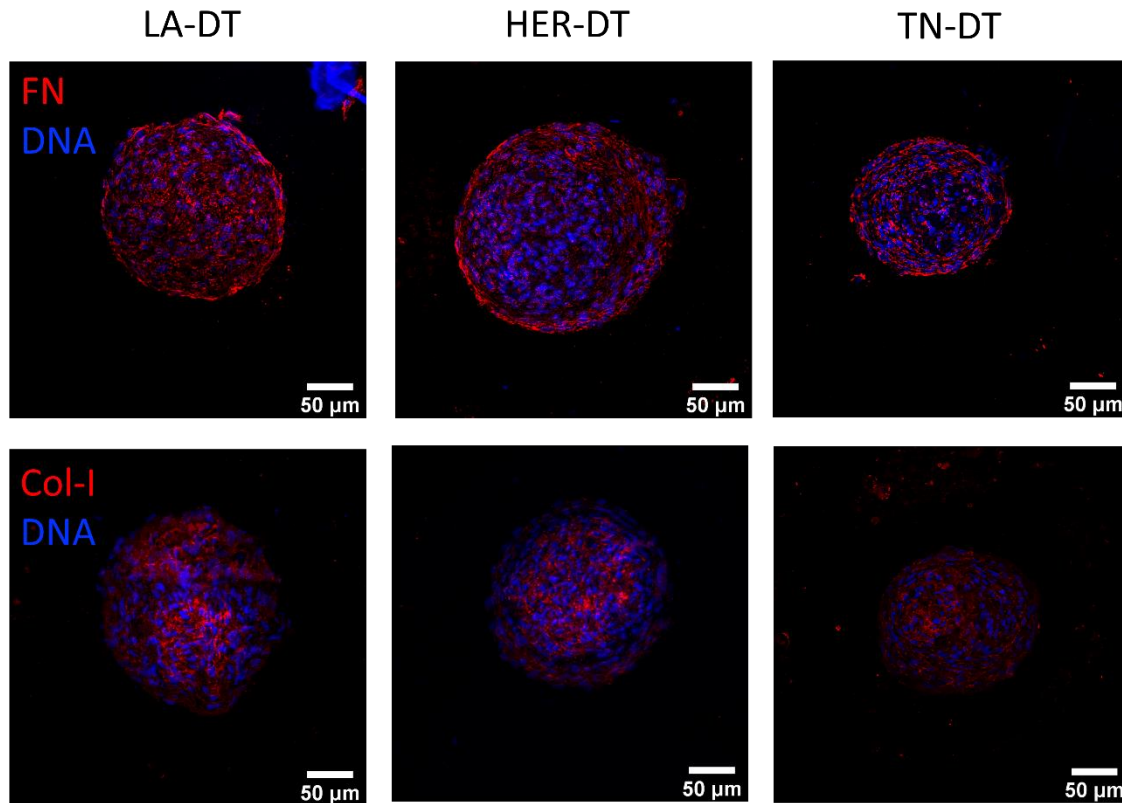


Figure 32. Fibronectin and Collagen I deposition and distribution in MCTS derived from DT specimens in passage 8 after 7 days of culture. Images acquired with a 40x magnification. Scale bar 50 µm.

6.3.3 Epithelial cells form the outer layer of MCTS

Previously 2D cellular characterisation of the DT specimens suggests that fibroblasts are the main cell type composing the MCTS. To assess epithelial and fibroblast distribution immunofluorescence staining's for epithelial (E-cad, CK8 and CK14) and fibroblast (vimentin) markers were performed.

In agreement with the 2D characterisation, CK8- and CK14-positive cells represent a small portion of the MCTS (**Figure 33**). Considering the cellular spatial organisation, fibroblasts establish at the spheroid core (vimentin-positive cells) (**Figure 34**). Considering E-cad expression (**Figure 34**), the pattern matches that of CK8 and 14 (**Figure 33**). Over time, epithelial cells are segregated to the periphery, which has been reported in previous works [128-130]. Therefore, the peripheral cell monolayer observed

in H&E staining (section 6.4.1) may correspond to epithelial cells stabilized by ECM which contribute to define the periphery of the spheroid.

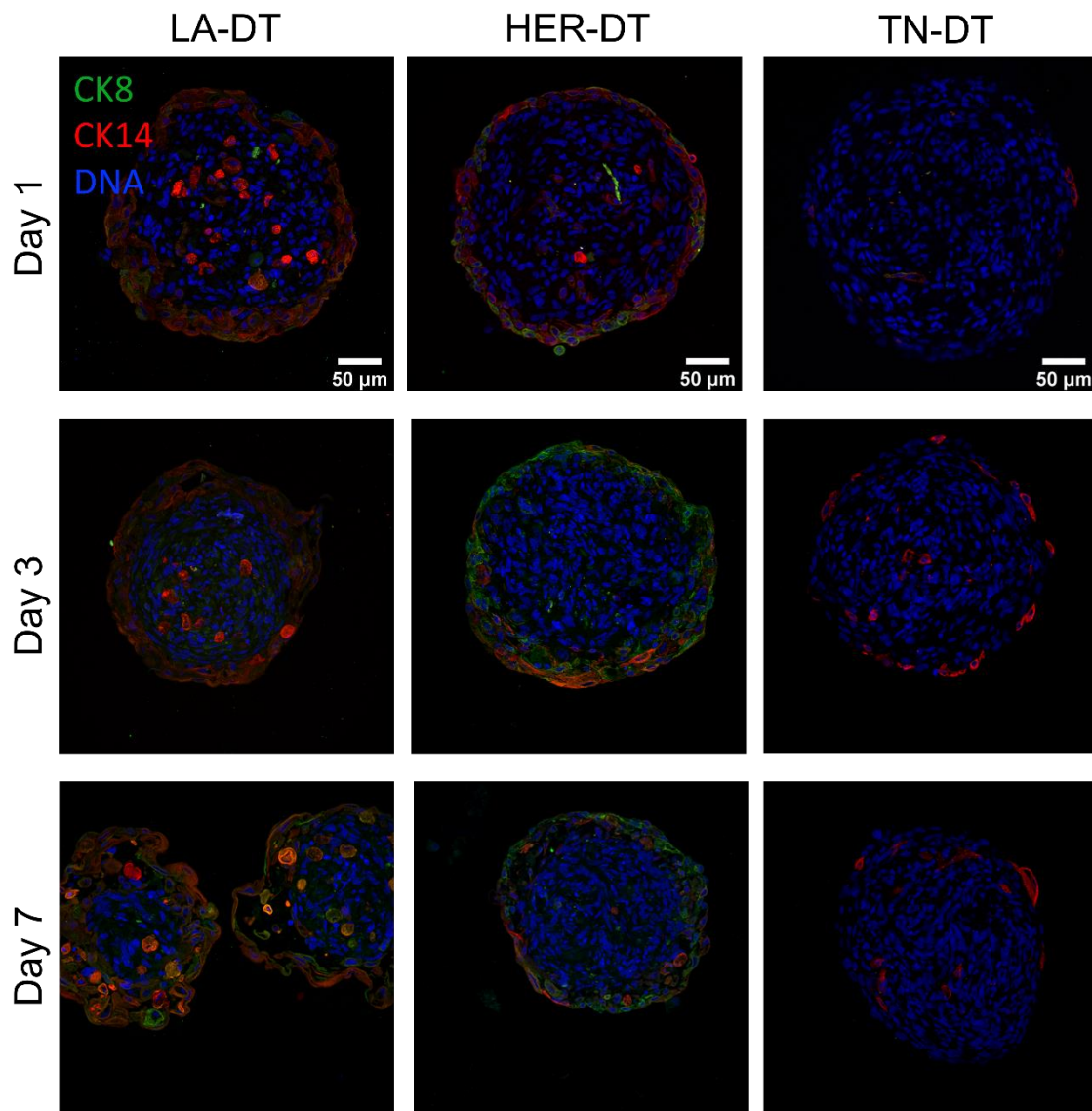


Figure 33. Expression of epithelial markers (CK8 and 14) in MCTS along 7 days in culture. Immunostaining of CK8 (green), CK14 (red) and DNA (blue). 3 μm paraffin-embedded sections of MCTS spheroids derived from LA-, HER- and TN-DT specimens (passage 2). Images acquired with a 40x magnification. Scale bar 50 μm.

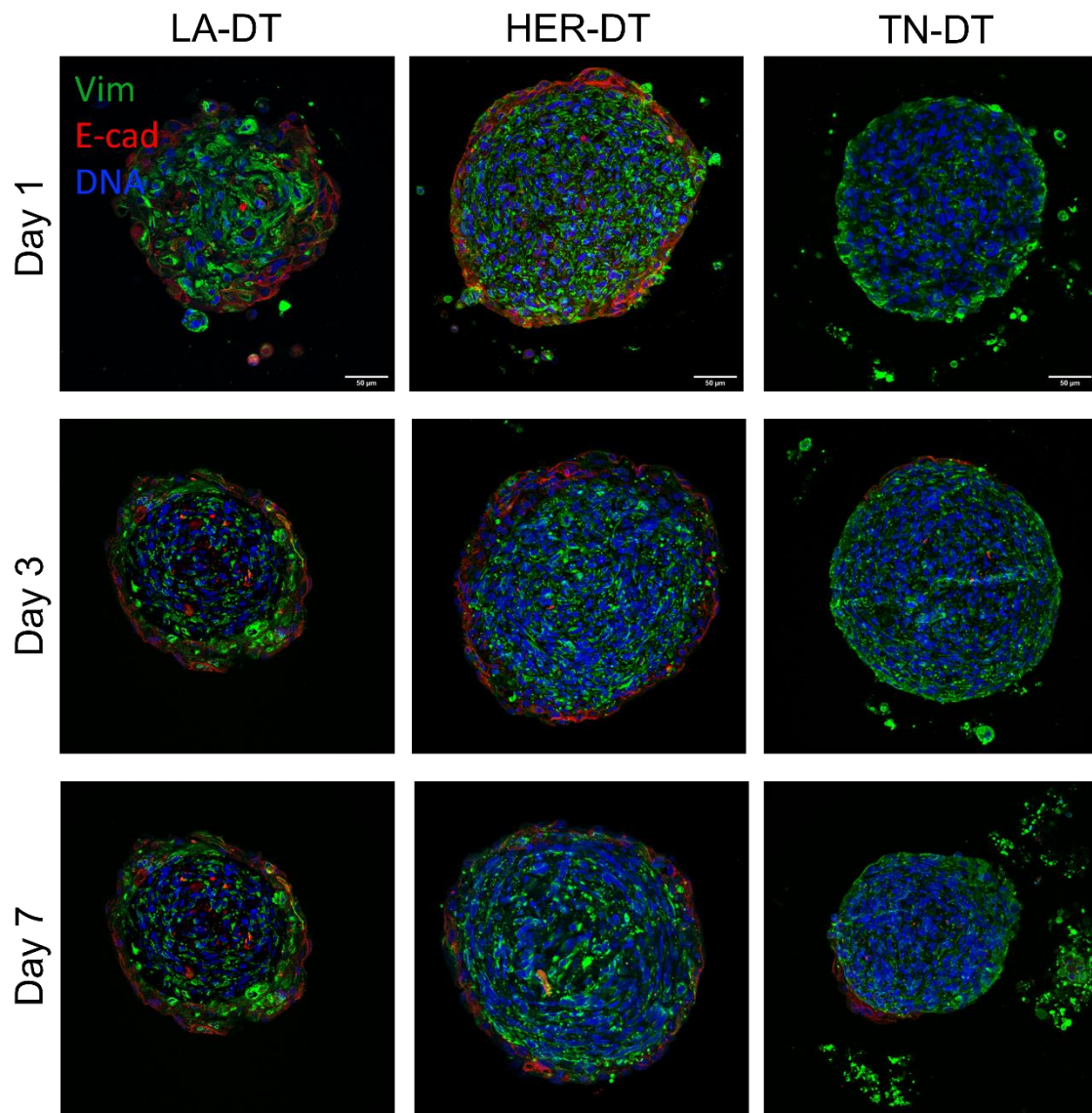


Figure 34. Expression of E-cadherin (epithelial marker) and vimentin (fibroblast marker) in MCTS along 7 days in culture. Immunostaining of vimentin (green), E-cadherin (red) and DNA (blue). 3 µm paraffin-embedded sections of MCTS spheroids derived from LA-, HER- and TN-DT specimens (passage 2). Images acquired with a 40x magnification. Scale bar 50 µm.

In MCTS obtained from cells in passage 8, the presence of epithelial cells is no longer detected (**Figure 35**). Considering that the expression patterns of FN and Col-I have not suffered alteration with higher cellular passages, the presence of epithelial cells are not determinant for ECM deposition in the MCTS and their final morphological properties.

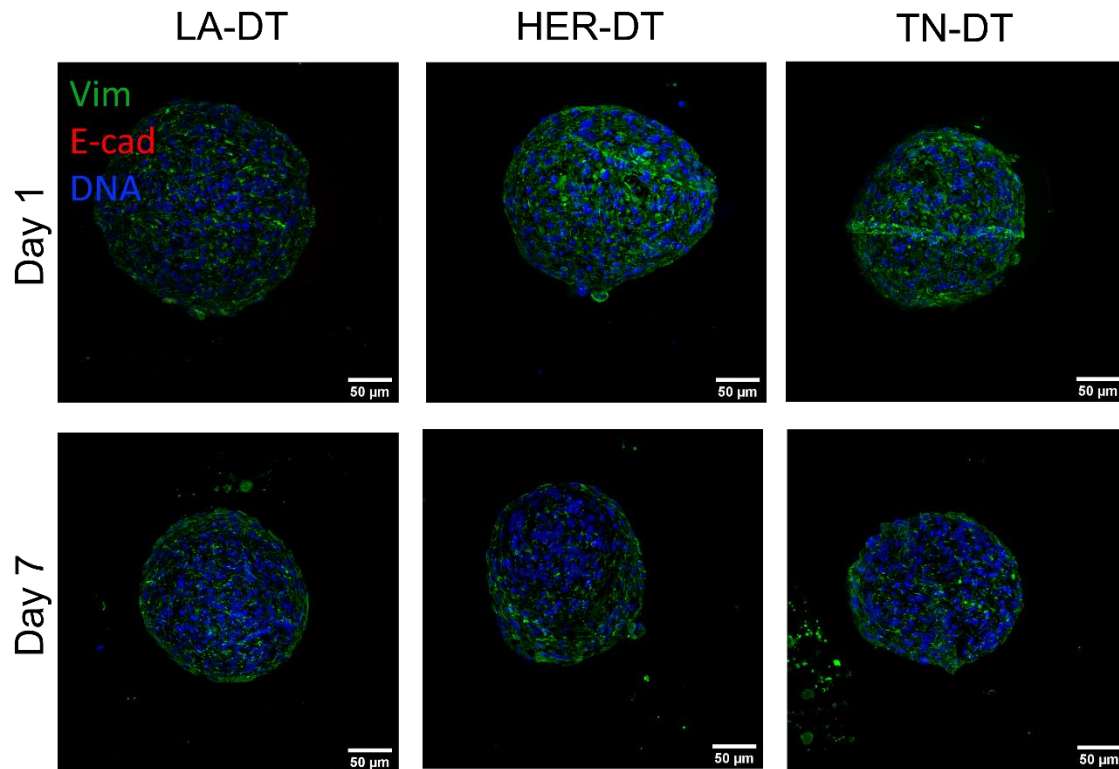


Figure 35. Vimentin and E-cadherin expression in MCTS derived from DT specimens in passage 8. Representative images of vimentin (green), E-cadherin (red) and DNA (blue) in LA-, HER- and TN-MCTS. Notice the absence of E-cadherin expression. Images acquired with a 40X objective. Scale bar 50 µm.

6.3.4 MCTS in fibrin as a model of cancer cells invasion

As reviewed before, the invasive capacity of cells is a critical parameter in BC development, namely during *in situ* – to invasive transition [14, 18]. The more traditional experimental setups to study cell motility *in vitro* are the scratch-wound assay and the transwell assay [131]. The establishment of cancer cell spheroid invasion assays allows to improve traditional methods and better mimic more physiologically relevant conditions *in vitro*.

In this work, cellular motility and migratory capacities were evaluated with MCTS embedded in fibrin [132]. This experiment was carried out only once and with spheroids produced with DT specimens in passage 6. Since a large depletion of epithelial cells had already been confirmed, it was decided to study only the behaviour of fibroblasts. Therefore the expression of vimentin - as a fibroblast marker - and of FN were studied. This experiment was carried out as a proof of concept on the application of fibrin gels to establish cancer cells spheroid invasion models.

Matrigel is the most common ECM-like substrate for cancer cell spheroid invasion assays [131, 133, 134]. However, Matrigel is not the desirable material for cell culture, since it is a xenogeneic material of unknown complete composition and is associated with batch-to-batch variability inducing variable culture conditions [135]. Moreover, Matrigel has been described to influence cells behaviour. But, since it is an undefined matrix, it is difficult to describe which biochemical property explain the acquired results.

The experimental setup here present is based on a fibrin gel. Fibrin is a biodegradable polymer formed from fibrinogen. Since it maintains cell adhesion motives, fibrin gels do not need prior functionalisation, as described for alginate hydrogels. Therefore, cells embedded in fibrin can degrade the matrix and migrate. Moreover, fibrin gels represent a more defined cell culture substrate [135, 136]. Taken together, we believe that fibrin presents advantages over Matrigel as a substrate to study cancer cells invasion *in vitro*.

Previous studies have demonstrated that the presence of FN is essential in the migratory capacity of tumour cells [117, 119, 120]. Therefore, an extended deposition of FN was expected in the fibrin gel, promoting conditions for cellular invasion. In fact, FN deposition is observed since day 2 in the fibrin gels (**Figure 36**), particularly with LA-DT. At this time point, LA-DT cells present the higher migratory capacity, which supports the correlation between FN deposition and cancer cells migration.

Results obtained after 7 days in culture (**Figure 37**) demonstrate a high localisation of fibroblasts in regions of intense FN deposition. At this timepoint, TN-DT cells present a more defined expression of vimentin. LA-DT cells continue to present an increased deposition of FN, which might be related to the presence of activated fibroblasts in these cultures (section 6.2.3). Overall, cells present a spread-like morphology, supporting the application of the system as a cancer cell invasive model. In future studies, it is important to conduct this experiment with cells from early passages to allow the characterisation of epithelial cells migratory behaviour.

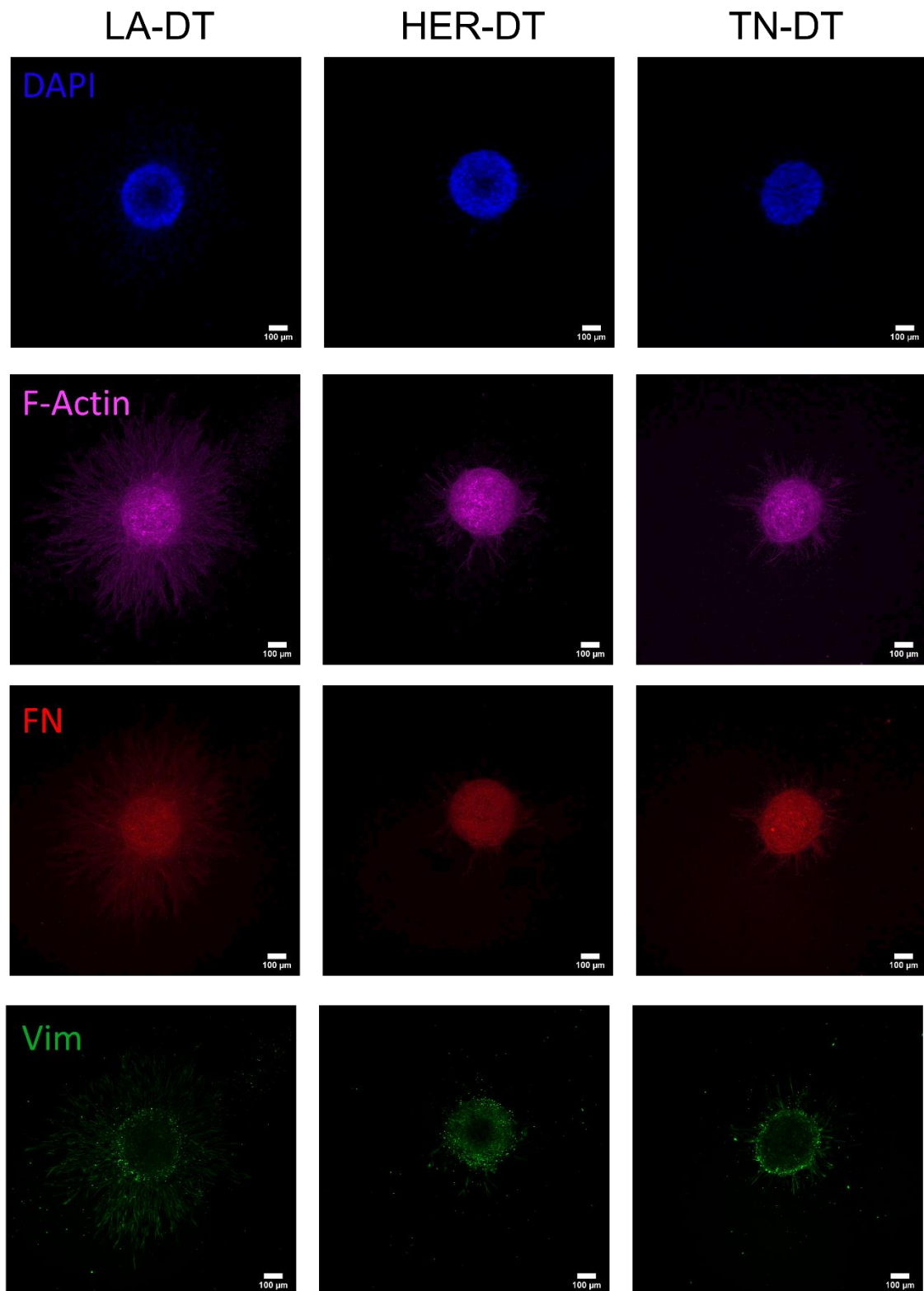


Figure 36. Expression of vimentin and fibronectin in MCTS embedded in fibrin gel for 2 days. Immunostaining of DNA (blue), F-actin (purple), fibronectin (FN, red), and vimentin (Vim, green). MCTS spheroids derived from LA-, HER-, TN-DT specimens in passage 6. Images acquired with a 10x magnification. Scale bar 100 μ m.

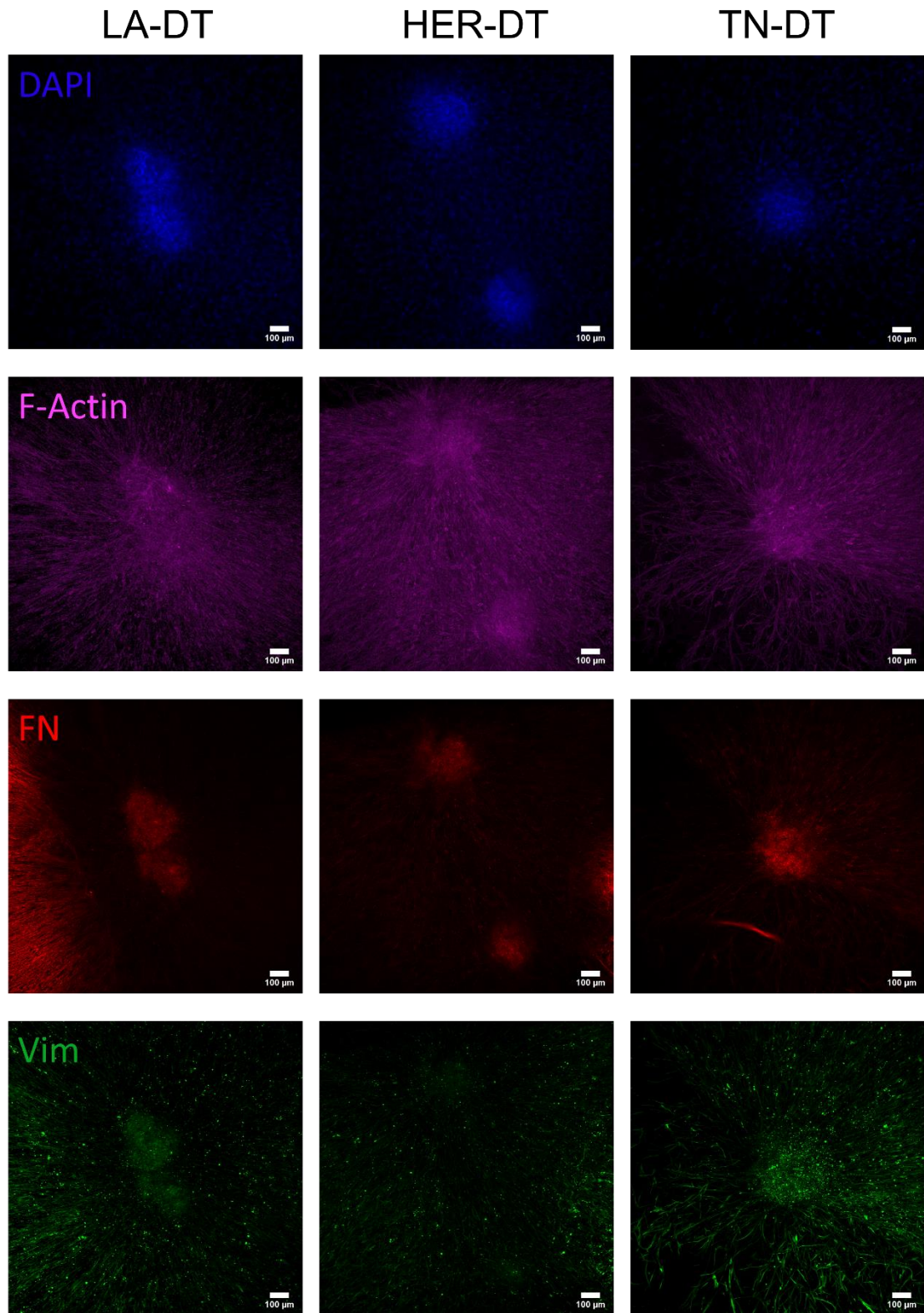


Figure 37. Expression of vimentin and fibronectin in MCTS embedded in fibrin gel for 7 days. Immunostaining of DNA (blue), F-actin (purple), fibronectin (FN, red), and vimentin (Vim, green). MCTS spheroids derived from LA-, HER-, TN-DT specimens in passage 6. Images acquired with a 10x magnification. Scale bar 100 μ m.

6.4 Formation of breast cancer organoids within RGD-alginate hydrogels

Organoids, self-organising multicellular structures that recapitulate key features of native tissues/organs, have emerged as physiologically relevant in vitro models to study cancer [137]. Still, they are commonly assembled in ECM-derived 3D matrices, such as collagen or Matrigel™, with poorly tunable biochemical/mechanical properties, high batch-to-batch variability, and intrinsic bioactivity, making it difficult to perform mechanistic studies and compare results between different laboratories or even different experiments. Biomaterial-based platforms and tissue engineering approaches have been translated into cancer research, creating improved models to study tumour biology [138, 139]. Models based on tumour ECM-mimetic hydrogels exhibit great potential as matrices for 3D cell culture and organisation [57, 140]. Among these, ultra-pure alginate hydrogels present key advantages such as low batch-to-batch variability, well defined and xeno-free composition, and precisely customisable biochemical/physical properties [141, 142]. We previously showed that molecularly-designed alginate 3D matrices recap key features of native ECMs supporting tissue morphogenesis [132, 143-146].

When embedded in a matrix, cells face the necessity to overcome the physical barrier imposed by the polymeric network to spread, proliferate, and migrate. It has been demonstrated that softer and more deformable matrices ($G' < 250$ Pa) promote fibroblasts spreading and proliferation [147]. Moreover, previous works in our lab have demonstrated that soft alginate hydrogels functionalized with RGD peptides, support epithelial morphogenesis, and promote the formation of acinar-like structures like the ones present in the mammary tissue [57]. Consequently, soft RGD-alginate matrices ($G' \approx 240$ Pa with 1 wt.% alginate, **Figure 38 A**) were selected for the embedding of DT specimens.

As expected, when embedded in alginate hydrogels, cells presented a round type morphology and formed cell clusters (**Figure 38 B**). In some regions, it was possible to identify cells with a spread-like morphology (**Figure 38 C**). The produced hydrogels were sufficiently soft to allow cells to escape the matrix and proliferate in the bottom of the well (**Figure 38 D**).

To characterise multicellular clusters in 3D (organoids), alginate discs were fixed at day 14 and organoids were measure based on the cytoskeleton (F-actin) and DNA staining (**Figure 38 E**). Moreover, alginate discs were kept in culture for 21 days to evaluate cells metabolic activity. Since cells present the capacity to extravasate the

alginate matrix, discs were moved to a clean well before each metabolic activity assay to dispose of the influence of cells cultured in 2D.

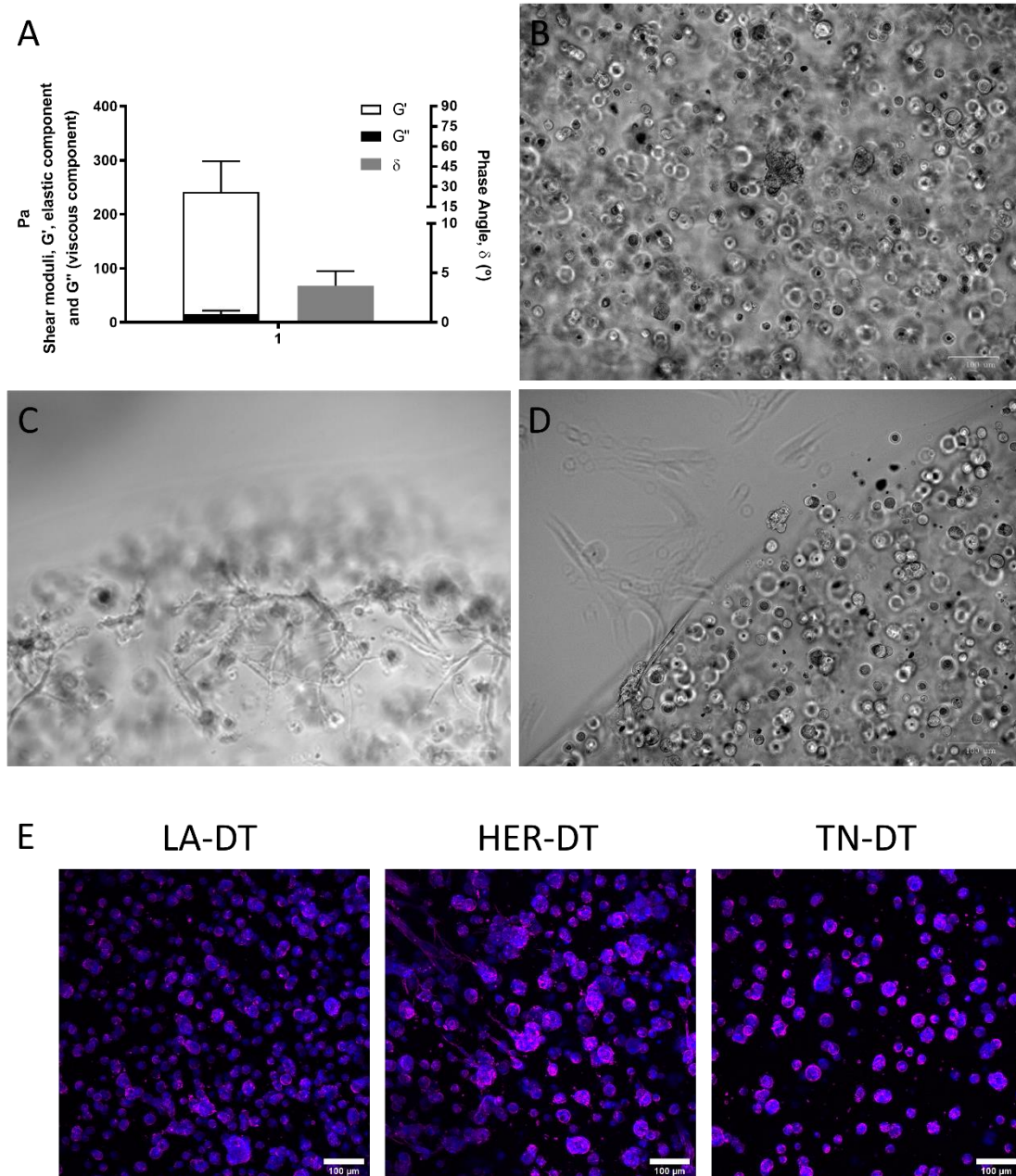


Figure 38. RGD-Alginate hydrogel for the culture of DT cells. (A) Mechanical properties of RGD-Alginate matrix (1 wt.% alginate). (B-D) Brightfield images of DT cells embedded in alginate matrices. Images acquired with ZOE Fluorescent Cell Imager (BioRad). Scale bar: 100 μ m. (E) Multicellular clusters within alginate 3D matrices. Immunostaining of DNA (blue) and F-actin (purple). Images acquired with a 20x magnification. Scale bar: 100 μ m.

Figure 39 presents the characterisation of organoids formation based on diameter measures. Although bigger spheroids have been formed from higher cell passages, the average organoids diameters are between 20 and 30 μ m. Cavo, Fato [60]

and co-workers have described similar diameters for MCF-7 cell clusters in alginate hydrogels with stiffnesses of 300–350 kPa. This highlights the idea that cells of primary origin and cell lines respond differentially in *in vitro* cultures.

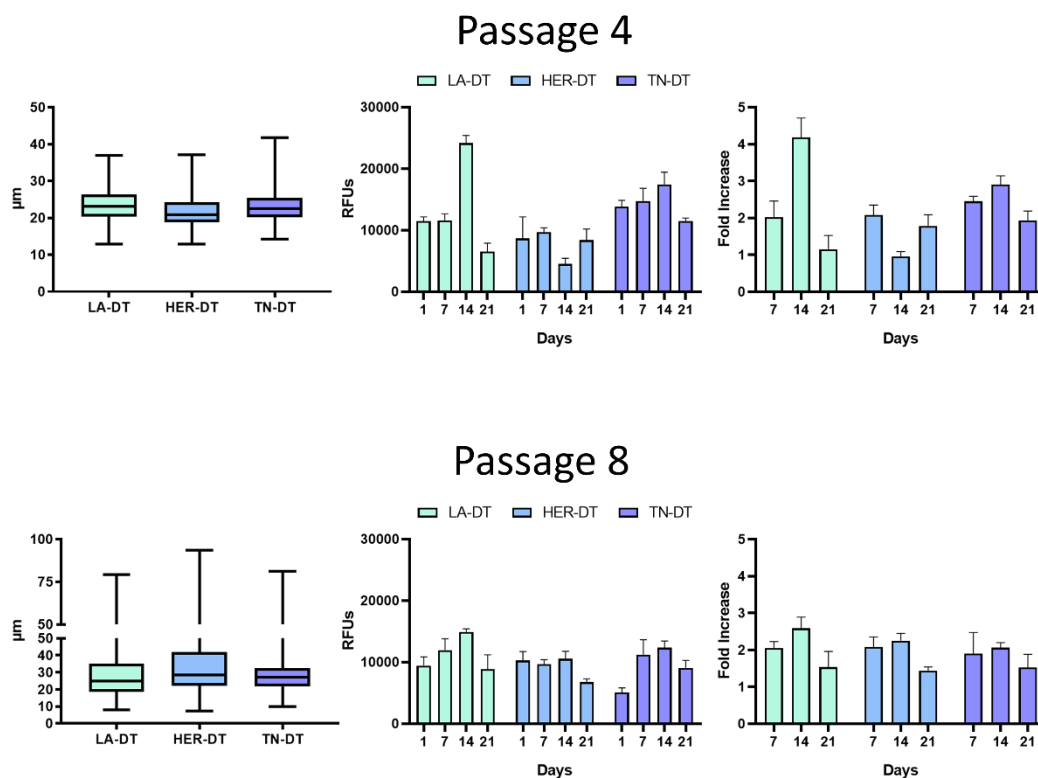


Figure 39. Characterisation of DT cells behaviour in 3D (passages 4 and 8). Diameter of cell clusters in 3D (passage 4 – top left, passage 8 – bottom left). Resazurin assay results presented with relative fluorescent units (RFUs) normalised to the autofluorescence of the resazurin solution (middle) and with the fold increase values in relation to day 1 (right). N = 3.

To evaluate metabolic activity a resazurin-based assay was performed on days 1, 7, 14 and 21 after embedding (**Figure 39** and **S2**, supplementary information). Considering the readouts with cells in passages 4 and 8 (**Figure 39**), it was not possible to define a correlation we organoids diameters. But we were able to observe a decrease in the overall metabolic activity from P4 to P8. This could be explained by the presence of both epithelial and fibroblast at P4, while in P8 the majority of the cells were fibroblast. Epithelial cells can grow within the alginate matrices as previously reported [56, 57]. On the other hand, fibroblast maintained their round shape without forming multicellular aggregates. One strategy to improve the fibroblast network could be the use of a protease-sensitive alginate matrix [148].

7 Concluding remarks

Breast cancer is a pathological condition that represents 29% of new cases of cancer and 14% of cancer deaths in women. BC comprises several subtypes with different clinical presentations and responses to treatment. Immunohistochemical profiling is the most common categorisation system. Considering the expression status of hormone receptors (ER and PR) and HER2, BC is commonly classified into four major molecular subtypes: Luminal (A and B), HER2-enriched and TNBC.

Over the past years, the scientific community have recognised the importance of establishing more reliable preclinical BC models. Since cancer cell lines have demonstrated limited capacity to mimic the diversity and complexity of human BC, primary tumour cells have come to the front.

In the present work, samples from primary Luminal A, HER2-enriched and TN tumours were used to establish different *in vitro* co-culture models. Establishing primary tumour derived cultures is associated with challenges such as fibroblast enrichment, as demonstrated. Even, it was possible to culture these cells and ensure their viability in different culture systems (2D, MCTS and alginate hydrogels) sustaining their possible application in *in vitro* models.

The impact of fibroblast enrichment was more significant after six passages suggesting that, with this type of approach, DT specimens must be used in the first passages. To develop scientific study/preclinical models, this is a limitation since the shelf life of cells is short. However, once a primary cell model has been validated, this limitation does not arise. Since isolated cells can be directly applied in the *in vitro* model that will be used to define the best therapeutic approach (personalised medicine). This approach gains special emphasis in TNBC since there is no targeted therapy available.

Considering the presented cellular characterisation, an important analysis should be considered in future studies. As reviewed, BC subtyping is highly accented in cells immunohistochemical profile in terms of hormone receptors (ER and PR) and HER2 expression. A reliable BC model must ensure the maintenance of these characteristics *in vitro*. Otherwise, the model will not have clinical relevance and will not be suitable for

personalised therapy approaches. Therefore, hormone receptors and HER2 expression must be assessed.

Concerning the expression of CKs 8 and 14, the presence was dual-positive cells was highlighted. Since an association between these and an EMT-phenotype is described in the literature, future studies must concern with cells genetic profile under these culture conditions. Upregulation of EMT associated genes enhances cell motility and enables migratory/metastatic capacities. Therefore, promoting these studies associated with the described cancer cell invasive model (MCTS embedded in fibrin gel) may allow to further describe these processes.

About MCTS formation, the adopted system allowed the production of reproducible spheroids with morphological characteristics maintained over six independent experiences. Considering the loss of epithelial cells, these results highlight that the morphological characteristics of MCTS, and their maintenance, is dependent on stromal cells and their ECM production capacity. Therefore, even opting for prior cell sorting, stromal cells must be present in high proportion in these models bringing advantages at the level of (1) spheroid production and (2) ability to mimic the TME. In future studies with prior cell sorting, it may be interesting to evaluate the ideal ratio of epithelial cells to fibroblast that maximises spheroid's production and better mimics the TME. Regarding the produced MCTS, it was not possible to prove the formation of an oxygen gradient and a hypoxic core. Since this is a characteristic of solid tumours with a proven impact on tumour cells behaviour, it must be further studied. For this purpose, analysis of HIF-1 α and/or Lox-1 expression may be considered [72].

Finally, we were able to generate primary breast cancer organoids in a well-defined 3D hydrogel matrix based on a peptide modified alginate. Future studies must rely on the expression of epithelial and mesenchymal markers to further understand cellular organisation. According to the literature, it is expected significant differences on cells organisation in comparison with our results with MCTS. In MCTS, epithelial cells are segregated to the periphery of a fibroblast core. However, Estrada, Rebelo [59] and co-workers establish a co-culture system of MCF-7 cells and fibroblasts in alginate and demonstrated the formation of aggregates of epithelial cells surrounded by fibroblasts.

Overall, we were able to culture and characterise primary breast cancer cells in 2D for the three BC subtypes. In the 3D field, MCTS were successfully established, and the first steps were given on the establishment of BC organoids (tumoroids). Our work represents a step forward to develop more physiologically relevant models with preclinical and clinical applicability

This page has been intentionally left blank.

References

1. Cardiff, R.D., et al., *Mammary Gland*, in *Comparative Anatomy and Histology (Second Edition)*, P.M. Treuting, S.M. Dintzis, and K.S. Montine, Editors. 2018, Academic Press: San Diego. p. 487-509.
2. Britannica. *Mammary gland*. 2020 February 16, 2021]; Available from: <https://www.britannica.com/science/mammary-gland>.
3. Srivastava, V., et al., *Organoid models for mammary gland dynamics and breast cancer*. *Current Opinion in Cell Biology*, 2020. 66: p. 51-58.
4. Nath, S. and G.R. Devi, *Three-dimensional culture systems in cancer research: Focus on tumor spheroid model*. *Pharmacology & Therapeutics*, 2016. 163: p. 94-108.
5. N. Lynn Henry, P.D.S., Irfanullah Haider, and R.J. Phoebe E. Freer, Michael S. Sabe, *Cancer of the Breast, in Abeloff's Clinical Oncology*. 2020, Elsevier.
6. ACS. *Invasive Breast Cancer (IDC/ILC)*. 2019 11-03-2021]; Available from: <https://www.cancer.org/cancer/breast-cancer/understanding-a-breast-cancer-diagnosis/types-of-breast-cancer/invasive-breast-cancer.html>.
7. ACS. *Ductal Carcinoma In Situ (DCIS)*. 2019 11-03-2021]; Available from: <https://www.cancer.org/cancer/breast-cancer/understanding-a-breast-cancer-diagnosis/types-of-breast-cancer/dcis.html>.
8. Erber, R. and A. Hartmann, *Histology of Luminal Breast Cancer*. *Breast Care*, 2020. 15(4): p. 327-336.
9. Sachs, N., et al., *A Living Biobank of Breast Cancer Organoids Captures Disease Heterogeneity*. *Cell*, 2018. 172(1): p. 373-386.e10.
10. Weigelt, B., F.C. Geyer, and J.S. Reis-Filho, *Histological types of breast cancer: How special are they?* *Molecular Oncology*, 2010. 4(3): p. 192-208.
11. Harbeck, N., et al., *Breast cancer*. *Nature Reviews Disease Primers*, 2019. 5(1): p. 66.
12. JHU. *Staging & grade - Breast cancer tumor* 10-04-2021]; Available from: <https://pathology.jhu.edu/breast/staging-grade/>.
13. Foulkes, W.D., I.E. Smith, and J.S. Reis-Filho, *Triple-Negative Breast Cancer*. *New England Journal of Medicine*, 2010. 363(20): p. 1938-1948.
14. Bahcecioglu, G., et al., *Breast cancer models: Engineering the tumor microenvironment*. *Acta Biomaterialia*, 2020. 106: p. 1-21.
15. Li, Y. and E. Kumacheva, *Hydrogel microenvironments for cancer spheroid growth and drug screening*. *Science Advances*, 2018. 4(4): p. eaas8998.
16. Drews-Elger, K., et al., *Primary breast tumor-derived cellular models: characterization of tumorigenic, metastatic, and cancer-associated fibroblasts in dissociated tumor (DT) cultures*. *Breast Cancer Res Treat*, 2014. 144(3): p. 503-17.
17. Inman, J.L., et al., *Mammary gland development: cell fate specification, stem cells and the microenvironment*. *Development*, 2015. 142(6): p. 1028-42.
18. Soysal, S.D., A. Tzankov, and S.E. Muenst, *Role of the Tumor Microenvironment in Breast Cancer*. *Pathobiology*, 2015. 82(3-4): p. 142-152.
19. Choi, S.Y.C., et al., *Lessons from patient-derived xenografts for better in vitro modeling of human cancer*. *Advanced Drug Delivery Reviews*, 2014. 79-80: p. 222-237.
20. Paterni, I., et al., *Estrogen receptors alpha (ERalpha) and beta (ERbeta): subtype-selective ligands and clinical potential*. *Steroids*, 2014. 90: p. 13-29.
21. Inic, Z., et al., *Difference between Luminal A and Luminal B Subtypes According to Ki-67, Tumor Size, and Progesterone Receptor Negativity Providing Prognostic Information*. *Clinical Medicine Insights. Oncology*, 2014. 8: p. 107-111.
22. Yanagawa, M., et al., *Luminal A and luminal B (HER2 negative) subtypes of breast cancer consist of a mixture of tumors with different genotype*. *BMC Research Notes*, 2012. 5(1): p. 376.

23. Yersal, O. and S. Barutca, *Biological subtypes of breast cancer: Prognostic and therapeutic implications*. World J Clin Oncol, 2014. 5(3): p. 412-24.
24. Tran, B. and P.L. Bedard, *Luminal-B breast cancer and novel therapeutic targets*. Breast Cancer Research, 2011. 13(6): p. 221.
25. Hashmi, A.A., et al., *Prognostic parameters of luminal A and luminal B intrinsic breast cancer subtypes of Pakistani patients*. World J Surg Oncol, 2018. 16(1): p. 1.
26. Creighton, C.J., *The molecular profile of luminal B breast cancer*. Biologics : targets & therapy, 2012. 6: p. 289-297.
27. Ismail-Khan, R. and M.M. Bui, *A Review of Triple-Negative Breast Cancer*. Cancer Control, 2010. 17(3): p. 173-176.
28. Criscitiello, C., et al., *Understanding the biology of triple-negative breast cancer*. Annals of Oncology, 2012. 23: p. vi13-vi18.
29. Zhang, J., et al., *Immune-related biomarkers in triple-negative breast cancer*. Breast Cancer, 2021.
30. Yehiely, F., et al., *Deconstructing the molecular portrait of basal-like breast cancer*. Trends Mol Med, 2006. 12(11): p. 537-44.
31. Podo, F., et al., *Triple-negative breast cancer: Present challenges and new perspectives*. Molecular Oncology, 2010. 4(3): p. 209-229.
32. Agorku, D.J., et al., *CD49b, CD87, and CD95 Are Markers for Activated Cancer-Associated Fibroblasts Whereas CD39 Marks Quiescent Normal Fibroblasts in Murine Tumor Models*. Front Oncol, 2019. 9: p. 716.
33. Mercier, I., et al., *Human breast cancer-associated fibroblasts (CAFs) show caveolin-1 downregulation and RB tumor suppressor functional inactivation: Implications for the response to hormonal therapy*. Cancer Biol Ther, 2008. 7(8): p. 1212-25.
34. Dykes, S.S., et al., *Stromal cells in breast cancer as a potential therapeutic target*. Oncotarget, 2018. 9(34): p. 23761-23779.
35. Denton, A.E., E.W. Roberts, and D.T. Fearon, *Stromal Cells in the Tumor Microenvironment*. Adv Exp Med Biol, 2018. 1060: p. 99-114.
36. Mao, Y., et al., *Stromal cells in tumor microenvironment and breast cancer*. Cancer Metastasis Rev, 2013. 32(1-2): p. 303-15.
37. Koh, T.J. and L.A. DiPietro, *Inflammation and wound healing: the role of the macrophage*. Expert Rev Mol Med, 2011. 13: p. e23.
38. Lopez de Andres, J., et al., *Cancer stem cell secretome in the tumor microenvironment: a key point for an effective personalized cancer treatment*. J Hematol Oncol, 2020. 13(1): p. 136.
39. Boudreau, N. and C. Myers, *Breast cancer-induced angiogenesis: multiple mechanisms and the role of the microenvironment*. Breast Cancer Research, 2003. 5(3): p. 140.
40. Sokol, E.S., et al., *Growth of human breast tissues from patient cells in 3D hydrogel scaffolds*. Breast Cancer Research, 2016. 18(1): p. 19.
41. Beri, P., et al., *Biomaterials to model and measure epithelial cancers*. Nature Reviews Materials, 2018. 3(11): p. 418-430.
42. Guimarães, C.F., et al., *The stiffness of living tissues and its implications for tissue engineering*. Nature Reviews Materials, 2020. 5(5): p. 351-370.
43. McNally, S. and T. Stein, *Overview of Mammary Gland Development: A Comparison of Mouse and Human*. Methods Mol Biol, 2017. 1501: p. 1-17.
44. Briem, E., et al., *Application of the D492 Cell Lines to Explore BreastMorphogenesis, EMT and Cancer Progression in 3D Culture*. J Mammary Gland Biol Neoplasia, 2019. 24(2): p. 139-147.
45. Bhimani, J., K. Ball, and J. Stebbing, *Patient-derived xenograft models—the future of personalised cancer treatment*. British Journal of Cancer, 2020. 122(5): p. 601-602.
46. Carter, E.P., et al., *A 3D in vitro model of the human breast duct: a method to unravel myoepithelial-luminal interactions in the progression of breast cancer*. Breast Cancer Res, 2017. 19(1): p. 50.
47. Alemany-Ribes, M. and C.E. Semino, *Bioengineering 3D environments for cancer models*. Adv Drug Deliv Rev, 2014. 79-80: p. 40-9.
48. Qiao, H. and T. Tang, *Engineering 3D approaches to model the dynamic microenvironments of cancer bone metastasis*. Bone Research, 2018. 6(1): p. 3.
49. Sitariski, A.M., et al., *3d Tissue Engineered In Vitro Models Of Cancer In Bone*. ACS biomaterials science & engineering, 2018. 4(2): p. 324-336.

50. Kawai, S., et al., *Three-dimensional culture models mimic colon cancer heterogeneity induced by different microenvironments*. Scientific Reports, 2020. 10(1): p. 3156.
51. Beri, P., et al., *Biomaterials to model and measure epithelial cancers*. Nature reviews. Materials, 2018. 3(11): p. 418-430.
52. Gu, L. and D.J. Mooney, *Biomaterials and emerging anticancer therapeutics: engineering the microenvironment*. Nature reviews. Cancer, 2016. 16(1): p. 56-66.
53. Lv, D., et al., *Three-dimensional cell culture: A powerful tool in tumor research and drug discovery*. Oncology letters, 2017. 14(6): p. 6999-7010.
54. Dalheim, M.Ø., et al., *Efficient functionalization of alginate biomaterials*. Biomaterials, 2016. 80: p. 146-156.
55. Lee, K.Y. and D.J. Mooney, *Alginate: Properties and biomedical applications*. Progress in Polymer Science, 2012. 37(1): p. 106-126.
56. Barros da Silva, P., et al., *Reshaping in vitro Models of Breast Tissue: Integration of Stromal and Parenchymal Compartments in 3D Printed Hydrogels*. Front Bioeng Biotechnol, 2020. 8: p. 494.
57. Bidarra, S.J., et al., *A 3D in vitro model to explore the inter-conversion between epithelial and mesenchymal states during EMT and its reversion*. Sci Rep, 2016. 6: p. 27072.
58. Cavo, M., et al., *A new cell-laden 3D Alginate-Matrigel hydrogel resembles human breast cancer cell malignant morphology, spread and invasion capability observed "in vivo"*. Scientific Reports, 2018. 8(1): p. 5333.
59. Estrada, M.F., et al., *Modelling the tumour microenvironment in long-term microencapsulated 3D co-cultures recapitulates phenotypic features of disease progression*. Biomaterials, 2016. 78: p. 50-61.
60. Cavo, M., et al., *Microenvironment complexity and matrix stiffness regulate breast cancer cell activity in a 3D in vitro model*. Sci Rep, 2016. 6(1): p. 35367.
61. Paredes Juarez, G.A., et al., *Immunological and technical considerations in application of alginate-based microencapsulation systems*. Front Bioeng Biotechnol, 2014. 2: p. 26.
62. Katt, M.E., et al., *In Vitro Tumor Models: Advantages, Disadvantages, Variables, and Selecting the Right Platform*. Frontiers in bioengineering and biotechnology, 2016. 4: p. 12-12.
63. Rodenhizer, D., et al., *The Current Landscape of 3D In Vitro Tumor Models: What Cancer Hallmarks Are Accessible for Drug Discovery?* Advanced Healthcare Materials, 2018. 7(8): p. 1701174.
64. Pal, A., et al., *A 3D Heterotypic Breast Cancer Model Demonstrates a Role for Mesenchymal Stem Cells in Driving a Proliferative and Invasive Phenotype*. Cancers, 2020. 12(8): p. 2290.
65. Mokhtari, R.B., et al., *3D Multicellular Stem-Like Human Breast Tumor Spheroids Enhance Tumorigenicity of Orthotopic Xenografts in Athymic Nude Rat Model*. Cancers, 2021. 13(11): p. 2784.
66. Halfter, K., et al., *Testing chemotherapy efficacy in HER2 negative breast cancer using patient-derived spheroids*. J Transl Med, 2016. 14(1): p. 112.
67. Hofmann, S., et al., *Patient-derived Tumor Spheroid Cultures as a Promising Tool to Assist Personalized Therapeutic Decisions*. 2020.
68. Burdall, S.E., et al., *Breast cancer cell lines: friend or foe?* Breast cancer research : BCR, 2003. 5(2): p. 89-95.
69. Faridi, N., et al., *Isolation and characterization of the primary epithelial breast cancer cells and the adjacent normal epithelial cells from Iranian women's breast cancer tumors*. Cytotechnology, 2018. 70(2): p. 625-639.
70. Andrade, F., J. Albuquerque, and A.V. Nascimento, *3.5 - Cell-based in vitro models for pulmonary permeability studies*, in *Concepts and Models for Drug Permeability Studies*, B. Sarmiento, Editor. 2016, Woodhead Publishing. p. 101-113.
71. Orlando, G., G. Remuzzi, and D.F. Williams, *Kidney Transplantation, Bioengineering, and Regeneration*, in *Kidney Transplantation, Bioengineering and Regeneration*, G. Orlando, G. Remuzzi, and D.F. Williams, Editors. 2017, Academic Press. p. xxv.
72. Imamura, Y., et al., *Comparison of 2D- and 3D-culture models as drug-testing platforms in breast cancer*. Oncol Rep, 2015. 33(4): p. 1837-43.
73. Dai, X., et al., *Breast Cancer Cell Line Classification and Its Relevance with Breast Tumor Subtyping*. Journal of Cancer, 2017. 8(16): p. 3131-3141.
74. Holliday, D.L. and V. Speirs, *Choosing the right cell line for breast cancer research*. Breast Cancer Research, 2011. 13(4): p. 215.

75. Ivanov, D.P., et al., *Multiplexing Spheroid Volume, Resazurin and Acid Phosphatase Viability Assays for High-Throughput Screening of Tumour Spheroids and Stem Cell Neurospheres*. PLOS ONE, 2014. 9(8): p. e103817.
76. Lemons, J.M.S., et al., *Quiescent Fibroblasts Exhibit High Metabolic Activity*. PLOS Biology, 2010. 8(10): p. e1000514.
77. Cserni, G., et al., *Distribution pattern of the Ki67 labelling index in breast cancer and its implications for choosing cut-off values*. The Breast, 2014. 23(3): p. 259-263.
78. Pathmanathan, N. and R.L. Balleine, *Ki67 and proliferation in breast cancer*. Journal of Clinical Pathology, 2013. 66(6): p. 512-516.
79. Soliman, N.A. and S.M. Yussif, *Ki-67 as a prognostic marker according to breast cancer molecular subtype*. Cancer biology & medicine, 2016. 13(4): p. 496-504.
80. Hashmi, A.A., et al., *Cytokeratin 5/6 and cytokeratin 8/18 expression in triple negative breast cancers: clinicopathologic significance in South-Asian population*. BMC research notes, 2018. 11(1): p. 372-372.
81. Aiad, H.A., et al., *Relationship of CK8/18 expression pattern to breast cancer immunohistochemical subtyping in Egyptian patients*. Ecancermedicallscience, 2014. 8: p. 404-404.
82. Korsching, E., et al., *Cytogenetic Alterations and Cytokeratin Expression Patterns in Breast Cancer: Integrating a New Model of Breast Differentiation into Cytogenetic Pathways of Breast Carcinogenesis*. Laboratory Investigation, 2002. 82(11): p. 1525-1533.
83. Rädler, P.D., et al., *Highly metastatic claudin-low mammary cancers can originate from luminal epithelial cells*. Nature Communications, 2021. 12(1): p. 3742.
84. Jones, C., et al., *CGH analysis of ductal carcinoma of the breast with basaloid/myoepithelial cell differentiation*. British Journal of Cancer, 2001. 85(3): p. 422-427.
85. Theriault, B.L., et al., *Establishment of primary cultures from ovarian tumor tissue and ascites fluid*. Methods Mol Biol, 2013. 1049: p. 323-36.
86. Yamada, S., et al., *Deconstructing the Cadherin-Catenin-Actin Complex*. Cell, 2005. 123(5): p. 889-901.
87. Lascombe, I., et al., *N-Cadherin as a Novel Prognostic Marker of Progression in Superficial Urothelial Tumors*. Clinical Cancer Research, 2006. 12(9): p. 2780-2787.
88. Senbanjo, L.T. and M.A. Chellaiah, *CD44: A Multifunctional Cell Surface Adhesion Receptor Is a Regulator of Progression and Metastasis of Cancer Cells*. Frontiers in cell and developmental biology, 2017. 5: p. 18-18.
89. Koike, N., *The Role of Stem Cells in the Hepatobiliary System and in Cancer Development: a Surgeon's Perspective*, in *Stem Cells and Cancer in Hepatology*. 2018. p. 211-253.
90. Li, W., et al., *Unraveling the roles of CD44/CD24 and ALDH1 as cancer stem cell markers in tumorigenesis and metastasis*. Scientific Reports, 2017. 7(1): p. 13856.
91. Morath, I., T.N. Hartmann, and V. Orian-Rousseau, *CD44: More than a mere stem cell marker*. The International Journal of Biochemistry & Cell Biology, 2016. 81: p. 166-173.
92. Jin, J., et al., *Phototheranostics of CD44-positive cell populations in triple negative breast cancer*. Scientific Reports, 2016. 6(1): p. 27871.
93. Zheng, Q., et al., *The Breast Cancer Stem Cells Traits and Drug Resistance*. Frontiers in Pharmacology, 2021. 11(2120).
94. Kisselbach, L., et al., *CD90 Expression on human primary cells and elimination of contaminating fibroblasts from cell cultures*. Cytotechnology, 2009. 59(1): p. 31-44.
95. Zhu, J., et al., *Overexpression of CD90 (Thy-1) in Pancreatic Adenocarcinoma Present in the Tumor Microenvironment*. PLOS ONE, 2014. 9(12): p. e115507.
96. Donnenberg, V.S., et al., *Localization of CD44 and CD90 positive cells to the invasive front of breast tumors*. Cytometry Part B: Clinical Cytometry, 2010. 78B(5): p. 287-301.
97. Yang, Z.F., et al., *Significance of CD90+ cancer stem cells in human liver cancer*. Cancer Cell, 2008. 13(2): p. 153-66.
98. Ridge, K.M., et al., *Chapter Fourteen - Methods for Determining the Cellular Functions of Vimentin Intermediate Filaments*, in *Methods in Enzymology*, M.B. Omary and R.K.H. Liem, Editors. 2016, Academic Press. p. 389-426.
99. Robinson-Bennett, B. and A. Han, *30 - Role of Immunohistochemistry in Elucidating Lung Cancer Metastatic to the Ovary from Primary Ovarian Carcinoma*, in *Handbook of*

- Immunohistochemistry and in Situ Hybridization of Human Carcinomas*, M.A. Hayat, Editor. 2006, Academic Press. p. 537-545.
100. Chen, M.H.-S., et al., *Expression of basal keratins and vimentin in breast cancers of young women correlates with adverse pathologic parameters*. *Modern Pathology*, 2008. 21(10): p. 1183-1191.
 101. Korsching, E., et al., *The origin of vimentin expression in invasive breast cancer: epithelial-mesenchymal transition, myoepithelial histogenesis or histogenesis from progenitor cells with bilinear differentiation potential?* *J Pathol*, 2005. 206(4): p. 451-7.
 102. Maehira, H., et al., *Vimentin Expression in Tumor Microenvironment Predicts Survival in Pancreatic Ductal Adenocarcinoma: Heterogeneity in Fibroblast Population*. *Ann Surg Oncol*, 2019. 26(13): p. 4791-4804.
 103. Sahai, E., et al., *A framework for advancing our understanding of cancer-associated fibroblasts*. *Nature Reviews Cancer*, 2020. 20(3): p. 174-186.
 104. Yamashita, M., et al., *Role of stromal myofibroblasts in invasive breast cancer: stromal expression of alpha-smooth muscle actin correlates with worse clinical outcome*. *Breast Cancer*, 2012. 19(2): p. 170-176.
 105. Kalluri, R. and M. Zeisberg, *Fibroblasts in cancer*. *Nature Reviews Cancer*, 2006. 6(5): p. 392-401.
 106. Watsky, M.A., et al., *Chapter Four - New Insights into the Mechanism of Fibroblast to Myofibroblast Transformation and Associated Pathologies*, in *International Review of Cell and Molecular Biology*, K.W. Jeon, Editor. 2010, Academic Press. p. 165-192.
 107. Kenny, P.A., et al., *The morphologies of breast cancer cell lines in three-dimensional assays correlate with their profiles of gene expression*. *Molecular Oncology*, 2007. 1(1): p. 84-96.
 108. Amaral, R.L.F., et al., *Comparative Analysis of 3D Bladder Tumor Spheroids Obtained by Forced Floating and Hanging Drop Methods for Drug Screening*. *Frontiers in Physiology*, 2017. 8(605).
 109. Gong, X., et al., *Generation of Multicellular Tumor Spheroids with Microwell-Based Agarose Scaffolds for Drug Testing*. *PloS one*, 2015. 10(6): p. e0130348-e0130348.
 110. Eilenberger, C., et al., *Effect of Spheroidal Age on Sorafenib Diffusivity and Toxicity in a 3D HepG2 Spheroid Model*. *Scientific Reports*, 2019. 9(1): p. 4863.
 111. Cruz-Matías, I., et al., *Sphericity and roundness computation for particles using the extreme vertices model*. *Journal of Computational Science*, 2019. 30: p. 28-40.
 112. Zaroni, M., et al., *3D tumor spheroid models for in vitro therapeutic screening: a systematic approach to enhance the biological relevance of data obtained*. *Scientific Reports*, 2016. 6(1): p. 19103.
 113. Friedrich, J., et al., *Spheroid-based drug screen: considerations and practical approach*. *Nature Protocols*, 2009. 4(3): p. 309-324.
 114. Kim, S.J., et al., *Engineering Multi-Cellular Spheroids for Tissue Engineering and Regenerative Medicine*. *Adv Healthc Mater*, 2020: p. e2000608.
 115. Horder, H., et al., *Bioprinting and Differentiation of Adipose-Derived Stromal Cell Spheroids for a 3D Breast Cancer-Adipose Tissue Model*. *Cells*, 2021. 10(4): p. 803.
 116. Oskarsson, T., *Extracellular matrix components in breast cancer progression and metastasis*. *The Breast*, 2013. 22: p. S66-S72.
 117. Park, H.J. and D.M. Helfman, *Up-regulated fibronectin in 3D culture facilitates spreading of triple negative breast cancer cells on 2D through integrin β -5 and Src*. *Scientific Reports*, 2019. 9(1): p. 19950.
 118. Bae, Y.K., et al., *Fibronectin expression in carcinoma cells correlates with tumor aggressiveness and poor clinical outcome in patients with invasive breast cancer*. *Human Pathology*, 2013. 44(10): p. 2028-2037.
 119. Ioachim, E., et al., *Immunohistochemical expression of extracellular matrix components tenascin, fibronectin, collagen type IV and laminin in breast cancer: their prognostic value and role in tumour invasion and progression*. *European Journal of Cancer*, 2002. 38(18): p. 2362-2370.
 120. Jeong, S.-Y., et al., *Co-Culture of Tumor Spheroids and Fibroblasts in a Collagen Matrix-Incorporated Microfluidic Chip Mimics Reciprocal Activation in Solid Tumor Microenvironment*. *PloS one*, 2016. 11: p. e0159013.
 121. Williams, C.M., et al., *Fibronectin expression modulates mammary epithelial cell proliferation during acinar differentiation*. *Cancer research*, 2008. 68(9): p. 3185-3192.

122. Attieh, Y., et al., *Cancer-associated fibroblasts lead tumor invasion through integrin- β 3-dependent fibronectin assembly*. The Journal of cell biology, 2017. 216(11): p. 3509-3520.
123. Acerbi, I., et al., *Human breast cancer invasion and aggression correlates with ECM stiffening and immune cell infiltration*. Integrative Biology, 2015. 7(10): p. 1120-1134.
124. Conklin, M.W., et al., *Aligned collagen is a prognostic signature for survival in human breast carcinoma*. The American journal of pathology, 2011. 178(3): p. 1221-1232.
125. Erler, J.T. and V.M. Weaver, *Three-dimensional context regulation of metastasis*. Clinical & experimental metastasis, 2009. 26(1): p. 35-49.
126. Gilkes, D., et al., *Hypoxia-inducible Factor 1 (HIF-1) Promotes Extracellular Matrix Remodeling under Hypoxic Conditions by Inducing P4HA1, P4HA2, and PLOD2 Expression in Fibroblasts*. The Journal of biological chemistry, 2013. 288.
127. Wong, C.C.-L., et al., *Hypoxia-inducible factor 1 is a master regulator of breast cancer metastatic niche formation*. Proceedings of the National Academy of Sciences, 2011. 108(39): p. 16369-16374.
128. Khawar, I.A., et al., *Three Dimensional Mixed-Cell Spheroids Mimic Stroma-Mediated Chemoresistance and Invasive Migration in hepatocellular carcinoma*. Neoplasia, 2018. 20(8): p. 800-812.
129. Yakavets, I., et al., *Advanced co-culture 3D breast cancer model for investigation of fibrosis induced by external stimuli: optimization study*. Scientific Reports, 2020. 10(1): p. 21273.
130. Yip, D. and C.H. Cho, *A multicellular 3D heterospheroid model of liver tumor and stromal cells in collagen gel for anti-cancer drug testing*. Biochemical and Biophysical Research Communications, 2013. 433(3): p. 327-332.
131. Berens, E.B., et al., *A Cancer Cell Spheroid Assay to Assess Invasion in a 3D Setting*. Journal of visualized experiments : JoVE, 2015(105): p. 53409.
132. Torres, A.L., et al., *Guiding morphogenesis in cell-instructive microgels for therapeutic angiogenesis*. Biomaterials, 2018. 154: p. 34-47.
133. Chrisafis, G., et al., *Collective cancer cell invasion requires RNA accumulation at the invasive front*. Proceedings of the National Academy of Sciences, 2020. 117(44): p. 27423-27434.
134. Lim, G.J., S.-J. Kang, and J.Y. Lee, *Novel invasion indices quantify the feed-forward facilitation of tumor invasion by macrophages*. Scientific Reports, 2020. 10(1): p. 718.
135. Allen, P., J. Melero-Martin, and J. Bischoff, *Type I collagen, fibrin and PuraMatrix matrices provide permissive environments for human endothelial and mesenchymal progenitor cells to form neovascular networks*. Journal of Tissue Engineering and Regenerative Medicine, 2011. 5(4): p. e74-e86.
136. Jockenhoevel, S., et al., *Fibrin gel – advantages of a new scaffold in cardiovascular tissue engineering*. European Journal of Cardio-Thoracic Surgery, 2001. 19(4): p. 424-430.
137. Drost, J. and H. Clevers, *Organoids in cancer research*. Nat Rev Cancer, 2018. 18(7): p. 407-418.
138. Papalazarou, V., M. Salmeron-Sanchez, and L.M. Machesky, *Tissue engineering the cancer microenvironment-challenges and opportunities*. Biophys Rev, 2018. 10(6): p. 1695-1711.
139. Gill, B.J. and J.L. West, *Modeling the tumor extracellular matrix: Tissue engineering tools repurposed towards new frontiers in cancer biology*. J Biomech, 2014. 47(9): p. 1969-1978.
140. Park, K.M., D. Lewis, and S. Gerecht, *Bioinspired Hydrogels to Engineer Cancer Microenvironments*. Annual Review of Biomedical Engineering, 2017. 19(1): p. 109-133.
141. Bidarra, S.J., C.C. Barrias, and P.L. Granja, *Injectable alginate hydrogels for cell delivery in tissue engineering*. Acta Biomater, 2014. 10(4): p. 1646-1662.
142. Bidarra, S.J., A.L. Torres, and C.C. Barrias, *Injectable Cell Delivery Systems Based on Alginate Hydrogels for Regenerative Therapies*, in *Reference Module in Materials Science and Materials Engineering*. 2016.
143. Araujo, M., et al., *Coumarin-grafted blue-emitting fluorescent alginate as a potentially valuable tool for biomedical applications*. J Mater Chem B, 2020. 8(4): p. 813-825.
144. Campiglio, C.E., et al., *Bottom-up engineering of cell-laden hydrogel microfibrillar patch for guided tissue regeneration*. Mater Sci Eng C Mater Biol Appl, 2020. 108: p. 110488.

145. Bidarra, S.J., et al., *Immobilization of human mesenchymal stem cells within RGD-grafted alginate microspheres and assessment of their angiogenic potential*. *Biomacromolecules*, 2010. 11(8): p. 1956-1964.
146. Bidarra, S.J. and C.C. Barrias, *3D Culture of Mesenchymal Stem Cells in Alginate Hydrogels*. *Methods Mol Biol*, 2019. 2002: p. 165-180.
147. Bott, K., et al., *The effect of matrix characteristics on fibroblast proliferation in 3D gels*. *Biomaterials*, 2010. 31(32): p. 8454-8464.
148. Fonseca, K., P. Granja, and C. Barrias, *Engineering proteolytically-degradable artificial extracellular matrices*. *Progress in Polymer Science*, 2014. 39.

This page has been intentionally left blank.

Supplementary information

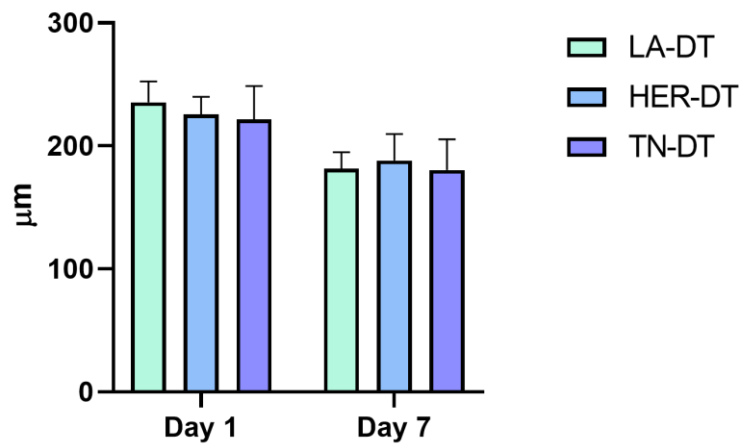


Figure S1. MSCT morphological characterisation – diameter. Average diameter of MCTS derived from DT cells in different passages.

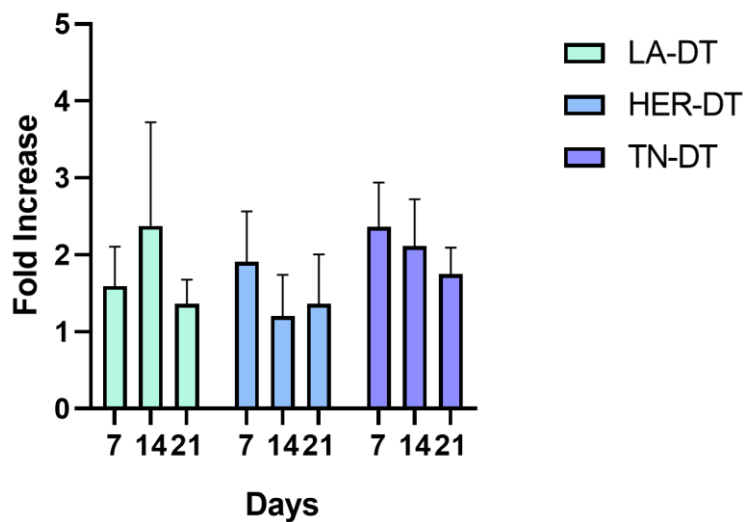


Figure S2 Metabolic activity studies of DT cells cultured in 3D alginate matrices. Resazurin assay performed with cells in passages 1, 4, 5, 8 and 9 - average results. Results present with the fold increase values in relation to day 1. N = 3